Quantitative Modelling of T cell Activation and Co-Stimulation

John Nguyen

Sir William Dunn School of Pathology

Somerville College

A thesis submitted for the degree of Doctor of Philosophy

Trinity Term 2019

Acknowledgements

Thinking back, no more than six years ago I would have struggled to even imagine being where I am today. In the four years of pursuing my doctoral degree, I have acquired a number of skills and experiences that would not have been possible without the support from many people.

My heartfelt thanks go out to my supervisor Dr Omer Dushek, whose contagious enthusiasm served to draw out the most of my potential. Especially starting computational modelling without any prior experience was daunting, but his continued guidance and the unique sense of collaboration in his multi-disciplinary group left me with no regrets. Omer would soon encourage me to voice my opinion and help steer the research of the lab, and he offered me numerous opportunities for personal growth, through teaching and supervision of students, representing the group at conferences, and managing collaborations. I can say that I owe him much of the confidence that I have in my abilities as a scientist today.

I am also indebted to all members of the Dushek, Brown and Van der Merwe labs for the stimulating discussions, helpful advice and support in the lab, and a friendlier work atmosphere than I could ever have wished for. The same is true for the Dunn School as a greatly supportive research department. I also appreciate the advice and comments I received during meetings and conferences, and particularly from the assessors of my *Transfer to DPhil Status* and *Confirmation of DPhil Status*, Professors Simon Davis and Michael Dustin, as well as Dr Audrey Gérard.

Furthermore, I am grateful for the financial support without which I would not have been able to complete this work: The Sir William Dunn School of Pathology Research Studentship, the Clarendon Fund Scholarship, the Mary Somerville Graduate Scholarship from Somerville College Oxford, as well as the Santander Graduate Awards. I also greatly appreciate the opportunity to complete manuscripts for publication within the next six months thanks to a postdoctoral extension award from the Cellular Immunology Unit Trust. The work of the lab

was further supported by the Wellcome Trust, the Royal Society and Cancer Research UK.

I would also like to extend my thanks to my family and friends for the continued emotional and moral support throughout the years.

Finally, I would like to express my gratitude to my final examiners, Professors David Sansom and Simon Davis, for taking the time to assess this thesis and my final viva.

Contributions

This work is part of a larger collaborative project in the lab, with other students applying similar methods to study other families of co-stimulatory and co-inhibitory receptors. Especially the mathematical modelling is a result of a group effort, with the base model for Chapter 3 having been developed over the years and recently published (Trendel et al., 2019), with contributions from Omer Dushek, Nicola Trendel, Philipp Kruger and myself. Parameter values of this model were based on the best fitting values for the data sets in (Trendel et al., 2019), estimated by an ABC-SMC algorithm written and run by Nicola Trendel and Omer Dushek, whereas I have built and simulated the extended models of co-stimulation shown in Chapter 3.

Abstract

Precisely regulated activity of T cells is crucial to effectively control pathogens while limiting immunopathology to a minimum. Even though T cell activation is predominantly governed by antigen recognition through the T cell receptor (TCR), the activity of an array of various accessory receptors can markedly alter this decision-making process, with the potential to serve as attractive therapeutic intervention points. Therefore, many of these co-stimulatory and co-inhibitory receptors and their molecular signalling pathways have been characterised. However, how exactly these receptors integrate with TCR signalling to affect the T cell response quantitatively remains poorly understood.

Here, we used *in vitro* expanded primary human T cells in a minimal stimulation platform to study co-stimulation through receptors of the TNF receptor superfamily (TNFRSF) in isolation. This allowed us to precisely define the ligand doses and stimulation times in order to capture the quantitative effects of TNFRSF signalling on the T cell cytokine response, with a particular focus on two representative TNFRSF members, 4-1BB and CD27. We found that 4-1BB co-stimulation was able to prolong the cytokine response, while engagement of CD27 increased the amount of cytokine produced without affecting the duration of the response and the T cells still became unresponsive after 8 hours. However, in combination with computational modelling, detailed analysis of our results showed that the distinct phenotypes of these receptors were mainly caused by their differential expression pattern in time, while the TNFRSF members share a common co-stimulatory mechanism, which we summarised in a minimal mathematical model. Simulations of the model predicted that co-stimulation through either of 4-1BB and CD27 could rescue TCR-dependent cytokine production in T cells which had become unresponsive through previous stimulation, and that CD27 could increase the potency of 4-1BB by enhancing its expression. We were then able to validate the model by confirming the both the rescue of the response and the synergy between TNFRSF members experimentally.

Table of Contents

Chapter 1: Introduction

1.1. The human immune system and the role of T cells

A functional immune system is indispensable to ensure our protection against pathogenic intruders. Epithelial barriers represent the first line of defence against invading pathogens from the outside (Fritz et al., 2008). Once these are breached, further mechanisms of the innate immune system are employed, starting with pattern recognition receptors (PRRs) which have evolved to detect conserved structures originating from pathogens and cellular damage, also known as pathogen- and damage-associated molecular patterns (PAMPs and DAMPs), respectively (Takeuchi and Akira, 2010). PRRs are represented by soluble components, such as the complement system, as well as receptors expressed on and inside various cell types, including professional phagocytes of the myeloid lineage such as granulocytes and macrophages (Iwasaki and Medzhitov, 2015; Janeway Jr. and Medzhitov, 2002). Once a threat is recognised, these cells inactivate and remove pathogenic structures while alarming surrounding tissues via an inflammatory response through soluble mediators such as the cytokine TNF (tumour necrosis factor).

Dendritic cells are phagocytes which bridge the innate and adaptive immune system (Reis E Sousa, 2006; Steinman, 1998). They patrol tissues and constantly ingest material through endocytosis and pinocytosis, which they can break down into peptides to present on major histocompatibility complex (MHC) molecules on their cell surface (Rock et al., 2016). These are recognised by T cells, which together with the primarily antibody-producing B cells represent the adaptive immune system. In contrast to the germline-encoded PRRs, the genes for antigen

receptors are generated by recombination of gene segments (VDJ recombination) during T and B cell development, giving rise to the vast repertoire of hypervariable receptors, each with the capacity to recognise a subset of antigens (Thompson, 1995). Since each of these individual antigen receptors will only be expressed by a few cells of a naïve T or B cell clone, rapid clonal expansion upon antigen encounter is required to produce sufficient cell numbers for an effective immune response. This can take several days, but it allows the adaptive immune system to respond with specificity to a given infection and also to develop memory of encountered pathogens, enabling enhanced and accelerated immune responses to re-encounters (Iwasaki and Medzhitov, 2015).

T cells play a central role in this. Their T cell antigen receptor (TCR) cannot recognise antigens directly, but only antigen-derived peptides presented on MHC molecules on the surface of antigen-presenting cells (APCs) (Zinkernagel and Doherty, 1974). Naïve T cells circulate through the body and especially in lymphoid tissues, they screen the surfaces of professional APCs, primarily dendritic cells, for cognate peptides presented on MHC (pMHCs). Upon encounter of such pMHCs in the context of an infection, naïve T cells become activated in a process called priming (Mempel et al., 2004). Successful priming initiates the clonal expansion and differentiation of T cells into a variety of effector T cells, as well as long-lived memory T cells which are retained after clearance of the pathogen.

The two major subsets of T cells are characterised by their co-receptors CD4 and CD8. $CD4^+$ T cells recognise peptides on MHC class II, which is largely confined to professional APCs, such as dendritic cells, macrophages and B cells. The functions

of the diverse $CD4^+$ effector T cells (also known as T helper cells) therefore predominantly include relaying information and orchestrating the immune response by activating the appropriate cell types for the present infection through cytokines (Zhu et al., 2010). Type 1 T helper cells (T_H1), for example, encourage a particular focus on eradication of intracellular pathogens by activating macrophages, natural killer (NK) cells and also $CD8^+$ T cells by secreting cytokines such as TNF and interferon gamma (IFN-γ). Which subtype of T_H cell a $CD4^+$ T cell differentiates into is largely influenced by the cytokine stimuli it receives during the differentiation process. These can originate from the priming dendritic cell itself, which can secrete the appropriate cytokines based on the type of pathogen they identified through their conserved PRRs (Iwasaki and Medzhitov, 2015). The cytokine environment is also shaped by pre-existing effector and memory T cells during an ongoing or reactivated immune response.

$CD8^+$ T cells, on the other hand, recognise class I pMHCs, which are found on all nucleated cells (Hewitt, 2003). However, their priming requires additional signals and thus still predominantly happens in the context of dendritic cells, with support from $CD4^+$ T cells (Mescher et al., 2006; Tham et al., 2002). Activated $CD8^+$ T cells differentiate into cytotoxic T lymphocytes (CTLs) whose major functions are the production of pro-inflammatory cytokines and targeted killing of infected cells. This is possible since the antigen presentation machinery on MHC class I samples from all peptides produced by a cell, including intracellular proteins (Rock et al., 2016). Widespread expression of MHC class I therefore enables CTLs to scan the surfaces of almost all body cells and identify targets which express non-self peptides, e.g. derived from viral proteins. In addition, tumour cells tend to

produce so-called neo-antigens, peptides derived from mutated proteins, which can potentially be identified as “non-self”, as well. This provides a mechanism of immune-surveillance and control of malignancies by CTLs.

1.2. Overview of T cell signalling

The α and β chains of the αβ T cell receptor (TCR) form the pMHC binding interface. As mentioned above, their genes are randomly generated through recombination of V, D (in the case of the β chain) and J gene segments during T cell development (Thompson, 1995), with additional nucleotide insertions and deletions adding to the hypervariability at the junctions that form the complementarity-determining regions (CDRs), which are the loops in the α and β chains that contribute most to the pMHC interaction (Davis and Bjorkman, 1988).

However, this heterodimer is not known to have inherent intracellular signalling capacity, but instead forms a complex with the CD3γϵ and δϵ heterodimers, as well as a CD3ζζ homodimer, which contain a total of ten immunoreceptor tyrosine-based activation motifs (ITAMs) in their intracellular tails (Alcover et al., 2018; Call et al., 2004; Reth, 1989). Each ITAM contains two tyrosine residues that can be reversibly phosphorylated by Src-family kinases, such as Lck which predominantly fulfils this role in T cells, and dephosphorylated by phosphatases such as the large transmembrane phosphatase CD45. Phosphorylated ITAMs act as docking sites for further signalling proteins such as the tyrosine kinase ZAP-70 (Courtney et al., 2018).

The exact mechanism of how extracellular pMHC-TCR interactions initiate intracellular phosphorylation and signalling is still controversial. Proposed hypotheses include binding-induced conformational changes in the TCR-CD3 complex which are transduced across the membrane (Minguet et al., 2007), receptor clustering and oligomerisation models, as well as the kinetic segregation

model, which is based on exclusion of phosphatases with bulky extracellular domains from close APC-T cell contacts, favouring phosphorylation of TCR-CD3 complexes within these tight interactions (Davis and van der Merwe, 2006). These models are not necessarily mutually exclusive and have been discussed in detail elsewhere (Van Der Merwe and Dushek, 2011).

Of note are the highly organised structures called immunological synapses, which are formed by the rearrangement of cytoskeletal structures, TCRs and other surface receptors during prolonged, stable APC-T cells interactions (Dustin, 2014; Monks et al., 1998). Centripetal movement of small TCR clusters is observed, which coalesce in the centre of the synapse, forming the central supramolecular activation complex (cSMAC), surrounded by the peripheral SMAC (pSMAC), a ring enriched with adhesion proteins such as LFA-1. It is in this pSMAC where an elevated density of signalling molecules is found in association with the TCR microclusters (Varma et al., 2006), whereas the cSMAC is regarded as a site of signal termination, where TCR is removed either by endocytosis or exosome formation (Dustin, 2014). The precise functions of the immunological synapse are still debated, but may include modulation of T cell activation by facilitating co-localisation of pMHC-TCR complexes with other co-signalling ligand-receptors pairs as well as exclusion of large phosphatases such as CD45, negative regulation of signalling by TCR downregulation and pMHC trogocytosis, and (especially in the case of cytotoxic T lymphocytes) targeted release of cytokines and cytolytic granules. However, it has been shown that synapse formation is not essential for the activation of T cells, and that signals can be integrated from multiple short-lived APC-T cell interactions (Dustin, 2008; Marangoni et al., 2013).

1.2.1. T cell receptor signalling pathways

Downstream of the CD3 ITAM phosphorylation by Lck and recruitment of ZAP-70, TCR signalling involves numerous signalling molecules which have been identified in the past decades (Courtney et al., 2018). ZAP-70 is activated through phosphorylation by Lck and trans-auto-phosphorylation, after which it can act as a tyrosine kinase itself to phosphorylate the scaffold proteins LAT and SLP-76 and other downstream components (Chan et al., 1992). Phosphorylated LAT and SLP-76 form the backbone of a signalosome, recruiting multiple other signalling proteins from which multiple pathways branch off (Balagopalan et al., 2010).

PLC-γ, for example, produces the second messengers IP_3 and DAG when phosphorylated. IP_3 initiates the calcium pathway, resulting in the activation of the transcription factor NFAT (Macian, 2005), while DAG activates PKC-θ, which contributes to several downstream pathways. These culminate in the canonical activation of the transcription factor NFκB and the MAP kinase JNK. DAG and the LAT signalosome also participate in the activation of the MAP kinase ERK, which together with JNK leads to the production and activation of c-fos and c-jun, the components that form the transcription factor AP-1. Besides triggering nuclear localisation of the main T cell activation-associated transcription factors NFAT, NFκB and AP-1, the LAT signalosome also contributes to cytoskeletal remodelling crucial to T cell functions by signalling through Vav and WASp (Courtney et al., 2018).

It is worth noting that even though we have a good grasp of the topology of the TCR signalling network, our understanding of how this network produces the properties of the T cell response (such as the speed, sensitivity and specificity of antigen recognition and the digital nature of T cell activation) is very limited. So far, the function of only few signalling motifs has been elucidated, such as the ultrasensitivity and bistability of the ERK MAPK cascade (Das et al., 2009; Huang and Ferrell, 1996).

1.2.2. Functional outcomes of T cell activation

The eventual outcomes of TCR signalling can differ based on the differentiation stage and subtype of the T cell, as well as the context in conjunction with other co-signalling and cytokine receptors on T cells. In naïve T cells, successful priming induces a dramatic metabolic switch from quiescence to one of the most rapidly growing and dividing cell types (Michalek and Rathmell, 2010). The activation of the main transcription factors NFAT, NFκB and AP-1 results in gene expression changes that affect not only proliferation, but also the expression of surface receptors including co-signalling (e.g. 4-1BB and PD-1, see also sub-chapter 1.3.2.) and cytokine receptors (e.g. CD25), T cell differentiation, as well as the secretion of subtype-specific sets of cytokines.

In the case of effector $CD8^+$ T cells, which are extensively used in this thesis, TCR stimuli also result in the expression of Fas-ligand and production and release of perforin and granzymes for directed killing of target cells (Ando et al., 1997;

Voskoboinik et al., 2015). Cytokine secretion (with the main cytokines produced being TNF, IFN-γ, and IL-2) may be regarded as a secondary function, as this role is likely dominated by other cell types *in vivo*, such as $CD4^+$ T cells (Kristensen et al., 2004; Nakanishi et al., 2009; Slifka and Whitton, 2000; Varga and Welsh, 2000). The initial capacity of $CD8^+$ T cells to produce IL-2, has been shown to be relatively limited in comparison to $CD4^+$ T cells (Tham et al., 2002). IL-2 is well-known as a T cell growth factor, but is also crucial for the effector differentiation of $CD8^+$ T cells, making them dependent on $CD4^+$ T cell help in several regards (Malek and Castro, 2010).

However, production of TNF and IFN-γ has been found to be a crucial $CD8^+$ T cell function in many models of infection and cancer, activating and recruiting other immune cells (Allie et al., 2013; Hausmann et al., 2005; Prévost-Blondel et al., 2000). Moreover, in $CD8^+$ T cell-dominated responses, e.g. to acute viral infections, it is plausible that cytokines from these cells become very relevant (Butz and Bevan, 1998). The progressive loss of cytokine production observed in T cell exhaustion (see also Section 1.3.3.) can also be considered a major obstacle in the clearance of tumours and chronic infections (Apetoh et al., 2015). Taken together, a large body of evidence suggests that cytokine production is indeed an important $CD8^+$ T cell effector mechanism.

1.3. Regulation of T cell activation

T cell receptors are formed by random rearrangement of gene segments, which accounts for the hypervariability of their pMHC binding interfaces, but also results in possible recognition of pMHCs derived from self-antigens (Janeway Jr. and Medzhitov, 2002). To limit the risk of autoimmunity, rigorous regulatory mechanisms have evolved to remove or inactivate self-reactive T cells.

1.3.1. Central tolerance shapes the naïve T cell repertoire

During their development in the thymus, T cells are presented with self-antigen-derived pMHCs on specialised APCs, the cortical and medullary thymic epithelial cells, as well as thymic dendritic cells. In the thymic cortex, T cells that produce a defective TCR incapable of binding pMHC are removed through death by neglect ("positive selection"), whereas in the thymic medulla, T cells with TCRs that exhibit high affinity to self-pMHCs undergo induced cell death ("negative selection"). Thus, this mechanism of "central tolerance" removes the majority of self-reactive T cells from the repertoire before they leave the thymus (Klein et al., 2014). However, not all self-antigens are simultaneously expressed by each medullary thymic epithelial cell. Therefore, there is a chance for some self-reactive T cells to escape central tolerance if they happen to not encounter their cognate epitopes in the thymic medulla (Derbinski et al., 2005; Gotter et al., 2004).

Furthermore, TCRs which recognise harmless environmental and food-derived antigens will have to be kept in check in order to prevent unnecessary immunopathology. Thus, further regulatory mechanisms in the periphery are essential to maintain T cell tolerance.

1.3.2. Co-stimulation and co-inhibition provide T cells with context

Besides being selected against self-reactivity, TCRs expressed by naïve T cells that have undergone thymic selection are still devoid of intrinsic context since their binding interfaces are randomly generated. With only the TCR stimulus alone, there is no way to ensure that the pMHCs recognised originate from a virulent pathogen that requires immediate attention, and not from a harmless environmental antigen against which a strong immune response would be inappropriate.

Naïve T cells receive contextual information for the first time during priming. Professional APCs such as dendritic cells will upregulate the expression of MHC and co-stimulatory molecules during a maturation process upon encountering PAMPs, DAMPs and inflammatory cytokines (Reis E Sousa, 2006). Antigens collected in such a context of infection or inflammation will thus be presented to the naïve T cells in conjunction with co-stimulation, which signals through co-stimulatory receptors on the T cells. This was shown for the first time for the archetypical co-stimulatory receptor CD28, which consolidated a “two-signal

hypothesis": To be fully activated, naïve T cells require co-stimulation in addition to TCR signals (June et al., 1987; Mueller et al., 1989). With the discovery of many other co-stimulatory ligand-receptor pairs, this view has been extended to define the various co-stimulatory receptors as modulators of TCR signalling with very limited effects on their own (Chen and Flies, 2013). Most co-stimulatory ligand-receptor pairs known to date are found either in the immunoglobulin superfamily (IgSF), e.g. CD80/CD86 – CD28, ICOS-L – ICOS and CD58 – CD2, or the TNF / TNF receptor superfamilies (TNFSF / TNFRSF), including CD70 – CD27 and 4-1BBL – 4-1BB, which will be discussed in further detail in this thesis.

Not only is co-stimulation crucial during the priming of naïve T cells; throughout all stages in the life of a T cell, co-stimulation can affect e.g. the effector response and maintenance of the memory pool through various receptors with both overlapping and non-redundant functions, due to tight and differential regulation of the expression these receptors on T cells, as well as their ligands on APCs. The same applies to co-inhibitory receptors such as CTLA-4 and PD-1, which fulfil the biological role opposite to co-stimulation: They limit immune responses, for instance by preventing effective priming of naïve cells under tolerogenic conditions, or directly inhibiting the function of effector T cells to limit tissue damage and to resolve the immune response after clearance of an infection (Chen and Flies, 2013). In summary, the combination of co-stimulation and co-inhibition (also referred to as co-signalling) regulates how T cells perceive a certain TCR stimulus, appropriately tuning the response to cues from the environment that are sensed by conserved mechanisms of the innate immune system and relayed to T cells via strictly regulated co-stimulatory and co-inhibitory ligands on APCs.

1.3.3. Mechanisms of peripheral T cell tolerance

While naïve T cells are effectively primed by mature dendritic cells in the presence of an infection, dendritic cells remain immature with low expression of co-stimulatory molecules in the absence of danger signals (Reis E Sousa, 2006). Rather than inducing clonal expansion and effector responses, T cells primed in this context are primarily subjected to alternative fates that limit immunopathology. Similarly to the removal of self-reactive T cells in the thymus by negative selection, repeated inadequate stimulation of T cells can also lead to clonal deletion in the periphery through induced apoptosis (Davey et al., 2002; Kurts et al., 1997).

However, early *in vitro* experiments where T cells were stimulated through the TCR without engaging co-stimulatory receptors such as CD28 demonstrated that incomplete T cell activation can also induce a hypo-responsive state without cell death, which was defined as T cell anergy (Mueller et al., 1989; Schwartz, 2003). Anergic T cells are characterised by growth arrest and inhibited production of cytokines, especially the paracrine T cell growth factor IL-2, even in the face of persistent antigen presence. A generally proposed mechanism for the unresponsive phenotype is the preferential activation of NFAT through TCR signalling in the absence of co-stimulation and cytokines, and this imbalance with the other main transcription factors of T cell activation (AP-1 and NFκB) results in a divergent gene expression profile, upregulating proteins like DGK-α and the E3 ubiquitin ligases Cbl-b, GRAIL and Itch which induce the degradation and

inactivation of various components of T cell signalling. In addition, chromatin remodelling is observed in anergic T cells to further inhibit the transcription of cytokine genes (Baine et al., 2009; Wells, 2009).

Nevertheless, it is worth noting that "anergy" appears to have become an umbrella term for various unresponsive phenotypes of T cells, including for instance the process of "adaptive tolerance" which is likely to have distinct underlying mechanisms (Chiodetti et al., 2006; Schwartz, 2003). Recent studies have also shown that many of the epigenetic changes in anergic T cells overlap with those found in regulatory T cells, reigniting the idea of a continuous spectrum between T cell anergy and clonal diversion towards a regulatory phenotype, which bestows immunosuppressive capabilities on inappropriately activated T cells (Kalekar et al., 2016; Morales and Mueller, 2018; Schwartz, 2003).

Regulatory T cells (also known as T_{reg}s) represent another important component of peripheral T cell tolerance. The most abundant population of regulatory T cells is represented by $CD4^+$ T cells expressing the master transcription factor FoxP3. These cells can be generated in the thymus as an alternative fate to negative selection for T cells with intermediate affinity to self-pMHCs (Itoh et al., 1999; Jordan et al., 2001; Kawahata et al., 2002), but are also induced in the periphery when $CD4^+$ T cells are primed under tolerogenic circumstances (Apostolou and Von Boehmer, 2004). Regulatory T cells can suppress conventional effector T cell responses through a multitude of mechanisms, including deprivation of co-stimulatory molecules and growth factors (such as IL-2) by active removal and competition, production of inhibitory cytokines and other mediators (e.g. IL-10, IL-35, TGF-β and adenosine), modulation of APC phenotypes, and contact-

dependent mechanisms (Schmidt et al., 2012; Vignali et al., 2008). The importance of regulatory T cells in immune homeostasis is attested to by the severe systemic autoimmunity observed in clinical cases of FoxP3 deficiency (Van Der Vliet and Nieuwenhuis, 2007).

Lastly, effector T cell responses are also limited by a phenomenon described as T cell exhaustion. This process is observed in cases of prolonged persistence of antigen, such as in chronic infections and cancer. Rather than to preserve tolerance, T cell exhaustion appears to be a mechanism to prevent excessive immunopathology when clearance of antigen remains unsuccessful. This phenotype is characterised by a gradual loss of effector functions and proliferative capacity, as well as metabolic dysfunction, but also upregulation of various inhibitory receptors, suggesting an important role of T cell co-inhibition in maintaining hyporesponsiveness in T cell exhaustion (Wherry, 2011). Interestingly, imbalanced or excessive NFAT activation through the calcium pathway also appears to contribute to the T cell exhaustion-related gene expression signature, including the induction of co-inhibitory receptors (Martinez et al., 2015).

At this point one may wonder about the purpose of T cell anergy and exhaustion, in place of removing unwanted or redundant T cells altogether through clonal deletion and contraction. As Ronald Schwartz puts it in his 2003 review of T cell anergy, these non-deletory mechanisms of peripheral tolerance allow the immune system to limit immunopathology while reassessing the situation when antigen persists. An attenuated immune response during an actual infection would lead to increasing levels of antigen and co-stimulation, in which case re-activation of

previously silenced T cell clones would be warranted (Schwartz, 2003). T cell anergy has indeed been shown to be reversible with sufficient co-stimulation (Bansal-Pakala et al., 2001; Boussiotis et al., 1994; Wilcox et al., 2004). Similarly, exhausted T cells can be reinvigorated by blocking co-inhibitory pathways and targeted co-stimulation (Kamphorst et al., 2017; Saeidi et al., 2018; Zhao et al., 2015).

1.4. Rationale for the study of T cell co-stimulation and co-inhibition

With their pivotal role in the immune system, T cells also play an important part in the aetiology of immune dysregulation. While undesired T cell activity can result in organ transplant rejection or devastating auto-immune diseases such as multiple sclerosis and type-I diabetes mellitus (Riedhammer and Weissert, 2015), insufficient or inhibited T cell responses fail to clear malignancies and chronic infections, e.g. caused by HIV, HBV and HCV (Saeidi et al., 2018). Therefore, modulating T cell activity has attractive clinical potential.

One such application has resulted in the development and improvement of chimeric antigen receptors (CARs) which are used to redirect T cells to attack tumours. CARs are synthetic cell surface receptors designed to mimic the TCR complex, comprising a single-chain variable fragment (scFv), which is a modified antigen-binding fragment of an antibody that recognises a tumour-associated antigen, coupled to the intracellular tail of CD3ζ (Dotti et al., 2014). T cells genetically engineered with such CARs were indeed able to respond to tumour cells *in vitro*. However, their efficacy in early *in vivo* experiments was disappointing (Kershaw et al., 2006; Lamers et al., 2013), due to incomplete activation in the absence of co-stimulation and rapid induction of unresponsiveness (Savoldo et al., 2011).

This led to the design of second-generation CARs, which include the intracellular domain of a co-stimulatory receptor such as CD28 or 4-1BB in addition to the

CD3ζ tail, markedly improving the *in vivo* performance and persistence of CAR-engineered T cells (Carpenito et al., 2009; Vera et al., 2006). Second-generation CAR T cells had remarkable clinical efficacy and were approved for the treatment of B cell malignancies in 2017 (Davila et al., 2014; Maude et al., 2018). However, solid tumours still prove to be resistant to CAR T cell immunotherapy, likely due to limited accessibility and a highly immunosuppressive microenvironment (Beatty et al., 2018; Heczey et al., 2017). To overcome these obstacles, attempts are being made to either improve the design of CARs further, e.g. by inclusion of additional domains from other co-stimulatory receptors, or to combine CAR T cell therapy with other interventions to enhance the T cell response.

Another promising leap in the field of T cell co-signalling was marked by the development of immune checkpoint inhibitors, antibodies that block co-inhibitory receptors on T cells. Ipilimumab, which targets CTLA-4 on T cells, was approved for the treatment of melanoma in 2011, and since then, ipilimumab and checkpoint inhibitors which target PD-1 and PD-L1, another T cell co-inhibitory axis, have been introduced for the therapy of several other malignancies, with impressive clinical improvement in many patients (Wolchok et al., 2017). Their presumed mechanism of action is the reversal of the exhaustion phenotype in tumour-infiltrating T cells reactive to tumour-associated antigens, which have become unresponsive in the immunosuppressive microenvironment of the tumours. Since T cell exhaustion is also a major hurdle in chronic viral infection, checkpoint inhibitors have also been suggested and shown pre-clinically to be beneficial in this context (Saeidi et al., 2018; Wang et al., 2019). Therefore, it is not surprising that the investigation of many other T cell co-inhibitory and also co-

stimulatory molecules as targets for clinical intervention is underway (Berman et al., 2015; Sanmamed et al., 2015).

However, manipulating the balance of the natural immune regulatory mechanisms is not without drawbacks. A large proportion of patients do not respond to currently available checkpoint inhibitor therapies, suggesting the need for alternative targets or combination therapies to cover a broader range of cohorts. Moreover, checkpoint inhibitors cause immune-related adverse effects in many patients (Wolchok et al., 2017). These sometimes severe symptoms of auto-immunity also hamper the development of further antibodies targeting T cell co-signalling molecules as potential drugs (Sanmamed et al., 2019; Sznol et al., 2008), narrowing the therapeutic window and limiting clinical efficacy significantly, emphasising the need for more sophisticated strategies.

Incidentally, agonistic antibodies against co-stimulatory receptors were found to have unexpected or unintuitive effects during pre-clinical and clinical investigation in many cases, demonstrating the glaring gaps in our understanding of T cell co-signalling. A prominent example was the CD28 super-agonist TGN1412 which caused life-threatening cytokine release syndrome in a phase-I clinical trial in 2006 at doses which were thought to be harmless when extrapolated from pre-clinical data (Hünig, 2016). Later investigations found this to be due to human effector memory T cells expressing CD28, which was not the case for the non-human primate counterpart. Interestingly, the CD28 super-agonist has been reintroduced as an immunosuppressant, as it was found to preferentially stimulate T_{reg}s when given at low doses. T_{reg}s also express high levels of TNFR family co-stimulatory molecules, and antibodies originally designed as agonists to

these receptors were often found to exert their immunostimulatory function in fact primarily through depletion of these regulatory T cells, although recent insights might enable the engineering of antibodies with dual function, capable of both depleting T_{reg}s and stimulating conventional T cells (Buchan et al., 2018; Bulliard et al., 2014).

At the current standpoint, it is thus clear that further advances in the field of T cell co-signalling molecules can have vast clinical potential. Despite the already available wealth of biochemical data, our understanding of co-stimulatory and co-inhibitory receptors has not gone very far beyond this binary classification, and the development of translational applications is still fundamentally based on a trial-and-error approach in various *in vitro* and *in vivo* models. While knowledge of expression patterns and the pathways engaged by T cell co-signalling receptors can certainly help us extrapolate qualitative effects (such as effects on gene expression, cell survival and proliferation in particular T cell subsets), the sheer complexity of T cell signalling only allows for very limited prediction of quantitative properties of co-signalling (Chen and Flies, 2013). These include the extent to which co-signalling through a particular receptor is able to modulate the magnitude of a T cell response, e.g. through altering rates, sensitivities and durations/timing of effector functions. Especially for the intelligent design of combination therapies to maximise efficacy at well-tolerated doses, additional quantitative data, ideally in the form of predictive models, would be useful. Therefore, this thesis is intended to provide an example of such a quantitative study with a focus on co-stimulatory receptors of the TNFR superfamily.

1.5. Quantitative modelling of T cell signalling

Models are verbal, graphical or mathematical constructs generated as a simplified representation of a subject of interest. As an integral component of the scientific method, they can be used to define and communicate our understanding of "observed phenomena" (according to John von Neumann, 1955). Contrary to common misconception, the power of a model is not measured by its level of detail, but its applicability and predictive capacity. As a good example, the Lotka-Volterra predator-prey model (a cornerstone of mathematical biology) reduces the properties of two animal species of interest to dependency on food supply, and rates of reproduction and predation (Volterra, 1928). Despite the gross simplification, the model can faithfully reproduce the dynamics of two interacting populations under a reasonable set of assumptions.

Similarly, in the context of the intricate network of T cell signalling in conjunction with the abundance of reported molecular interactions in the literature, it is tempting to include as many of these components in a "grand unified model". However, such attempts to model T cell activation and co-stimulation in the past have not yielded very useful quantitative predictions (Konstorum et al., 2019; Lee et al., 2003). The main reason for this is the sheer number of parameters (e.g. protein expression levels, binding and catalytic rates, etc.) that have to be either reliably estimated or over-simplified, as it is often unfeasible to measure them experimentally with sufficient precision. The resulting uncertainty of any possible simulation using these models reduces their applicability greatly.

This is why we decided to use an alternative approach, known as phenotypic modelling (Lever et al., 2014, 2016; Proulx-Giraldeau et al., 2017). Instead of building a high-complexity molecular model based on the literature, we characterise quantitative phenotypes experimentally, which we then use to calibrate a model with the simplest possible architecture. More precisely, by stimulating T cells with a defined input (e.g. a quantifiable dose-range of pMHC with known binding parameters), we can observe and measure the resulting T cell phenotypes (for example as changes in cell surface receptor expression and functionally relevant outputs such as the production of cytokines). With this information, we can systematically derive the minimal set of processes necessary to faithfully reproduce the input-output relationship. In other words, we construct a model to helps us understand the decision-making process and its underlying rules which the T cell employs to convert cell-extrinsic signals into its response.

We have shown an example of this method previously in a study of the early cytokine response of *in vitro*-expanded primary human $CD8^+$ T cells to pMHC, where we observed a universal shutdown of cytokine production after 4-8 hours despite the constant presence of cognate pMHC (Trendel et al., 2019). This was reminiscent of adaptation in other cellular systems, where downregulation or inactivation of the receptor converts a constant input into a transient response. Interestingly, we were also able to reproduce this phenotype in a simple model solely based on the observed TCR downregulation and a threshold switch (Fig. 1.1), suggesting the possibility of an additional, rapid T cell regulatory mechanism distinct from anergy and exhaustion. This process of adaptation can potentially

tune the threshold for activation of T cells in the periphery and render them co-stimulation dependent.

Naturally, due to its simplicity, this model cannot be directly compared to molecular networks, which are often used to visualise signal transduction pathways. Instead, the components of this model, such as the threshold switch, are abstract representations of the net function of signalling modules, which can potentially comprise interactions of numerous signalling proteins. While this model is thus unable to predict the changes caused by modulation of particular signalling proteins, it is still sufficient to reproduce the functional outcomes of T cell stimulation with pMHC. Furthermore, its relatively few free parameters can be calibrated to available experimental data in order to then simulate T cell responses to different inputs, e.g. variations in pMHC dose and TCR binding affinities. Such predictions can then be formulated into hypotheses which can be tested experimentally for further insights.

Moreover, this model can be extended upon to include T cell co-stimulation in order to gain a deeper understanding of TCR signalling modulation by co-signalling receptors, which will be demonstrated in Chapters 3 and 4.

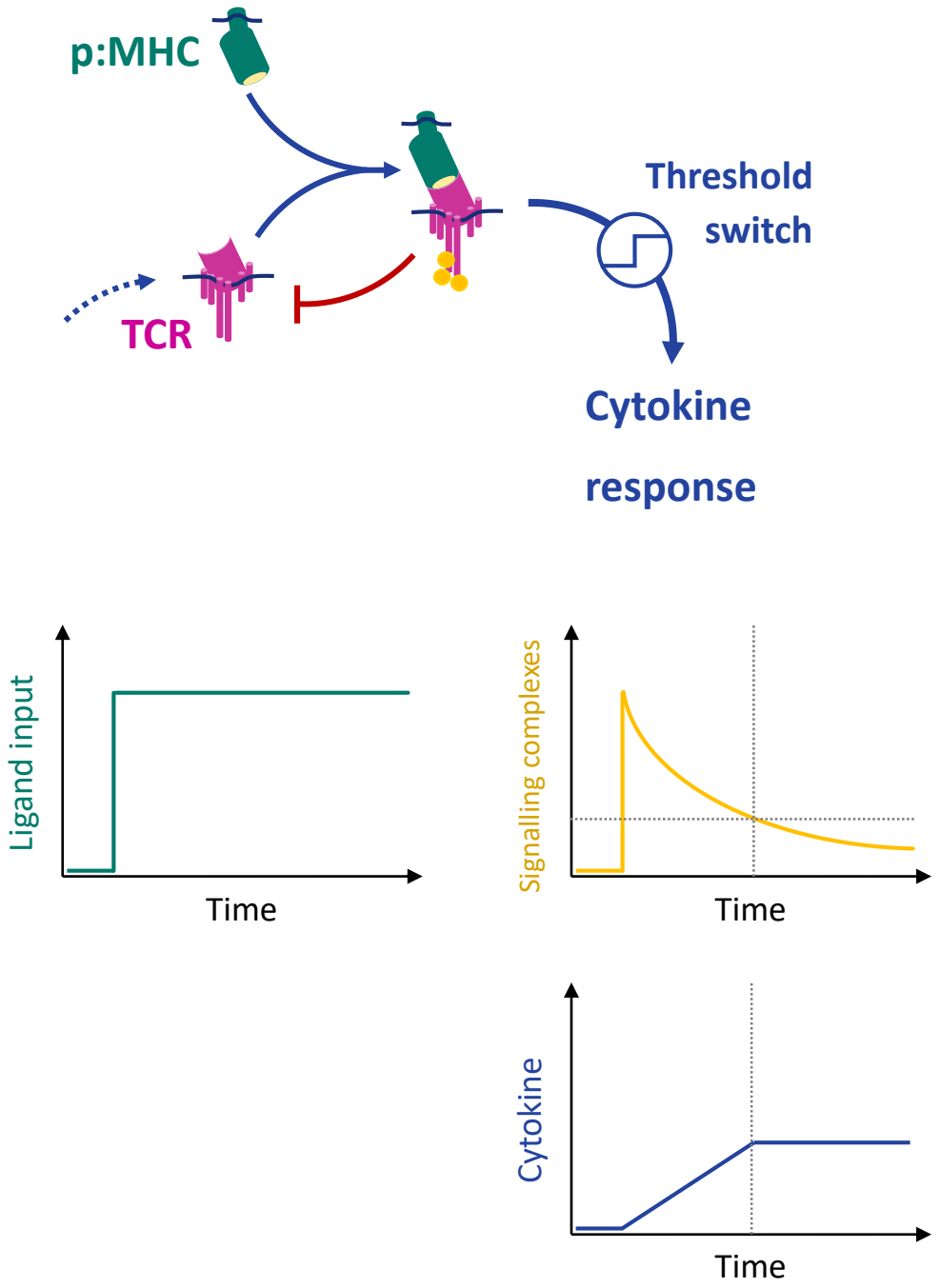

Figure 1.1: Schematic of a phenotypic model of T cell activation and adaptation, modified from Trendel & Kruger et al. (2019). T cell receptor (TCR) and peptide-major histocompatibility complex (pMHC) form a receptor-ligand complex that induces the cytokine response, gated by a threshold switch. At the same time, ligand binding causes downregulation of the TCR. As a result, downregulation of the TCR will reach a point where the amount of signalling complexes is insufficient to overcome the activation threshold, and the cells cease to produce cytokine despite continuous presence of pMHC ligand.

Chapter 2: The phenotype of $CD8^+$ T cell co-stimulation through members of the TNF receptor superfamily

2.1. T cell co-stimulatory receptors of the TNF receptor superfamily

The majority of co-stimulatory receptors belong to either the immunoglobulin superfamily (IgSF) or the tumour necrosis factor receptor superfamily (TNFRSF), the most prominent members of which are found in the Type V (or divergent) subfamily, which includes the receptors 4-1BB, CD70, GITR and OX40 (Chen and Flies, 2013). These have been characterised as glycoproteins with extracellular cysteine-rich domains (CRDs), expressed as monomers or dimers on the cell surface (van Lier et al., 1987; Pollok et al., 1993). Upon binding to their trimeric ligands of the TNF superfamily, they form trimers and multimers of trimers, a process which is generally accepted as the main triggering mechanism.

Signalling is initiated by the recruitment of TNF receptor-associated factors (TRAFs) to the intracellular tails of the trimerised receptors (Zapata et al., 2018), potentially leading to the formation of extensive signalosomes which strongly activate transcription factors of the NFκB family (via canonical and non-canonical NFκB pathways) and can also engage the ERK, JNK and p38 MAPK pathways. Involvement of the PI3K-AKT axis has been suggested (So et al., 2011a), although this is likely to be indirect or in conjunction with other signalling cascades.

Activation of these common pathways generally results in enhancement of T cell growth, survival and effector functions by TNFRSF-mediated co-stimulation. Many qualitative biological functions of TNFRSF members indeed become apparent with the available biochemical literature: MAPK and AKT activity affect cell metabolism

and the expression of cell cycle-related proteins such as cyclin D and thus stimulate proliferation (Lavoie et al., 1996; Muise-Helmericks et al., 1998), while NFκB signalling, amongst other pleiotropic effects, induces anti-apoptotic survival factors such as Bcl-2 and Bcl-x_L (Khoshnan et al., 2000; Lee et al., 2002). However, despite the shared similarities in molecular mechanisms, different TNFRSF members can display discrepancies in biological roles (Croft, 2003; Hendriks et al., 2005).

4-1BB (also known as CD137 and TNFRSF9) mediates signalling mainly through TRAF1 and 2 homo- and heterotrimers (Arch and Thompson, 1998; Saoulli et al., 1998; Zheng et al., 2010). It is known to be expressed transiently on activated $CD4^+$ and $CD8^+$ T cells, whereas its ligand 4-1BBL (TNFSF9) is found on activated professional APCs (DCs, macrophages, B cells) (Alderson et al., 1994; Pollok et al., 1994). Interestingly, 4-1BBL is more highly expressed on monocyte-derived inflammatory dendritic cells compared to conventional dendritic cells in lymphoid tissues (Chang et al., 2017; Hendriks et al., 2005). These expression patterns suggest a role of 4-1BB predominantly during the effector response in the periphery rather than initial priming of T cells. Indeed, 4-1BB co-stimulation has been shown *in vitro* and in murine models to have positive effects on T cell clonal expansion, survival & memory (Giardino Torchia et al., 2015; Lee et al., 2002), as well as the cytokine response and tumour clearance (Saoulli et al., 1998; Vinay and Kwon, 2012). In the context of cellular immunotherapy, 4-1BB also confers enhanced persistence of adoptively transferred T cells and resistance to anergy and exhaustion (Long et al., 2015; Wilcox et al., 2004; Zhao et al., 2015).

CD27 (TNFRSF7) signals predominantly through TRAF2 and 5 (Akiba et al., 1998). In contrast to 4-1BB, it appears to be constitutively expressed on $CD4^+$ and $CD8^+$ T cells, and is absent on terminally differentiated T cells (Hendriks et al., 2003; Romero et al., 2007). However, its ligand CD70 (also known as CD27L and TNFSF7) is tightly regulated and found on activated professional APCs, but also others such as activated NK and T cells, and non-hematopoietic cell types where its physiological relevance is unknown (Kashii et al., 1999; Krause et al., 2009; Seko et al., 2002). Unlike other TNFSF members, CD70 is also expressed by some conventional DCs (cDC1) at high levels (Chang et al., 2017). Together with the expression pattern of CD27, this indicates the additional ability of CD27 co-stimulation to act early during the T cell response, e.g. the priming of naïve T cells. In viral infection models this has been shown, where CD27 co-stimulation appears to broaden the TCR repertoire by including lower-affinity T cell clones in the response (van Gisbergen et al., 2011). The importance and non-redundancy of CD27 for the mounting and maintenance of the effector T cell response is illustrated by cases of human CD27 or CD70 deficiency, where patients typically struggle with the control of EBV (Izawa et al., 2017). In direct comparison in a murine vaccination model, CD27 co-stimulation has been shown to drive T cells into a proliferative effector phenotype, whereas 4-1BB co-stimulation resulted in superior long-lived memory formation.

GITR (glucocorticoid-induced TNFR-related, also AITR, CD357 or TNFRSF18) and **OX40** (also known as CD134 or TNFRSF4) signal through TRAF2 and 5 (Kawamata et al., 1998; Snell et al., 2010) and are induced on activated T cells similarly to 4-1BB, while their ligands GITRL (AITRL, TNFSF18) and OX40L

(CD252, TNFSF4) are found on similar APC populations as 4-1BBL (Chang et al., 2017). They are reported to preferentially co-stimulate $CD4^+$ T cells during the effector response, with effects on effector $CD8^+$ T cells potentially being indirect (Clouthier et al., 2015; Serghides et al., 2005; Yu et al., 2006), whereas 4-1BB shows a bias towards $CD8^+$ T cells (Shuford et al., 1997; Takahashi et al., 1999). However, GITR appears to play an important role in the maintenance and persistence of $CD8^+$ memory T cell in mouse models, in conjunction with 4-1BB (Lin et al., 2013; Snell et al., 2012).

Receptor	Main signalling adapters	Receptor expression on conventional T cells	Ligand	Ligand expression
4-1BB	TRAF1 and TRAF2	Activation-induced	4-1BBL	Highly expressed on activated inflammatory monocyte-derived DCs (moDCs), at lower levels also on activated conventional DCs (cDCs), macrophages, B and T cells
GITR	TRAF2 and TRAF5		GITRL	
OX40			OX40L	
CD27		Constitutive, is lost on terminally differentiated effectors	CD70	Highly expressed on activated moDCs and cDC1, at lower levels also on activated cDC2, macrophages, B, T and NK cells

Table 2.1: Summary of selected TNFR superfamily members, their adapters, ligands and expression patterns.

As summarised in Table 2.1, disparities between TNFRSF members can likely be attributed to differences in expression pattern and time of action in the life of a T cell, rather than fundamental qualitative differences, since their reported signalling pathways are highly similar, resulting in improved T cell proliferation, function and survival. However, how co-stimulation through TNFRSF members interacts with TCR signalling, and chiefly, how these co-signalling receptors affect the T cell effector response quantitatively remains poorly understood. For example, increases in the magnitude of a T cell response could potentially arise through either

1. increases in intensity of response (e.g. cytokine production rate per single cell)
2. enhancement of T cell sensitivity to pMHC (allowing for effective responses particularly to low antigen doses)
3. or temporal prolongation of otherwise transient responses (i.e. prevention and rescue of T cells from states of unresponsiveness, see also Fig. 2.1).

This chapter focuses on collecting the data necessary to determine which of these (or combinations of these) features are exhibited by co-stimulation through TNFRSF members, as well as to assess potential quantitative differences between these receptors.

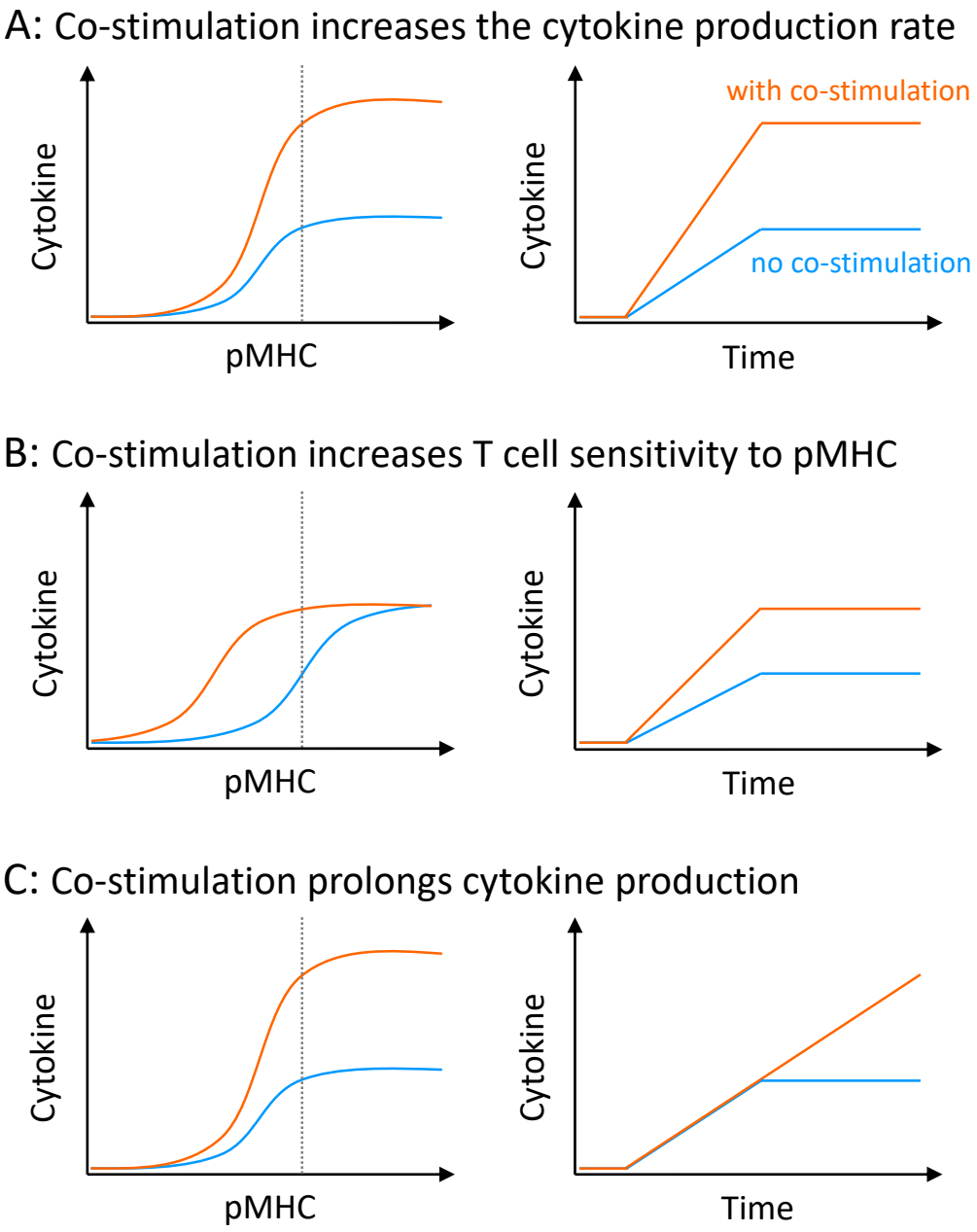

Figure 2.1: Potential quantitative effects of co-stimulation on the effector T cell response. Simplified schematic of three quantitatively different effects of T cell co-stimulation on the cytokine response, shown as dose-response at the endpoint, and time course at the pMHC dose indicated by the dotted line. The response to pMHC without co-stimulation is assumed to be transient, as shown in (Trendel et al., 2019).

2.2. A quantitative study of T cell co-stimulation through TNFRSF members – experimental design

For the purposes of this study, a previously published *in vitro* T cell stimulation system was employed where primary human $CD8^+$ T cells were lentivirally transduced with the c58/c61 TCR and stimulated with plate-immobilised recombinant pMHC (Lever et al., 2016; Trendel et al., 2019). Of the available library of peptide ligands spanning six orders of magnitude in affinity, the M4A-Q8K-C9V mutant of the NY-ESO-$1_{157\text{-}165}$ peptide in complex with HLA-A2 was chosen as a pMHC with a physiologically relevant affinity to the TCR (K_D = 7.23 µM (Trendel et al., 2019)).

In order to capture effects at sub-optimal pMHC doses as well as high doses that already induce good responses without co-stimulation, the plate layout was designed to cover more than one order of magnitude of pMHC doses above and below the expected EC_{50}. In addition, multiple doses of co-stimulatory ligand were used to observe and confirm titrating effects. Appropriate ranges of doses were determined in prototype co-stimulation experiments where saturation of the co-stimulatory effect was observed (see Methods Figure 6.2 for plate layout). To ensure functional activity for the duration of the experiment when immobilised on the plates, stabilised trimers of recombinant ligands to the respective co-stimulatory receptors were produced as described by Wajant and colleagues (Wyzgol et al., 2009), summarised in Methods Sections 6.2. and 6.3 (see also Fig. 6.1).

As time points, 4, 8, 16 and 24 hours were chosen, since we previously found that T cell adaptation sets in within 4-8 hours. We did not attempt to go beyond 24 hours, so as not to be confounded with effects on T cell proliferation and survival, because our primary aim was first and foremost to characterise how effector functions are modulated. Production of the cytokines IFN-γ, IL-2, TNF was measured as effector function, as well as surface receptors including TCR, CD27 and 4-1BB. The raw data sets and experimental repeats can be found as dose-response plots in the appendix (Supplementary Figures S.1-S.6).

2.3. Results

2.3.1. 4-1BB co-stimulation prevents T cell adaptation

At first glance, the raw data (Supplementary Figures S.1-S.2) suggest that 4-1BB-costimulation hardly affects the T cell cytokine response at the earlier time points, in comparison to the sizable boost in cytokine produced at 16 and 24 hours with increasing amounts of 4-1BBL added. For better visualisation, measured cytokine levels were plotted as function of time (Fig. 2.2A) for one representative experiment, where it becomes apparent that the previously described adaptation phenotype of cytokine production (in absence of co-stimulation) is completely prevented at all doses of pMHC when the T cells are presented with a sufficient amount of 4-1BBL, resulting in the pronounced increase of cytokines especially at later time points.

In order to demonstrate the titratable nature of this 4-1BB co-stimulation effect and to perform statistical analysis, the data sets were simplified by fitting the pMHC dose-response curves and extracting the E_{max} (peak cytokine response) and EC_{50} (pMHC dose at which the elicited cytokine response is 50% of the E_{max}) from the fits for each time point and 4-1BBL dose (as described in Methods Section 6.6. and Fig. 6.3). Fig. 2.2B shows the normalised E_{max} for each time point and 4-1BBL dose, averaged from three independent experimental repeats, whereas the E_{max} values at 4 hours for pMHC alone or with the highest 4-1BBL dose were directly compared in Fig. 2.2D. The adaptation phenotype in the absence of co-stimulation was reproducible, with IFN-γ levels staying constant after 8 hours (2.2B). In the

case of IL-2 and TNF, however, the measured cytokine apparently decreased after adaptation, likely due to decay and/or consumption of these soluble mediators by the T cells. While the effects of 4-1BB were negligible at 4 hours (Fig. 2.2D), the cytokine response was rescued from adaptation in presence of increasing amounts of 4-1BBL in a dose-dependent manner (Fig. 2.2B).

The F-test was chosen to statistically evaluate these phenotypic changes. When two different models (e.g. simple linear models) are fit to a set of data points, an F-test is commonly performed to determine whether one model fits the data significantly better than the other. In this case, linear functions were fit to the time series of E_{max} values for each 4-1BBL dose, starting from 8 hours (i.e. after adaptation without co-stimulation). The slope of these functions would be an estimate of the average cytokine production rate between 8 and 24 hours. These fits were tested in an F-test against the alternative model (null hypothesis) of a linear function with the slope of the condition without co-stimulation in order to assess whether co-stimulation affects cytokine production post-adaptation (Fig. 2.2C). For 4-1BBL doses above 100ng/well, this test shows that the cytokine production rates were significantly different from the condition without 4-1BBL (F-test p-value < 0.05), confirming that sufficient 4-1BB co-stimulation prevented adaptation for all three cytokines measured.

To summarise, we found that T cell co-stimulation through 4-1BB boosts the amount of cytokines produced mainly by prolonging the response, which in the absence of co-stimulation is very transient and typically adapts within 4 to 8 hours.

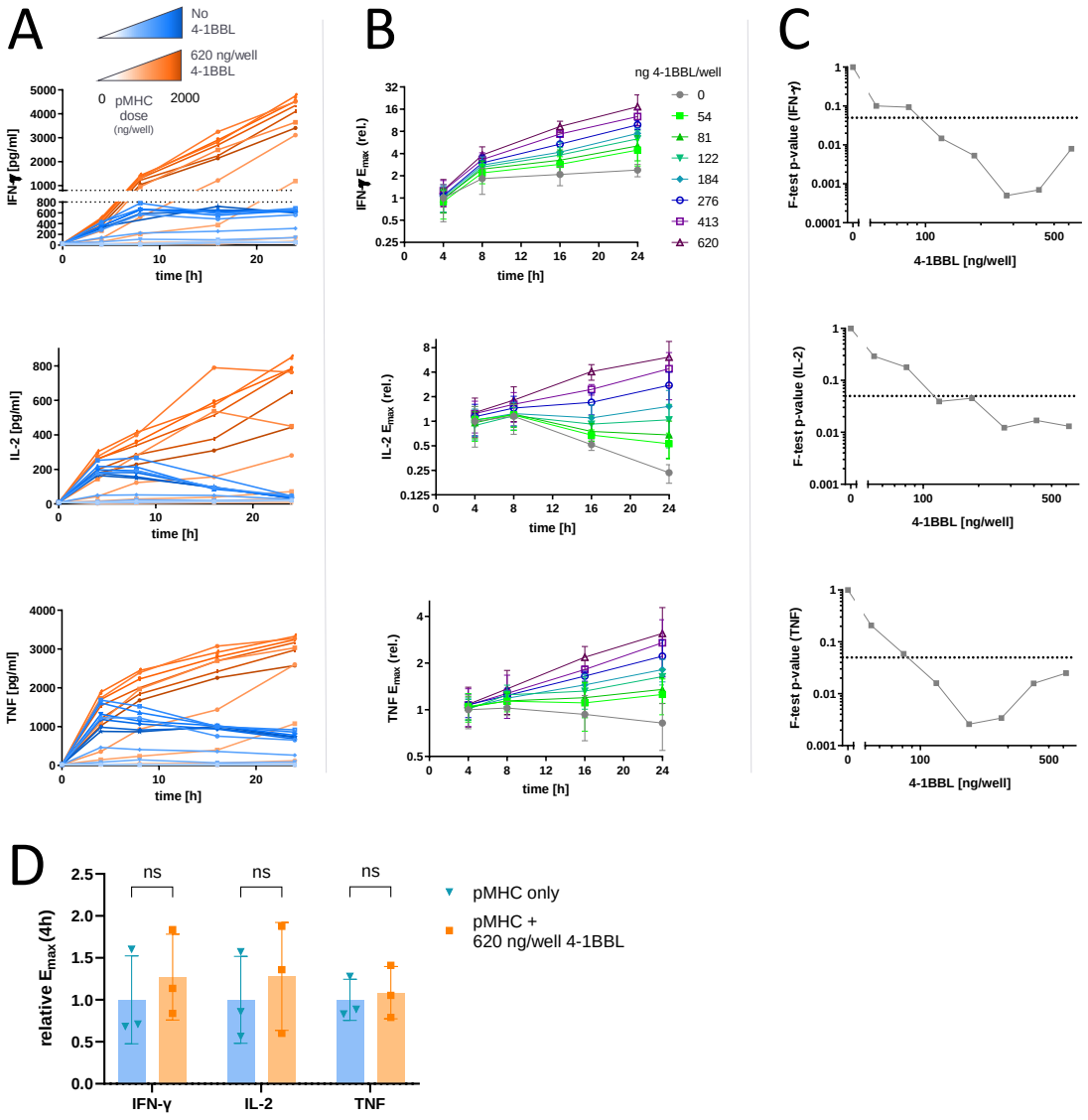

Figure 2.2: Co-stimulation through 4-1BB prevents adaptation of T cell cytokine production. Primary human CD8$^+$ T cells transduced with the c58/c61 TCR were stimulated for 4, 8, 16 and 24 hours with pMHC, with or without 4-1BBL, at the indicated doses. The production of the cytokines IFN-γ, IL-2 and TNF into the culture medium supernatant was quantified by ELISA. **(A)** Time course of measured supernatant cytokines in the absence (blue) or presence (orange) of 4-1BBL from one representative experiment. The colour shades represent the pMHC doses ranging from 0 (brightest) to 2000 ng/well (darkest). **(B)** E_{max} values from three separate experimental repeats were extracted from dose-response curve fits, normalised to the means of each individual experiment and plotted as fold change relative to the cytokine produced without co-stimulation at the 4 h time point. **(C)** To quantify adaptation, datasets from (B) (excluding the 4 h time point) were fit using linear functions and the slopes tested against the condition without co-stimulation in an F-test. The dotted line indicates a p-value of 0.05. **(D)** Normalised E_{max} values at 4 hours were plotted as fold-change of the condition without co-stimulation. E_{max} for pMHC with and without 4-1BBL were compared using paired two-tailed t-tests. Abbreviations: ns (not significant) = p-value > 0.05. All statistical analyses were performed in GraphPad Prism 8.

2.3.2. CD27 co-stimulation is unable to prevent T cell adaptation

A similar analysis of CD27 revealed a surprisingly different phenotype compared to the related receptor 4-1BB. The time courses of cytokine levels (Fig. 2.3A) after stimulation of $CD8^+$ T cells with pMHC in absence or presence of CD70 showed that CD27 co-stimulation mainly boosted cytokine production at the earlier time points (4 and 8 hours) without preventing adaptation at later stages. In the representative experiment shown, adaptation appeared to be slightly delayed for IL-2 and TNF, as the cytokine levels continued to rise between 4 and 8 hours when CD70 was added, while they began to decrease in absence of co-stimulation at all pMHC doses. However, the time courses of averaged E_{max} values extracted from three experimental repeats suggested that this trend may not be consistently reproducible (Fig. 2.3B).

Statistical analysis as in Section 2.3.1., by estimating the post-adaptation cytokine production rates as slopes of linear fits to the E_{max} time courses from 8 hours onwards, confirmed that the T cell adaptation behaviour remained unaffected by CD27 co-stimulation, as the slopes did not significantly differ regardless of CD70 dose (Fig. 2.3C), and that it is predominantly the early cytokine production that was boosted by CD27 co-stimulation (Fig. 2.3D).

In conclusion, contrary to 4-1BB, co-stimulation through CD27 in our experimental system mainly led to increased cytokine production within the first few hours of the response, while it could not prevent T cell adaptation.

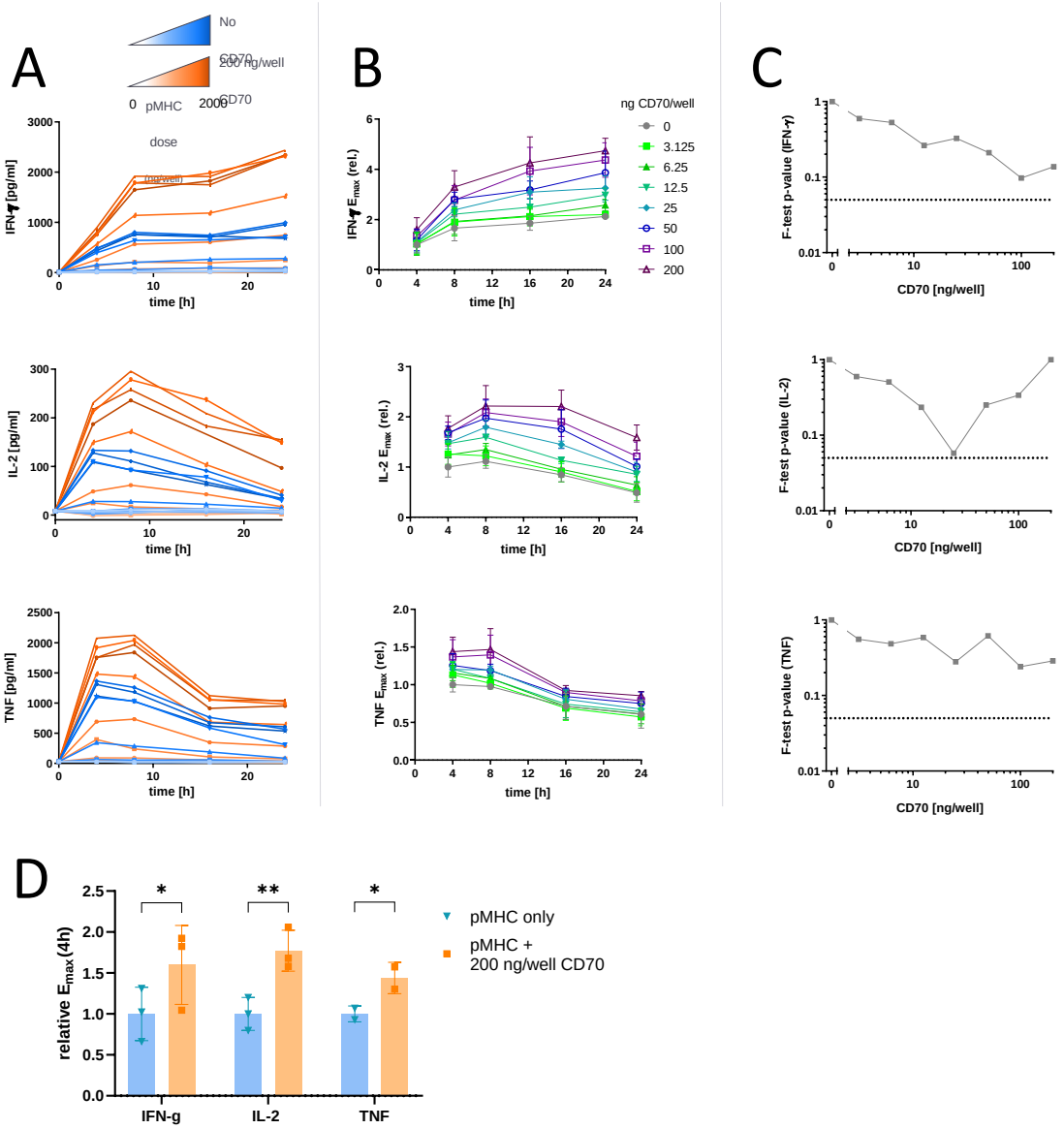

Figure 2.3: Co-stimulation through CD27 does not prevent adaptation of T cell cytokine production. Primary human CD8⁺ T cells transduced with the c58/c61 TCR were stimulated for 4, 8, 16 and 24 hours with pMHC, with or without CD70, at the indicated doses. The production of the cytokines IFN-γ, IL-2 and TNF into the culture medium supernatant was quantified by ELISA. **(A)** Time course of measured supernatant cytokines in the absence (blue) or presence (orange) of CD70 from one representative experiment. The colour shades represent the pMHC doses ranging from 0 (brightest) to 2000 ng/well (darkest). **(B)** E_{max} values from three separate experimental repeats were extracted from dose-response curve fits, normalised to the means of each individual experiment and plotted as fold change relative to the cytokine produced without co-stimulation at the 4 h time point. **(C)** To quantify adaptation, datasets from (B) (excluding the 4 h time point) were fit using linear functions and the slopes tested against the condition without co-stimulation in an F-test. The dotted line indicates a p-value of 0.05. **(D)** Normalised E_{max} values at 4 hours were plotted as fold-change of the condition without co-stimulation. E_{max} for pMHC with and without CD70 were compared using paired two-tailed t-tests. Abbreviations: ns (not significant) = p-value > 0.05; * = p-value < 0.05; ** = p-value < 0.01. All statistical analyses were performed in GraphPad Prism 8.

2.3.3. Expression of 4-1BB and CD27 is differentially regulated on $CD8^+$ T cells

The literature suggests that divergent phenotypes of 4-1BB and CD27 co-stimulation could be explained by differential expression patterns (see Section 2.1.). Since the T cells used for this series of experiments were also analysed for 4-1BB and CD27 surface expression using flow cytometry, we can confirm that 4-1BB is not expressed on resting T cells and is induced upon activation through the TCR (Fig. 2.4). Surface expression peaked between 8 and 16 hours and appears to be declining afterwards, roughly following the trend of cytokine production in absence of co-stimulation.

CD27, on the other hand, was highly expressed on resting T cells and hardly affected by TCR stimulation, whereas it was rapidly downregulated (within <4 hours) upon engagement of its ligand CD70 (Fig. 2.5A) in a dose-dependent manner (Fig. 2.5B). In the case of 4-1BB, this ligand-induced downregulation appears to be counteracted by its activation-induced upregulation to some extent, as surface expression remained well above baseline even in the presence of high doses of 4-1BBL (Fig. 2.4).

These observations provide plausible explanations as for why 4-1BB co-stimulation is ineffective in the very early cytokine response and sustained during later stages, while CD27 signalling only boosts early cytokine production and disappears later when CD27 is downregulated, unable to stop adaptation.

Interestingly, 4-1BB expression was enhanced by CD27 co-stimulation (Fig. 2.5C and D), which suggests the possibility of a synergy between these receptors.

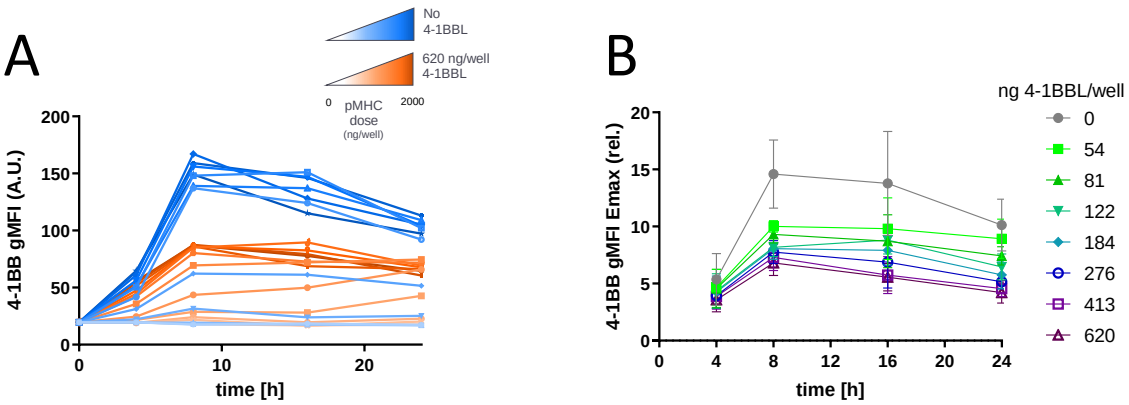

Figure 2.4: 4-1BB expression is induced upon T cell activation and is downregulated by its ligand. Primary human $CD8^+$ T cells transduced with the c58/c61 TCR were stimulated for 4, 8, 16 and 24 hours with pMHC, with or without 4-1BBL, at the indicated doses. Surface 4-1BB was labelled with a fluorescent anti-4-1BB antibody and quantified by flow cytometry. **(A)** Time course of measured surface 4-1BB as geometric mean fluorescence intensity (gMFI) in the absence (blue) or presence (orange) of 4-1BBL from one representative experiment. The colour shades represent the pMHC doses ranging from 0 (brightest) to 2000 ng/well (darkest). **(B)** E_{max} values from three separate experimental repeats were extracted from dose-response curve fits, normalised to the means of each individual experiment and plotted as fold change relative to baseline 4-1BB gMFI before stimulation.

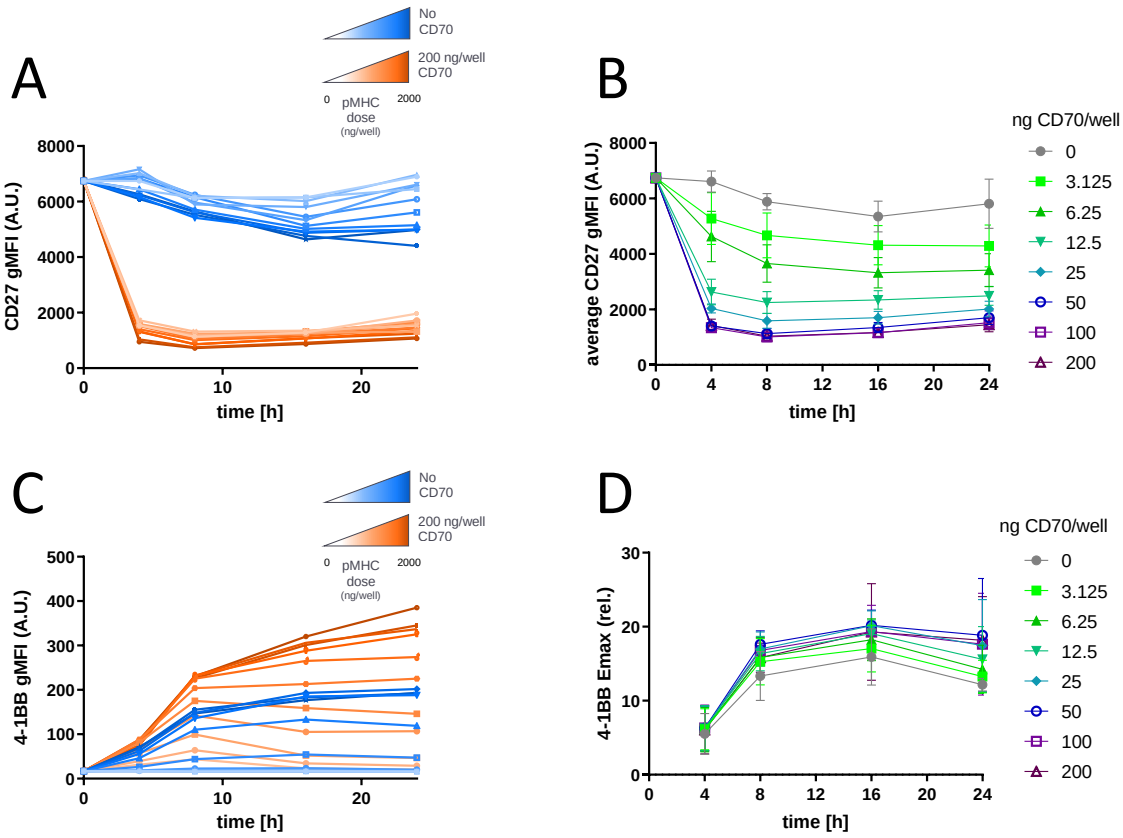

Figure 2.5: CD27 is highly expressed on resting T cells and rapidly downregulated by its ligand. Primary human $CD8^+$ T cells transduced with the c58/c61 TCR were stimulated for 4, 8, 16 and 24 hours with pMHC, with or without CD70, at the indicated doses. Surface CD27 and 4-1BB were labelled with a fluorescent anti-CD27 and anti-4-1BB antibodies and quantified by flow cytometry. **(A)** Time course of measured surface CD27 as geometric mean fluorescence intensity (gMFI) in the absence (blue) or presence (orange) of CD70 from one experiment. The colour shades represent the pMHC doses ranging from 0 (brightest) to 2000 ng/well (darkest). **(B)** Time course of measured surface CD27 as geometric mean fluorescence intensities (gMFI) from the same experiment, averaged across all pMHC doses. Colours represent indicated doses of CD70. **(C)** Time course of measured surface 4-1BB as geometric mean fluorescence intensity (gMFI) in the absence (blue) or presence (orange) of CD70 from one representative experiment. The colour shades represent the pMHC doses ranging from 0 (brightest) to 2000 ng/well (darkest). **(D)** E_{max} values from three separate experimental repeats were extracted from dose-response curve fits, normalised to the means of each individual experiment and plotted as fold change relative to baseline 4-1BB gMFI before stimulation.

2.3.4. TCR downregulation is unaffected by co-stimulation through 4-1BB and CD27

Given the previous study on T cell adaptation conducted by our lab, in which we found that TCR downregulation is sufficient to explain the adaptation of the T cell response, a potential mechanism for 4-1BB co-stimulation to prevent this unresponsive state could be the inhibition of TCR downregulation.

Unfortunately, the flow cytometry staining panel was found to be unsuitable for the analysis of changes in TCR expression (Supplementary Figure S.3). The dynamic range was poor due to the relatively weak fluorophore (AlexaFluor488) conjugated to the pMHC tetramers used for TCR staining. In addition, the signal-to-noise ratio was further decreased by the sensitivity of the detection channel to changes in cell morphology, resulting in an apparent increase in fluorescence when cells respond and grow upon stimulation, and a decrease in fluorescence when cells atrophy in the absence of TCR stimulus and cytokines. Only one 4-1BB co-stimulation data set was collected with an improved staining panel with PE-conjugated pMHC tetramers, which was able to minimise these artefacts.

The initial hypothesis that co-stimulation might sustain cytokine production by impairing TCR downregulation can most likely be rejected based on the available data. On the contrary, slow recovery of TCR expression after 16h in absence of co-stimulation seems to be prevented when 4-1BBL is present (Fig. 2.6A). A possible explanation for this small difference could be that cells detach from the plate surface after downregulating TCR and losing stimulus, allowing for TCR

expression to recover, while 4-1BB-4-1BBL interactions might prevent this either by sustaining the stimulus or physically mediating adhesion.

Changes in the EC_{50} of TCR downregulation in the presence of 4-1BBL were smaller than 2-fold, and indicated an enhancement rather than inhibition of TCR downregulation (Fig. 2.6B). While there are no replicates for this data set per se, there are independent repeats of a prototype experiment where TCR was measured with PE-conjugated tetramers at 8 hours in absence or presence of three doses of 4-1BBL (Fig. 2.6C), showing the same trend of EC_{50} (Fig. 2.6D).

These small reproducible fluctuations can perhaps be explained as artefacts of our plate-based stimulation system without ligands for adhesion proteins. Lower doses of 4-1BBL could mediate a weak adhesion effect (decreasing EC_{50}), while high doses could sterically impair access to pMHC for the TCR (increasing EC_{50}), which we also see when inert biotinylated proteins are co-immobilised on the plates (unpublished data).

An analogous set of experiments showed that TCR downregulation is even less affected by CD27 co-stimulation (Fig. 2.6E and F), although lower doses of CD70 were used here compared to experiments with 4-1BBL.

Taken together, effects on TCR downregulation caused by 4-1BB and CD27 co-stimulation are very small and can likely be ruled out as the main mechanism underlying the phenotypes observed, the identification of which will require a more in-depth approach.

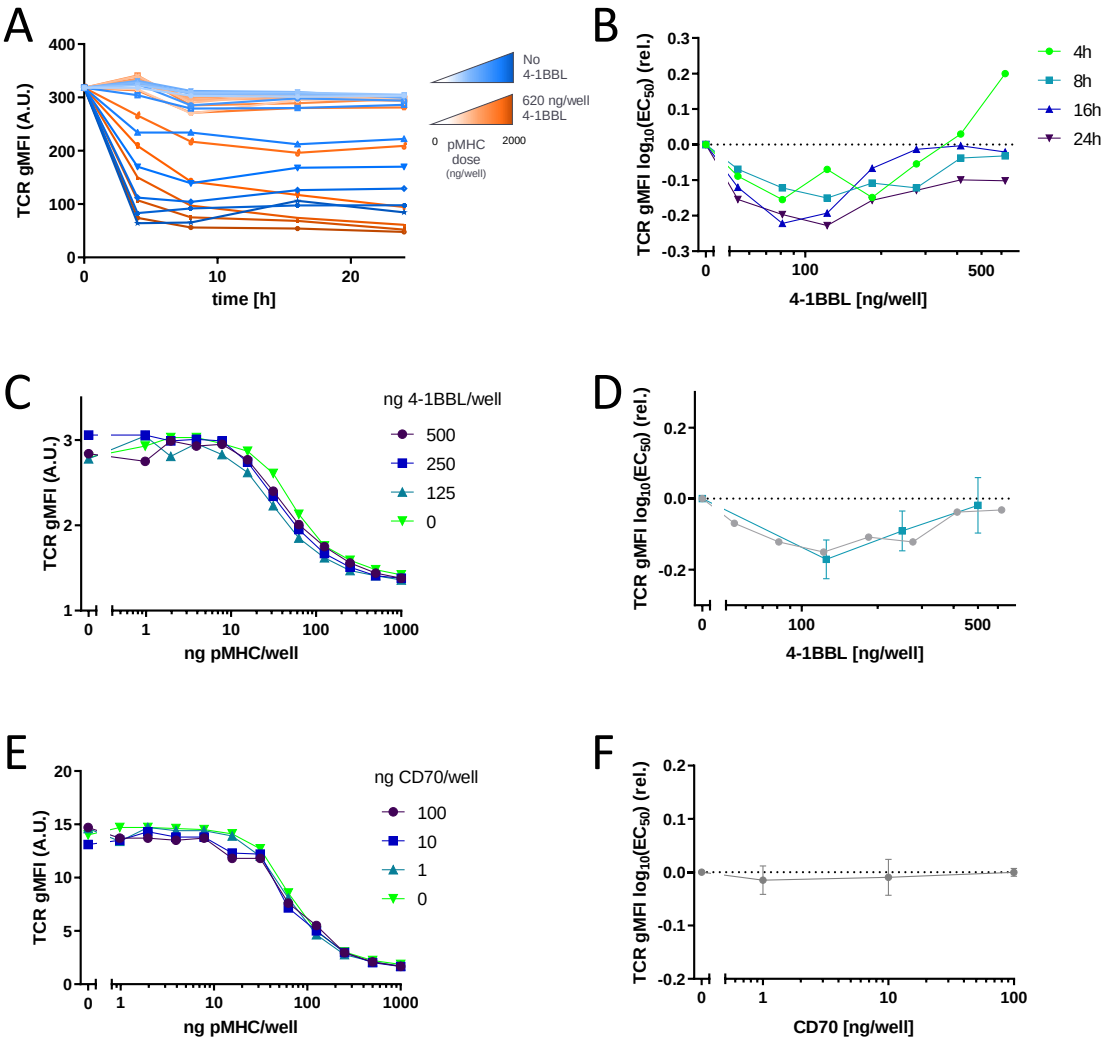

Figure 2.6: 4-1BB and CD27 co-stimulation barely affect TCR downregulation. Primary human CD8$^+$ T cells transduced with the c58/c61 TCR were stimulated with pMHC, either with or without 4-1BBL or CD70 at the indicated doses. Surface TCR was labelled with fluorescent pMHC tetramers and quantified by flow cytometry. **(A)** Time course of measured surface TCR expression as geometric mean fluorescence intensity (gMFI) in the absence (blue) or presence (orange) of 4-1BBL. The colour shades represent the pMHC doses ranging from 0 (brightest) to 2000 ng/well (darkest). **(B)** EC_{50} values were extracted from dose-response curve fits and plotted as fold change relative to the condition without co-stimulation. **(C)** Measured surface TCR expression at 8 hours in the absence or presence of indicated 4-1BBL doses. **(D)** EC_{50} values were extracted from dose-response curve fits of three independent repeats of (C) and plotted as fold change relative to the condition without co-stimulation (blue). The 8 hour time point of (B) is included in grey as comparison. **(E)** Measured surface TCR expression at 8 hours in the absence or presence of indicated CD70 doses. **(F)** EC_{50} values were extracted from dose-response curve fits of three independent repeats of (E) and plotted as fold change relative to the condition without co-stimulation.

2.3.5. Effects of 4-1BB and CD27 on T cell sensitivity are detectable but relatively small

After finding that co-stimulation mainly increases the magnitude of cytokine responses by preventing adaptation in the case of 4-1BB and by boosting the initial cytokine production rate in the case of CD27, we wanted to see whether co-stimulation through these receptors could also enhance T cell sensitivity to pMHC. T cells with improved sensitivity would require lower doses of pMHC to trigger a response, effectively lowering the EC_{50} of dose-response curves.

To determine whether this is the case in the presence of 4-1BB co-stimulation, EC_{50} values were thus extracted from cytokine dose-response curves from the 4-1BB co-stimulation time series and plotted against the 4-1BBL doses used (Fig. 2.7A). Decreases in cytokine EC_{50} remained smaller than 2-fold, although they followed a trend being essentially non-existent at the earliest time point of 4 hours and becoming larger over time, eventually becoming statistically significant at 24 hours (Fig. 2.7B). Interestingly, 4-1BB surface expression behaved similarly, with its EC_{50} decreasing with time and increasing amounts of 4-1BBL added, reaching a maximum decrease of approximately 2.6-fold at 24 hours and the highest 4-1BBL dose (Fig. 2.7A), at which point it became statistically significant (Fig. 2.7B). This change over time for all readouts is consistent with 4-1BB being absent from the surface of resting T cells and being induced over the course of T cell activation.

CD27 co-stimulation, on the other hand, exhibited stronger CD70-dependent EC_{50} decreases at the earliest time point measured (4 hours), when cytokines were

produced with an up to 2.5-fold lower EC_{50} and 4-1BB was expressed with up to 12-fold lower EC_{50} in the presence of CD27 co-stimulation (Fig. 2.8A). This trend became weaker with later time points, in line with the downregulation of CD27, and with it the disappearance of its co-stimulatory effect. However, the EC_{50} decrease remained statistically significant for IFN-γ and TNF (Fig. 2.8B). Despite the statistical significance, the biological relevance of such small changes remains questionable in the context of adhesion proteins, as will be discussed in Section 2.4.1.

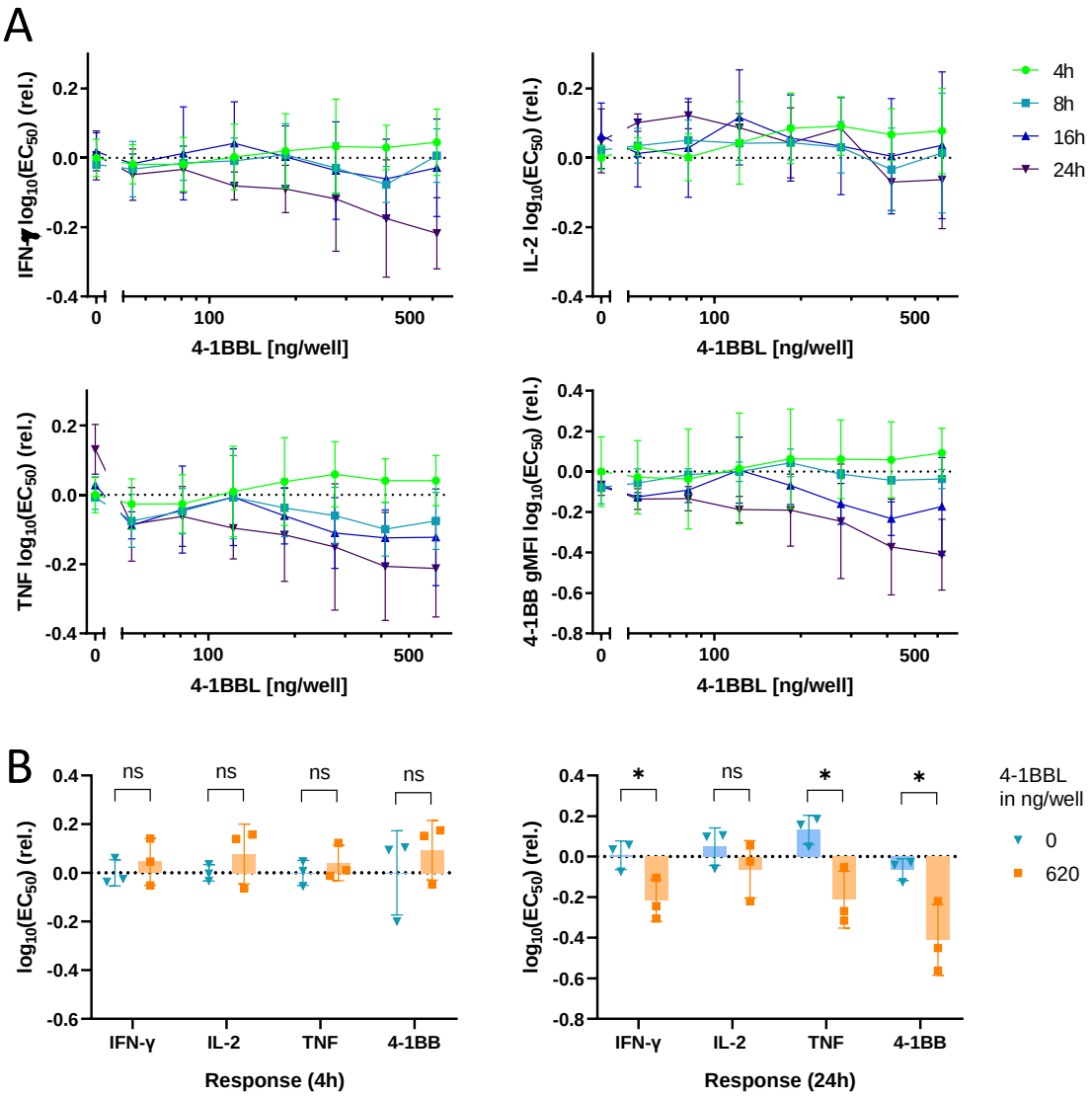

Figure 2.7: A slight increase in T cell sensitivity is observed at later time points with 4-1BB co-stimulation. Primary human $CD8^+$ T cells transduced with the c58/c61 TCR were stimulated for 4, 8, 16 and 24 hours with pMHC, with or without 4-1BBL, at the indicated doses. The production of the cytokines IFN-γ, IL-2 and TNF into the culture medium supernatant was quantified by ELISA. Surface 4-1BB was labelled with a fluorescent anti-4-1BB antibody and quantified by flow cytometry. **(A)** EC_{50} values from three separate experimental repeats were extracted from dose-response curve fits, normalised to the means of each individual experiment and plotted as log_{10}(fold change) relative to the 4 h time point without co-stimulation. **(B)** To quantify statistically significant effects on sensitivity, EC_{50} values at 4 or 24 hours were compared with two-tailed t-tests between the conditions without and with 620ng/well 4-1BBL. This statistical analysis was performed in GraphPad Prism 8. Abbreviations: ns (not significant) = p-value > 0.05; * = p-value < 0.05

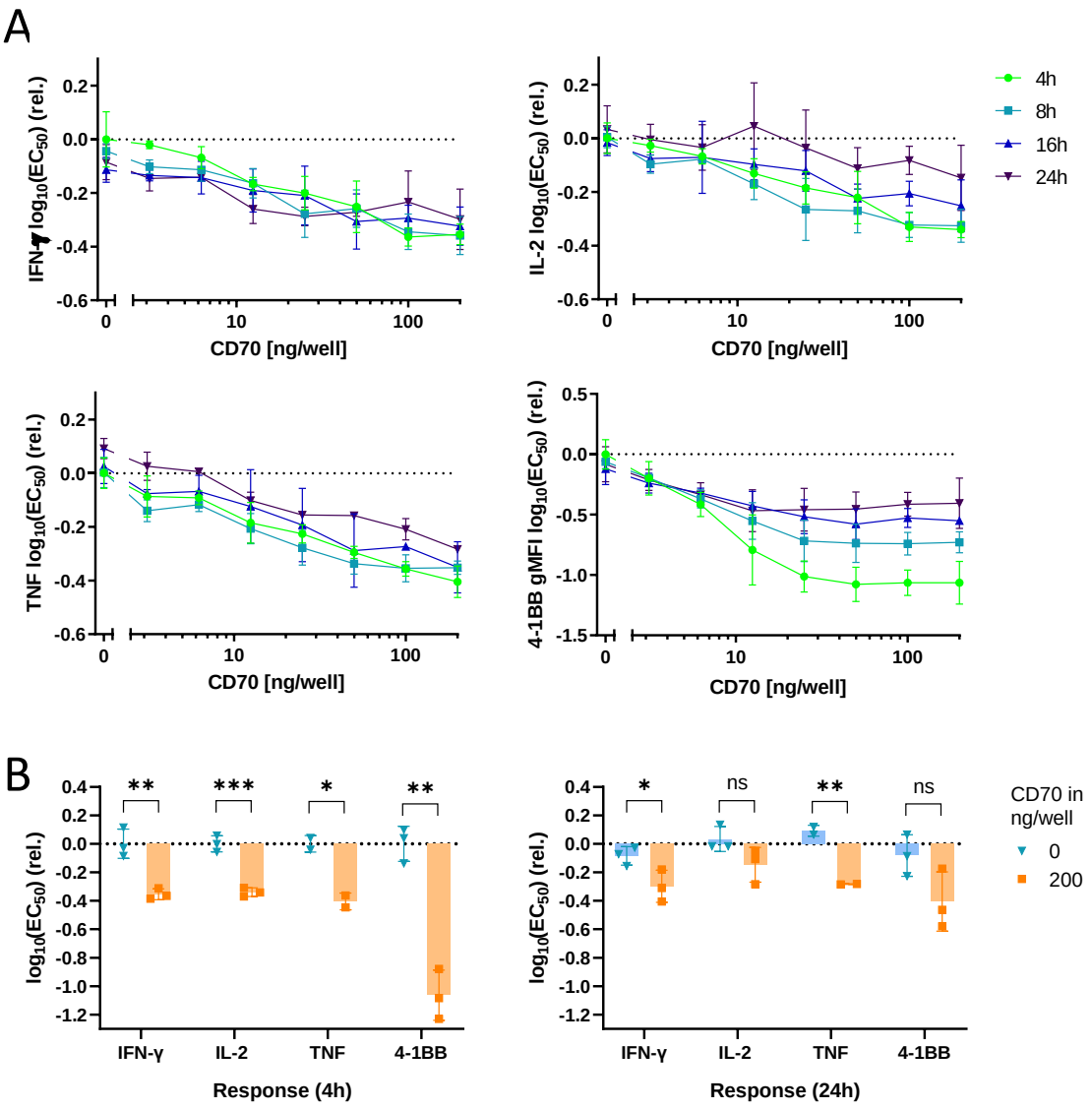

Figure 2.8: CD27 co-stimulation slightly increases T cell sensitivity. Primary human CD8⁺ T cells transduced with the c58/c61 TCR were stimulated for 4, 8, 16 and 24 hours with pMHC, with or without CD70, at the indicated doses. The production of the cytokines IFN-γ, IL-2 and TNF into the culture medium supernatant was quantified by ELISA. Surface 4-1BB was labelled with a fluorescent anti-4-1BB antibody and quantified by flow cytometry. **(A)** EC_{50} values from three separate experimental repeats were extracted from dose-response curve fits, normalised to the means of each individual experiment and plotted as log_{10}(fold change) relative to the 4 h time point without co-stimulation. **(B)** To quantify statistically significant effects on sensitivity, EC_{50} values at 4 or 24 hours were compared with two-tailed t-tests between the conditions without and with 200ng/well CD70. This statistical analysis was performed in GraphPad Prism 8. Abbreviations: ns (not significant) = p-value > 0.05; * = p-value < 0.05; ** = p-value < 0.01; *** = p-value < 0.001

2.3.6. Expression of GITR and OX40 is inducible but weak on CD8+ T cells

With the previous results indicating that timing and levels of expression are crucial for the function of co-stimulatory receptors, and the literature suggesting that GITR and OX40 co-stimulation affect primarily CD4+ T cells rather than the CD8+ T cells which our experimental system is based on (Clouthier et al., 2015; Yu et al., 2006), we first sought to compare the expression of these two receptors on CD4+ and CD8+ T cells. For this purpose, CD4+ and CD8+ T cells were separately isolated and expanded *in vitro* with our usual protocol, excluding lentiviral transduction.

Polyclonal stimulation with plate-immobilised anti-CD3 antibodies overnight (Fig. 2.9) showed that GITR and OX40 are induced on T cells upon activation, while they are largely absent from resting T cells, with only a small fraction of unstimulated cells expressing intermediate levels of GITR. Most importantly, these receptors are more strongly upregulated on CD4+ T cells, with OX40 expression being barely above baseline for stimulated CD8+ T cells. Considering the comparatively high expression levels of 4-1BB and CD27 which we previously focused on, co-stimulatory effects through GITR and especially OX40 can be expected to be weak in our CD8+ T cell-restricted experimental system.

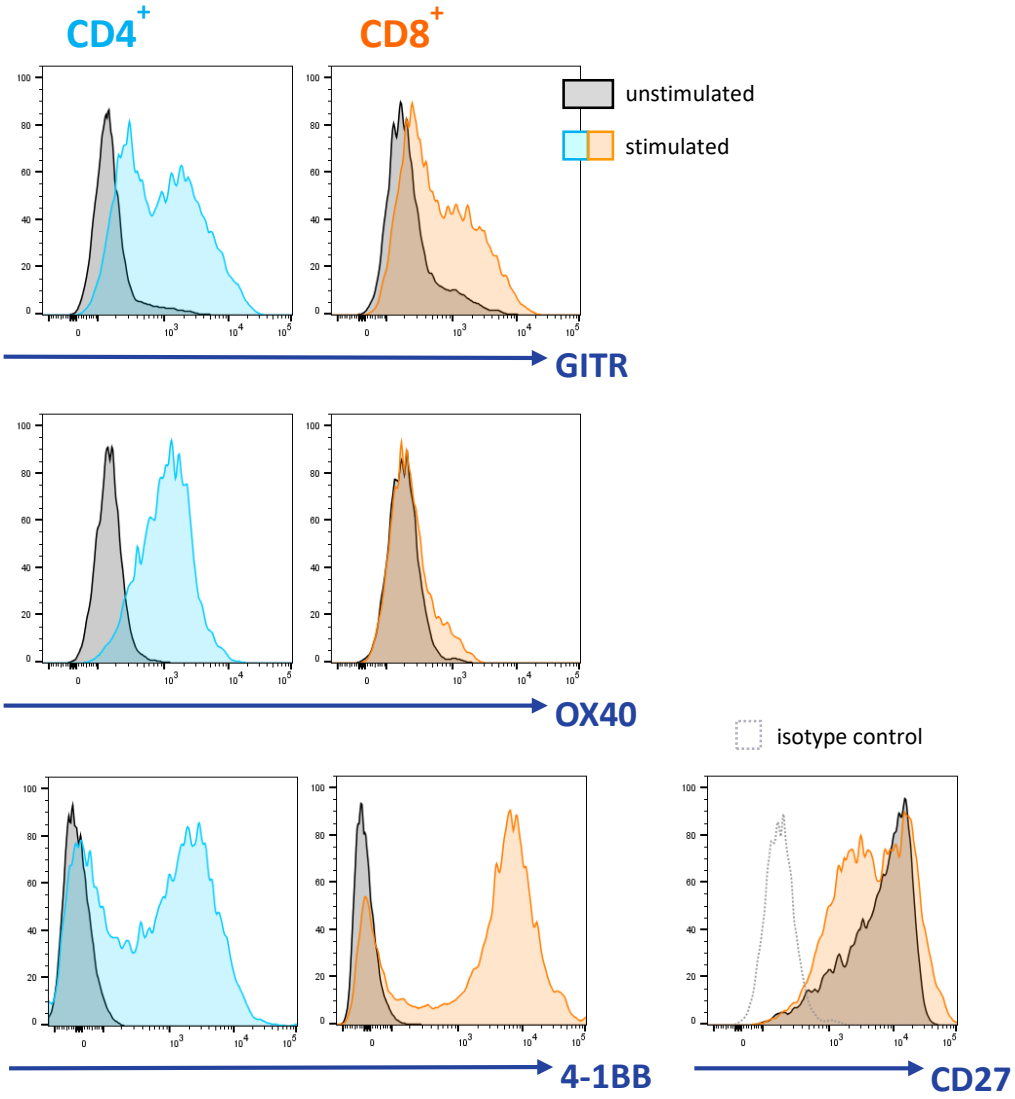

Figure 2.9: GITR and OX40 expression is induced, on CD8⁺ T cells to a lesser extent than on CD4⁺ T cells, upon activation through the TCR. Expanded primary human CD4⁺ and CD8⁺ T cell blasts (day 10-13) were stimulated with plate-immobilised anti-CD3 antibodies (clone UCHT1, 1µg/ml) for 18 hours. The indicated surface receptors were labelled with fluorescent antibodies and analysed by flow cytometry. Shown here are flow cytometry histograms for unstimulated (grey) and stimulated (blue/orange) T cells.

2.3.7. Effects of GITR and OX40 co-stimulation on CD8+ T cell responses are comparatively small

We conducted time course experiments with dose-ranges of pMHC and co-stimulatory ligands for GITR and OX40 as we did previously for 4-1BB and CD27.

Interestingly, even though it was induced upon T cell activation like 4-1BB, GITR expression appears to have different dynamics (Fig. 2.10A). In absence of ligand-induced downregulation, expression levels slowly rose after 4 hours and continued to increase at 24 hours instead of plateauing or decreasing at the later time points like 4-1BB (Fig. 2.4). This suggests that the 24 hours of our experiment may not be the biologically relevant time window for GITR, as its expression might peak at later time points and higher levels. Nevertheless, we could measure a detectable increase in cytokine production (Fig. 2.10B, C and D), although fairly weak in comparison to 4-1BB (Fig. 2.2).

OX40 expression, on the other hand, barely increased above baseline fluorescence throughout the experiment (Fig. 2.11A). Accordingly, the effects of added OX40L on the cytokine response were barely measurable (Fig. 2.11B, C and D).

It is important to note, however, that for unknown reasons, the IFN-γ and TNF responses did not adapt in these two cases as they did in all previous data sets. Further repeats are necessary for statistical tests and to draw more meaningful conclusions.

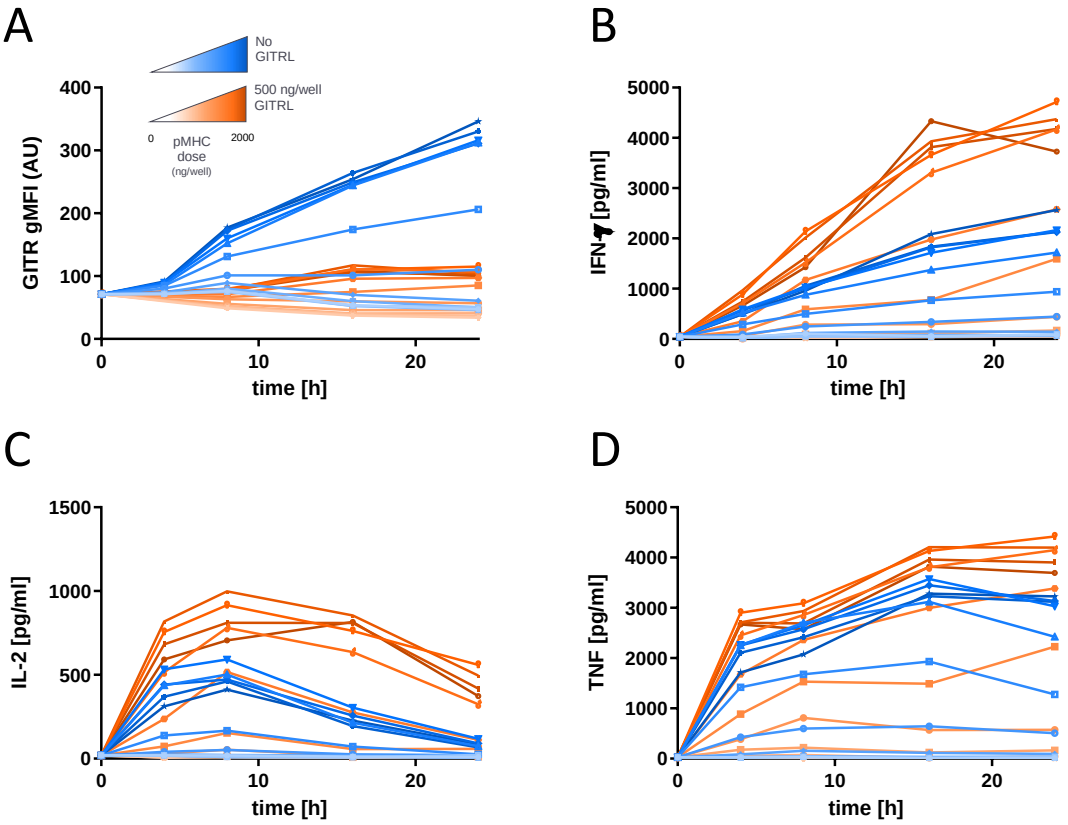

Figure 2.10: GITR co-stimulation weakly enhances cytokine production. Primary human CD8$^+$ T cells transduced with the c58/c61 TCR were stimulated for 4, 8, 16 and 24 hours with pMHC, with or without 500ng/well GITRL. Surface GITR was labelled with a fluorescent anti-GITR antibody and quantified by flow cytometry. The production of the cytokines IFN-γ, IL-2 and TNF into the culture medium supernatant was quantified by ELISA. Time courses of measured surface GITR as geometric mean fluorescence intensity (gMFI) **(A)**, IFN-γ **(B)**, IL-2 **(C)** and TNF **(D)** are shown in the absence (blue) or presence (orange) of GITRL. The colour shades represent the pMHC doses ranging from 0 (brightest) to 2000 ng/well (darkest).

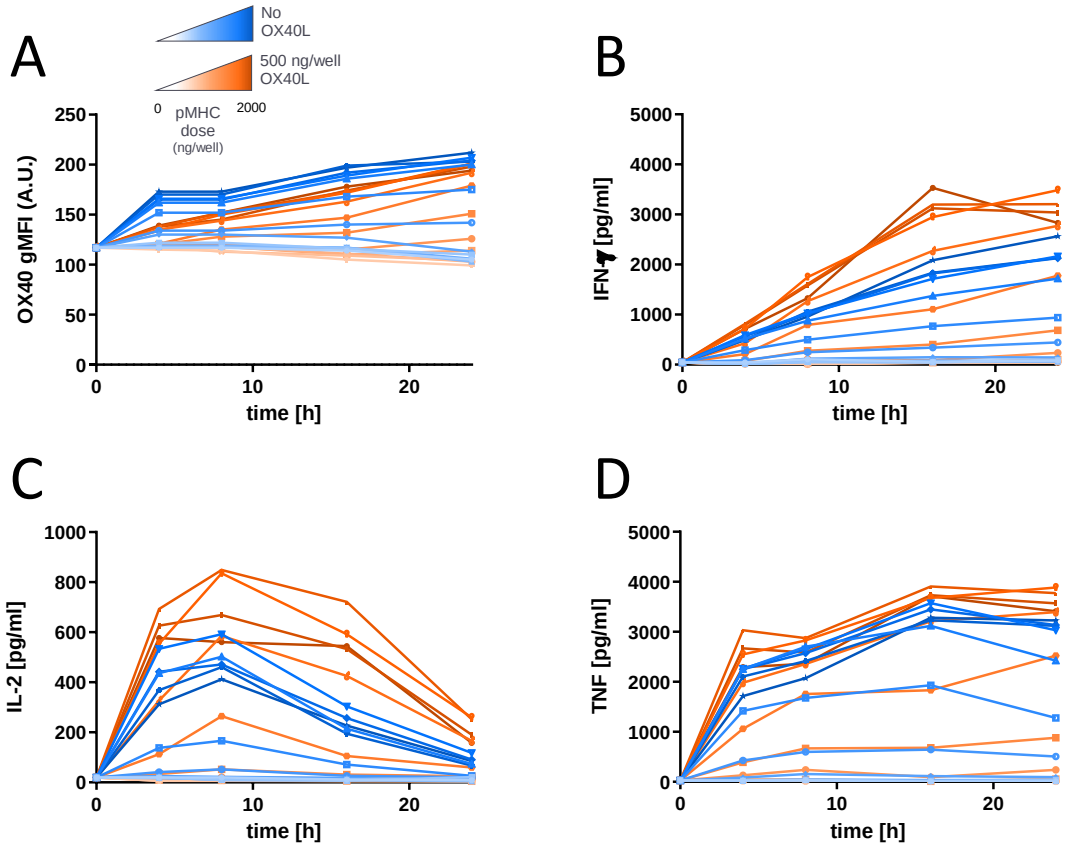

Figure 2.11: OX40 co-stimulation hardly enhances cytokine production. Primary human CD8$^+$ T cells transduced with the c58/c61 TCR were stimulated for 4, 8, 16 and 24 hours with pMHC, with or without 500ng/well OX40L. Surface OX40 was labelled with a fluorescent anti-OX40 antibody and quantified by flow cytometry. The production of the cytokines IFN-γ, IL-2 and TNF into the culture medium supernatant was quantified by ELISA. Time courses of measured surface GITR as geometric mean fluorescence intensity (gMFI) **(A)**, IFN-γ **(B)**, IL-2 **(C)** and TNF **(D)** are shown in the absence (blue) or presence (orange) of OX40L. The colour shades represent the pMHC doses ranging from 0 (brightest) to 2000 ng/well (darkest).

2.4. Discussion

2.4.1. Phenotypes of TNFRSF co-stimulation in context

Our minimal plate-based T cell stimulation platform enabled us to collect the data necessary for a quantitative analysis of T cell co-stimulation through receptors of the TNFR superfamily. Here we show in primary human $CD8^+$ T cells that 4-1BB and CD27 co-stimulation produce distinct phenotypes, which are consistent with their differential expression patterns in time.

4-1BB is not expressed on resting $CD8^+$ T cell blasts and therefore has no significant effect on the very early cytokine response. However, this receptor is rapidly upregulated between 4-8 hours after stimulation with pMHC, with a peak surface expression between the 8- and 16-hour time points. It is during this later stage that the production of IFN-γ, IL-2 and TNF is strongly increased in the presence of 4-1BBL, mainly due to the fact that the transient cytokine response which typically stops after 4-8 hours in the absence of co-stimulation is markedly prolonged by 4-1BB signalling. We conclude from this observation that the main effect of 4-1BB co-stimulation on $CD8^+$ T cell cytokine response is the prevention of adaptation, a TCR downregulation-associated unresponsive T cell phenotype which we have characterised previously (Trendel et al., 2019). This is in line with reports of 4-1BB co-stimulation preventing or reducing T cell anergy (Wilcox et al., 2004), and to some extent also T cell exhaustion in several *in vitro* and *in vivo* models (Long et al., 2015; Zhao et al., 2015). Even though these are unresponsive phenotypes which are likely distinct from adaptation, the reverting effect of 4-1BB

might have a common underlying mechanism. Interestingly, 4-1BB co-stimulation does not affect TCR downregulation in a way that would explain its effects on adaptation, further suggesting an involvement with more downstream TCR signalling.

CD27, on the other hand, is highly expressed on resting T cells and becomes rapidly downregulated in the presence of its ligand CD70. This is in line with the boosting effects of CD27 co-stimulation primarily on the early cytokine response and the inability of CD27 signalling to affect T cell adaptation. Interestingly, *in vivo* results also show that, rather than preventing unresponsiveness, dysregulated and constitutive CD70 expression in chronic infections actually drives $CD8^+$ T cells into an exhausted effector phenotype and impairs memory formation (van Gisbergen et al., 2009).

While the improvements of cytokine responses we observed with 4-1BB and CD27 co-stimulation particularly affect the overall amounts of cytokine produced (E_{max}), statistically significant 2- to 12-fold changes in the EC_{50} of dose-responses are observed, as well. However, the biological relevance of such small effects on T cell sensitivity is questionable. It is mainly receptors with a predominant role in mediating adhesion such as CD2 (Bachmann et al., 1999; Koyasu et al., 1990), and LFA-1 (Bachmann et al., 1997) that have been found to enhance T cell sensitivity, chiefly by stabilising close contacts between the plasma membranes of T cells and APCs (Bromley et al., 2001; Dustin et al., 1997). In the case of LFA-1, ~100-fold EC_{50} decreases of T cell responses were observed (Bachmann et al., 1997). In our plate-based *in vitro* T cell stimulation system, we obtain EC_{50} decreases of two orders of magnitude or more in the presence of CD58 or ICAM-1 (the ligands to

CD2 and LFA-1, respectively; unpublished data) compared to pMHC alone, suggesting that modulation of T cell sensitivity by 4-1BB or CD27 is likely overshadowed by adhesion receptors *in vivo*, where ligands to adhesion receptors are present.

However, if the EC_{50} decreases observed in our hands with 4-1BB and CD27 co-stimulation are indeed a consequence of their signalling and adhesion-independent, this would suggest potential multiplicative effects in combination with adhesion receptors that can become biologically significant. In fact, *in vivo* studies using murine systems have found that CD70-CD27 interactions allow for T cell clones with low affinity to antigens to accumulate and survive during viral infections (van Gisbergen et al., 2011; Hendriks et al., 2003), although it is worth noting that low affinities are not equivalent to low doses of antigen (Gottschalk et al., 2012). Given what is known about the molecular pathways downstream of TNFRSF members, it is plausible that by providing alternative mechanisms to activate major transcription factors of T cell activation, their signalling can lower the thresholds that TCR signalling has to overcome to induce a T cell response. Minor effects on T cell sensitivity to pMHC would then be a logical consequence, while such a mechanism would have more profound effects on other quantitative properties of the T cell response.

2.4.2. Limitations of our experimental platform

Considering the fact that our plate-based T cell stimulation platform differs from the surface of an antigen-presenting cell in many aspects, some of our observations might not reflect T cell behaviour *in vivo*. We designed this minimal system with the aim to precisely control the doses, combinations and timings of the ligands, with high throughput, and to an extent that is virtually impossible when using antigen-presenting cells. Despite the advantages, herein already lie several issues that must be considered.

To study the effects of each co-stimulatory receptor in isolation, the T cells are only co-presented with pMHC and the respective co-stimulatory ligand, while contacts between T cells and actual antigen-presenting cells involve a large number of different receptor-ligand interactions, especially the participation of adhesion molecules which stabilise close contacts and are therefore likely to have a global effect on the binding properties of various other receptors. This is reflected in the relatively high doses of pMHC necessary to induce T cell responses in our system, whereas in the context of professional antigen-presenting cells, cytokine responses have been reported to require as little as one pMHC (Huang et al., 2013). In the presence of adhesion molecules and other receptors, the doses of 4-1BBL and CD70 necessary for potent co-stimulatory effects would presumably be lower, as well.

Different co-stimulatory receptors themselves, by nature of their signalling pathways, may not only integrate with TCR signalling but are likely to interact in ways that are often exceedingly difficult to predict due to the high complexity of

signalling networks. Receptors with highly dynamic expression pattern, such as 4-1BB, would be particularly sensitive to such interplay, since even within the TNFRSF, we have observed that CD27 co-stimulation enhances the surface expression of 4-1BB, which will most probably have functional consequences.

We chose to use recombinant versions of the endogenous ligands over widely used alternatives such as agonistic antibodies in order to obtain more physiologically relevant findings, but we realise that by immobilising these ligands on the plates, we have foregone several biological properties of the natural ligands. Firstly, the elasticity and forces which T cells would experience on the plasma membrane of an opposing antigen-presenting cell will likely differ from the surface of the plate, and the relevance of these mechanical properties is becoming more and more recognised in the field of T cell receptor biology (Dushek and Dustin, 2018; Hong et al., 2018; Ma et al., 2012). Secondly, instead of being confined to the area of single cells, ligands on the plate form a virtually infinite stimulatory surface which the T cells cannot move away from. The slow rate of receptor replenishment and unresponsiveness of T cells might be the result of the constant stimulation, which mimics only the most extreme situations *in vivo*, such as severe infections and inflammatory tumour environments.

However, and most importantly, our ligands are anchored in place and do not allow for lateral mobility of the receptors, which is necessary to form supramolecular structures such as immunological synapses (Dustin, 2014; Monks et al., 1998). While natural pMHC-TCR and many other receptor-ligand complexes move and rearrange in distinct patterns, it is presently unclear how receptors of the TNFRSF behave relative to other molecules in contacts between T cells and

antigen-presenting cells. Their signalling pathways suggest an integration with other T cell activation pathways at the level of transcription factors, indicating that specific localisation within the immunological synapse or in relation to the TCR may not be as essential for TNFRSF members as it is for IgSF members such as CD28 or PD-1 (Chen and Flies, 2013). Keller et al. describe synchronised intracellular trafficking of CD70 with MHC class II in professional antigen-presenting cells towards the immunological synapse (Keller et al., 2007), but the functional importance of this coordination remains unclear.

We have accepted these caveats due to the limits of the available technology. While for example supported lipid bilayers allow for mobility of ligands, they do not fully recapitulate the properties of cell membranes, either. Moreover, they are more commonly used for short term assays, and over the course of 24 hours the limited stability of ligand anchors and the bilayers themselves is likely to become an issue, as well. With advances in experimental techniques, we hope to reproduce our quantitative data in more physiological settings.

Chapter 3: Construction of a phenotypic model of $CD8^+$ T cell co-stimulation through members of the TNF receptor superfamily

3.1. Extension of a minimal model of T cell activation to include co-stimulation

Our experimental work presented in Chapter 2 has shown that two representative co-stimulatory receptors of the TNFR superfamily, have very distinct effects on the $CD8^+$ T cell cytokine response, with 4-1BB preventing T cell adaptation and thereby prolonging the cytokine response, whereas CD27 led to early increases in cytokine without affecting adaptation, despite very similar signalling pathways reported for both receptors in the literature. While conventional analysis of our data is unable to determine the underlying mechanisms, it is plausible that the differential surface expression kinetics of these receptors might be sufficient to explain the differences in phenotype without inferring divergent signalling mechanisms. In this chapter, we apply our phenotypic modelling approach in order to confirm this, and to build a phenotypic model of T cell co-stimulation in the process.

We have previously generated such a model of T cell activation which was solely based on surface expression and downregulation dynamics of the TCR and a threshold switch (Trendel et al., 2019). Despite its simplicity, it was capable of faithfully reproducing quantitative properties of the T cell response to pMHC in our plate-based stimulation system, including the adaptation behaviour to stimulation with a constant dose of pMHC. This model is used as the basis to extend upon in order to include co-stimulation through 4-1BB and CD27.

Multiple parameters in this base model could potentially be modulated by co-stimulation (Fig. 3.1). K_A (association constant, also known as inverse of the dissociation constant K_D) is a summary of the effective binding properties of the pMHC-TCR interaction. These interactions can, for instance, be facilitated by adhesion molecules which stabilise close contacts between the plasma membranes of T cell and antigen-presenting cell. The parameter k_1 determines the (re)expression rate of surface TCR, while k_2 and k_3 represent signalling-dependent and ligand binding-dependent rates of TCR downregulation, respectively; molecular mechanisms for both acting in parallel have been proposed and demonstrated previously (von Essen et al., 2002; Monjas et al., 2004; San José et al., 2000). The rate of cytokine production is scaled by k_4. As additional potential mechanisms of co-stimulation, two new parameters have been added, with k_{amp} amplifying the signalling upstream of the threshold switch (which is mathematically equivalent to lowering the threshold of the switch) and k_{act} activating the cytokine response directly, independently from TCR signalling.

In the following sections, various models will be discussed where CD27 and 4-1BB co-stimulation affect these parameters. Simulations of these models will be tested for consistency with the experimental results from Chapter 2, with the objective to identify the effective integration points of TNFRSF co-stimulation with TCR signalling in a phenotypic model.

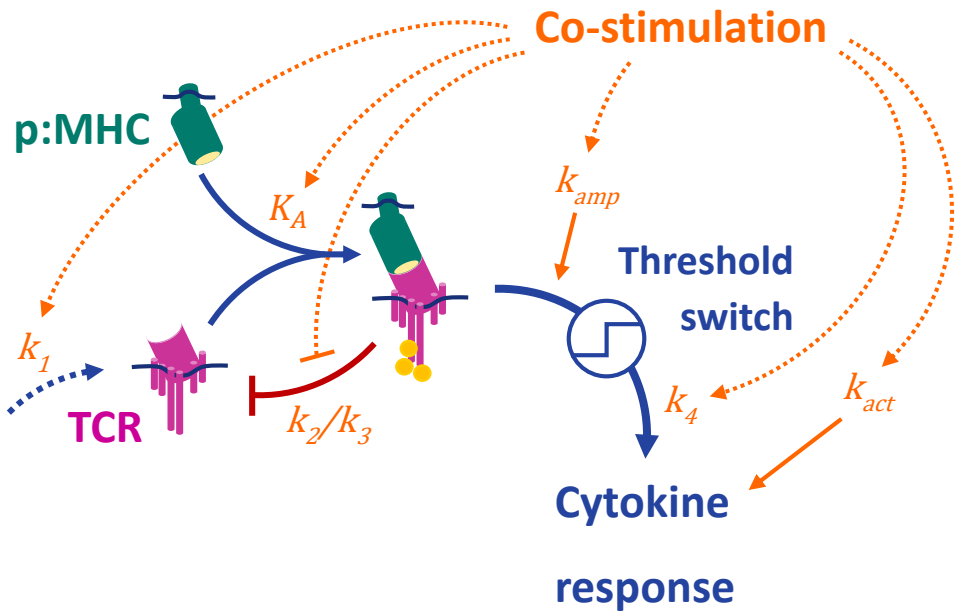

Figure 3.1: Schematic of the basic phenotypic model of T cell activation from Trendel & Kruger et al. (2019) with potential integration points for co-stimulation. As in Fig. 1.1, with parameters which can theoretically be modulated by co-stimulation highlighted in orange. K_A: association constant, k_1: rate of TCR (re)expression, k_2: rate of signalling-induced TCR downregulation, k_3: rate of ligand binding-induced TCR downregulation, k_4: rate of cytokine production, k_{amp}: rate of signalling amplification, k_{act}: rate of direct (TCR-independent) cytokine production. Further details can be found in the Methods Section 6.7.1.

3.2. Results

3.2.1. CD27 co-stimulation is likely to modulate either k_{amp} or k_4

A first screen, simulating responses while simply decreasing or increasing single parameters in the model (Supplementary Figures S.7 and S.8), shows that changes in K_A only shift the dose-response curves of TCR downregulation and cytokine production along the x-axis (changing the EC_{50}) without affecting temporal dynamics or the amplitude of the response at all (Supplementary Figure S.7A). Since the data generated in Chapter 2 show that co-stimulation through 4-1BB and CD27 mainly change the magnitude of the response rather than TCR downregulation or EC_{50}, effects on K_A can be ruled out as the main mechanism and will not be included in further model simulations.

While effects on TCR expression and downregulation are also unlikely based on our experimental results in Section 2.3.4., these have a less intuitively predictable impact on the dose-responses in our model and were included for the sake of completeness.

Since the dynamics of co-signalling receptor expression are likely to play an important role in regulating timing and effectiveness of 4-1BB and CD27 co-stimulation, modelling them as a constant change in parameters as above will not be able to appropriately recapitulate their function. In this case, CD27 is simpler to model since its expression is mostly affected by the presence of its ligand and does

not otherwise significantly change as a consequence of T cell activation on our time scale of interest (24 hours). This removes the necessity of feedback loops with TCR signalling, which will be addressed in the 4-1BB co-stimulation models.

Fig. 3.2A visualises our approach to model CD27 expression. As seen in the experimental data, CD27 is present on the surface of resting cells and forms complexes with its ligand CD70, the amount of which determines the magnitude of co-stimulatory effect. At the same time, binding its ligand results in rapid downregulation of CD27. In presence of a high dose of CD70, CD27 decreases to an equilibrium close to background levels within 4 hours (Fig. 2.4A), which is reproduced by the simulation in Fig. 3.2A. CD27 will not be affected by pMHC doses, as there are no direct feedbacks from TCR signalling onto CD27 itself.

Using this module to describe CD27 expression, we simulated co-stimulation affecting single parameters of our base model, with its strength scaling with the amount of CD70-CD27 complexes present. Interestingly, CD27 co-stimulation increasing k_1 or decreasing k_2 and k_3 can result in large increases of the cytokine response with barely noticeable changes in TCR downregulation (Fig, 3.2B-D).

Our TCR downregulation data in Section 2.3.4. does not support the hypothesis of TCR downregulation being affected, nor does the literature of signalling downstream of TNFRSF indicate any involvement of these receptors with TCR surface expression. However, due to the low resolution of TCR measurements in our CD27 co-stimulation data sets, one can argue that it is difficult to convincingly rule out such small changes in TCR levels with the available data. On the other hand, simulated co-stimulation on the parameter k_1 (TCR expression rate) has

distinct effects on the cytokine response, predominantly at high pMHC doses, where adaptation is overcome (Fig. 3.2B). This is inconsistent with the experimental data, which is why the model connecting co-stimulation to k_1 can indeed be rejected with confidence.

Co-stimulation through k_4, k_{amp} and k_{act} has no effect on TCR downregulation, with increases in k_4 boosting the cytokine production rate early during the first 8 hours without any impact on the adaptation behaviour (Fig. 3.3C), which appears to represent the experimental results best. On the other hand, in the models where CD27 signalling boosts k_{amp} (Fig. 3.3B), increases of the early cytokine response are mainly due to delays in adaptation, with no change in the first 4 hours.

While this is not quite reflected in the experimental data, our models are limited by the fact that they simulate the behaviour of a population of identical T cells (discussed in detail in Chapter 3.3.2.). In reality, the natural heterogeneity in the T cell population would have caused variability in reaction rates and thresholds, resulting in cells initiating cytokine production and adapting at variable times. Delays in adaptation would then cause cells which would have stopped early to continue their response, thereby increasing the amount of cytokine produced in a given amount of time and boosting the apparent cytokine production rate of the cell population (Fig. 3.4). It is also possible that such delays would go unnoticed in our data sets, given the measurement intervals of 4 and 8 hours. We thus decided not to reject this model. However, k_{act} can be excluded as a mechanism of co-stimulation, since it would lead to TCR-independent cytokine responses (Fig. 3.3D), which we do not observe for CD27.

In the end, the models with co-stimulation through k_4 and and k_{amp} could not be rejected, leaving us with two different models as potential mechanisms for CD27 function at this point (Table 3.7). For simplicity, we chose not to include the steady cytokine decay/consumption rate which we observe past 8 hours for IL-2 and TNF, which is why the modelled cytokine response best reflects the IFN-γ data in our experiments.

Figure 3.2: (next page) **Simulation of CD27 co-stimulation modulating TCR expression and downregulation.** CD70 and CD27 were modelled as ligand-receptor pair, where binding forms the signalling complex but also induces downregulation of CD27. **(A)** Simulated surface expression of CD27 over time and across pMHC doses in the absence (blue) or presence of CD70 (orange). In addition, TCR expression and cytokine response were simulated over time and across pMHC doses for models in which the CD70-CD27 complex either increases k_1 **(B)** or decreases k_2 **(C)** or k_3 **(D)**. k_1: rate of TCR (re)expression, k_2: rate of signalling-induced TCR downregulation, k_3: rate of ligand binding-induced TCR downregulation.

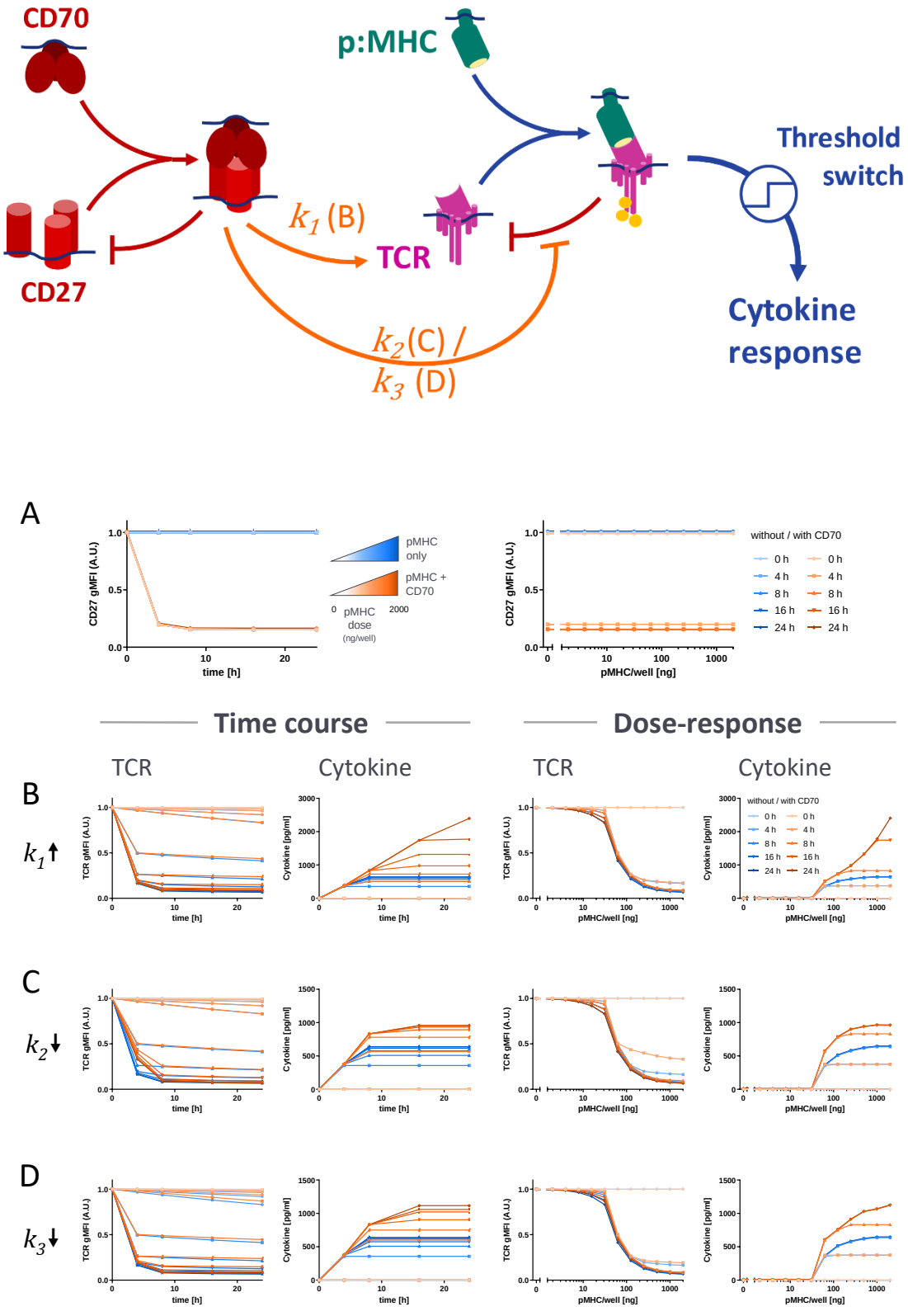

Figure 3.2: Simulation of CD27 co-stimulation modulating TCR expression and downregulation. (Description on previous page.)

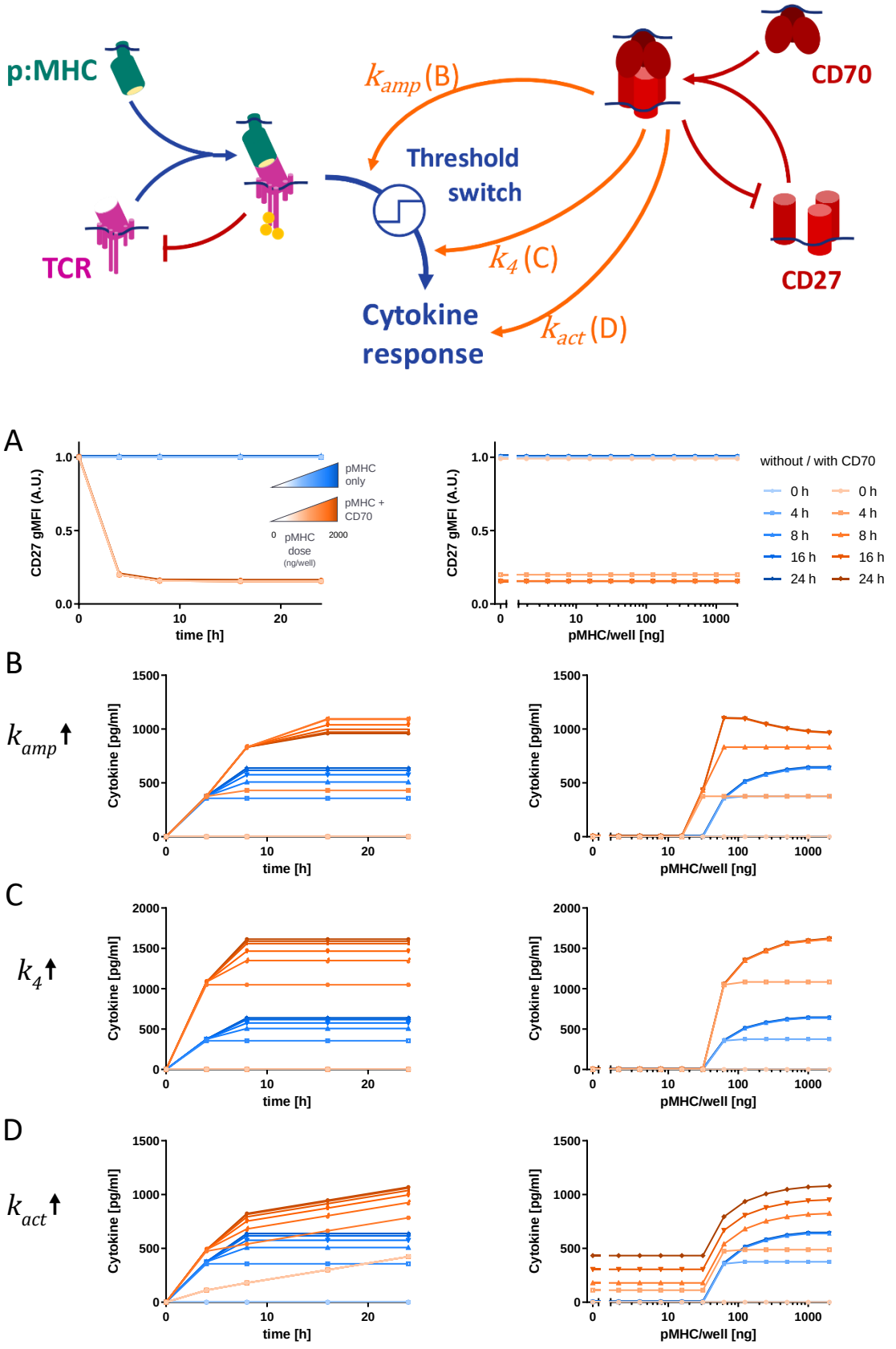

Figure 3.3: Simulation of CD27 co-stimulation modulating downstream signalling.
(Description on next page.)

Figure 3.3: (previous page) **Simulation of CD27 co-stimulation modulating downstream signalling.** CD70 and CD27 were modelled as in Fig. 3.2. **(A)** Simulated surface expression of CD27 over time and across pMHC doses in the absence (blue) or presence of CD70 (orange). In addition, the cytokine response was simulated over time and across pMHC doses for models in which the CD70-CD27 complex increases k_{amp} **(B),** k_4 **(C)** or k_{act} **(D)**. k_4: rate of cytokine production, k_{amp}: rate of signalling amplification, k_{act}: rate of direct (TCR-independent) cytokine production.

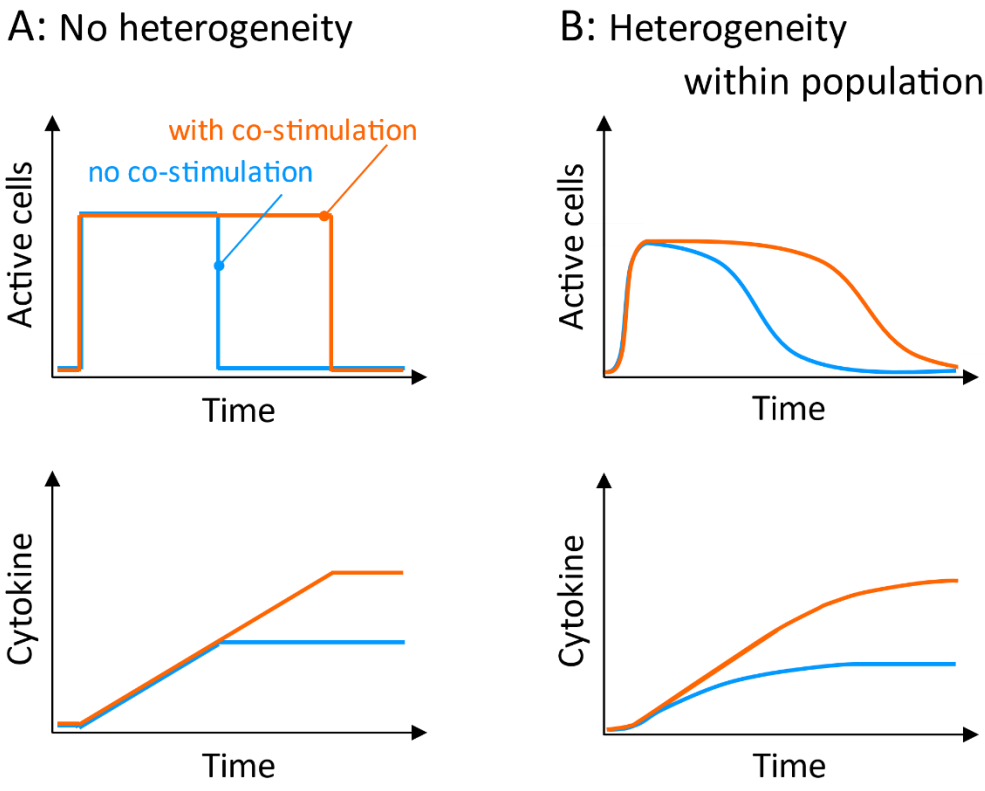

Figure 3.4: Population heterogeneity leads to differences in apparent cytokine production rate which are not captured by our deterministic modelling approach. Since our current model assumes a population of identical cells, their activity will be switched on and off in unison **(A)**. Co-stimulation modulating k_{amp} would therefore not result in any changes of the cytokine production rate pre-adaptation, as simulated in Fig. 3.3B. **(B)** In reality, population heterogeneity, e.g. variability in parameters such as the threshold of the switch, would result in a more slowly increasing fraction of the cells switching on or off over time, resulting in differences in the apparent cytokine production rate of the population even when identical cytokine production rates per cell are assumed.

3.2.2. 4-1BB co-stimulation is likely to modulate either k_{amp} or k_{act}

We applied the same approach to 4-1BB co-stimulation, only with 4-1BB expression being dependent on T cell activation. This implies that, as long as T cell activation is sustained, the activation-induced expression rate would counterbalance the 4-1BBL-induced downregulation of 4-1BB, allowing for a more prolonged co-stimulatory effect compared to CD27. This is supported by our experimental observations in Chapter 2.3.3. On the other hand, it is 4-1BB co-stimulation which sustains T cell activation by preventing adaptation, suggesting that through this positive feedback loop, co-stimulation through 4-1BB in fact supports its own expression. While this is more difficult to demonstrate experimentally due to ligand-induced downregulation, we find that CD27 co-stimulation, which is likely to share similar molecular pathways, does increase 4-1BB expression.

For modelling 4-1BB co-stimulation this means that parameter changes will have to reflect the behaviour of both the cytokine responses and 4-1BB expression, which may aid us in narrowing down the list of plausible models. More generally speaking, this also means that the most important feature that the model has to reproduce is the prevention of T cell adaptation.

Since k_4 only scales the cytokine production rate of activated cells, changes in this parameter (no matter how large) are unable to remove adaptation (Fig. 3.6B)

which is governed by the threshold switch further upstream. This model can therefore be rejected.

Models where 4-1BB co-stimulation affects TCR expression via k_1, k_2 and k_3 can indeed remove adaptation, but rely on inhibition of TCR downregulation (Fig. 3.5). While the changes are very small, the experimental data suggests that TCR downregulation is affected rather in the opposite direction in presence of 4-1BBL, if at all (Chapter 2.3.4.). In addition, the T cell response in these simulations is preferentially enhanced at higher pMHC doses, effectively increasing the EC_{50} of both cytokine and 4-1BB expression at later time points, which is also inconsistent with the data (Chapter 2.3.5.).

This leaves the models with 4-1BB co-stimulation through k_{amp} and k_{act} (Fig. 3.6A and C) as the most plausible ones (Table 3.7). In both, adaptation is prevented without changes in TCR expression. In the case of k_{amp}, the T cell response is sustained by amplification of the residual TCR signalling over the threshold, while co-stimulation through k_{act} induced a TCR-independent response which is masked by the fact that 4-1BB expression requires TCR signalling in the first place.

Figure 3.5: (next page) **Simulation of 4-1BB co-stimulation modulating TCR expression and downregulation.** 4-1BBL and 4-1BB were modelled as ligand-receptor pair, where binding forms the signalling complex but also induces downregulation of 4-1BB. 4-1BB is absent at start of the simulation and induced by TCR signalling. TCR expression, cytokine response and 4-1BB expression were simulated over time and across pMHC doses in the absence (blue) or presence of 4-1BBL (orange) for models in which the 4-1BBL-4-1BB complex either increases k_1 **(A)** or decreases k_2 **(B)** or k_3 **(C)**. k_1: rate of TCR (re)expression, k_2: rate of signalling-induced TCR downregulation, k_3: rate of ligand binding-induced TCR downregulation.

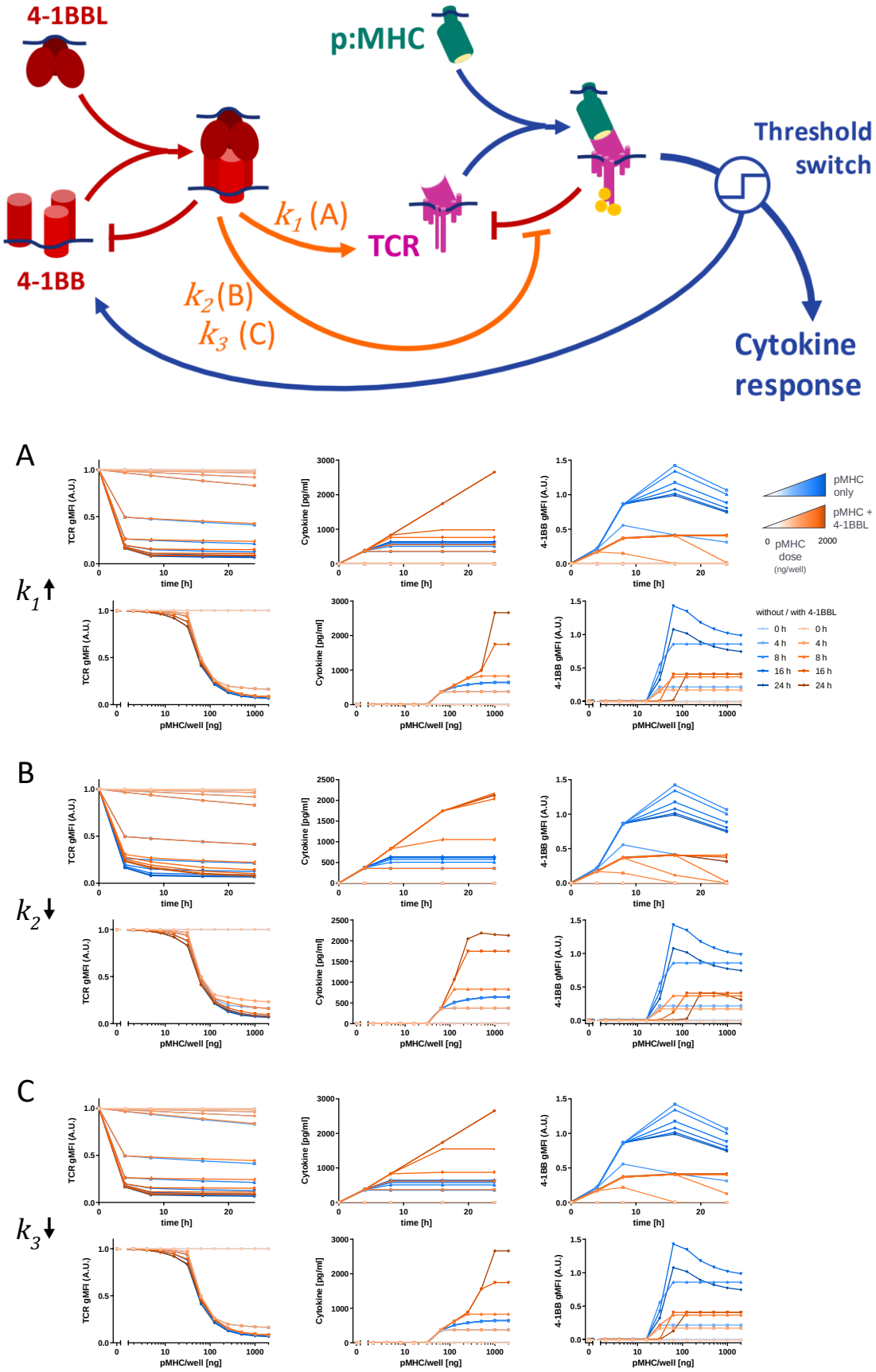

Figure 3.5: Simulation of 4-1BB co-stimulation modulating TCR expression and downregulation. (Description on previous page.)

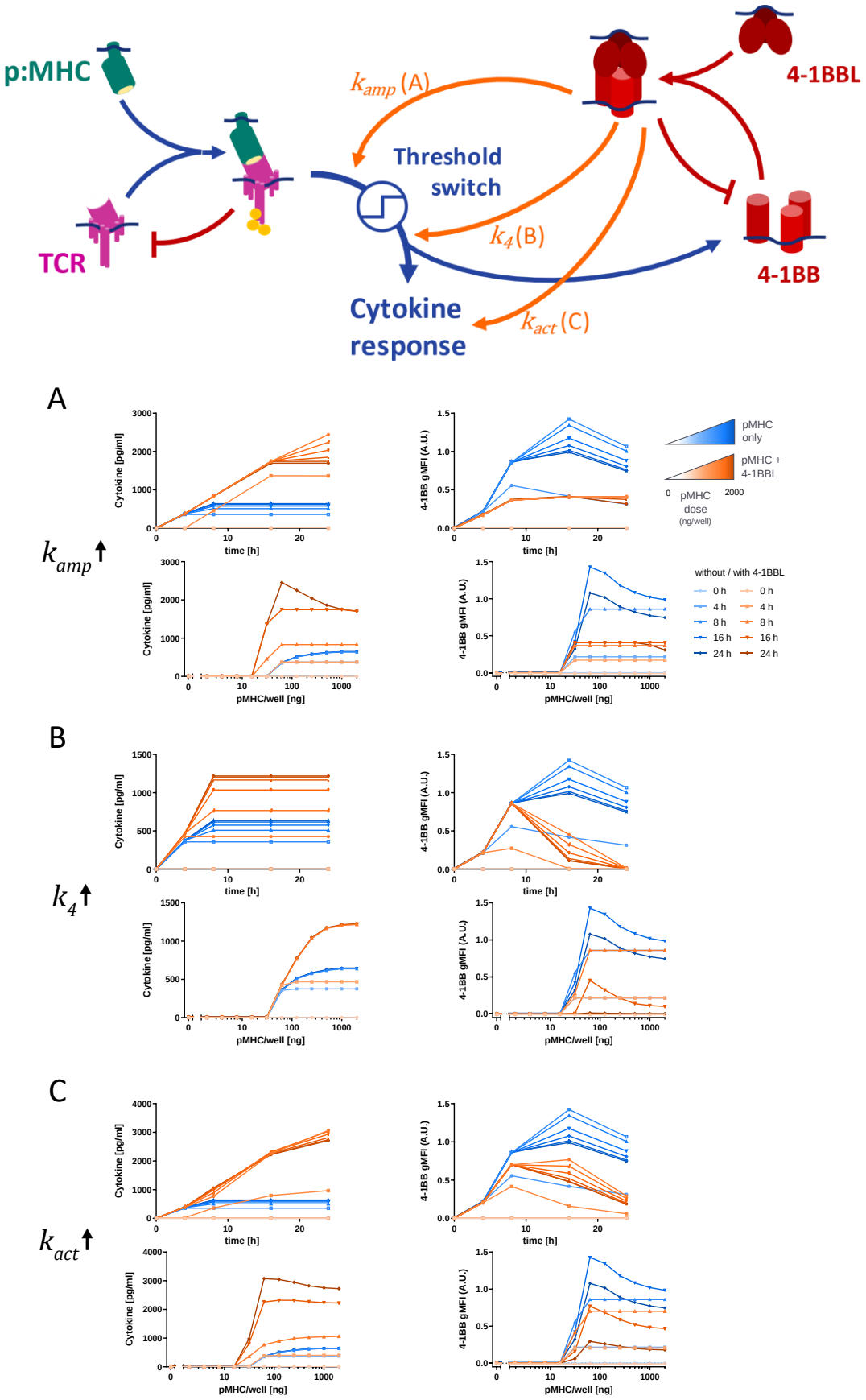

Figure 3.6: Simulation of 4-1BB co-stimulation modulating downstream signalling.
(Description on next page.)

Figure 3.6: (previous page) **Simulation of 4-1BB co-stimulation modulating downstream signalling.** 4-1BBL and 4-1BB were modelled as in Fig. 3.5. Cytokine response and 4-1BB expression were simulated over time and across pMHC doses in the absence (blue) or presence of 4-1BBL (orange) for models in which the 4-1BBL-4-1BB complex increases k_{amp} **(A)**, k_4 **(B)** or k_{act} **(C)**. k_4: rate of cytokine production, k_{amp}: rate of signalling amplification, k_{act}: rate of direct (TCR-independent) cytokine production.

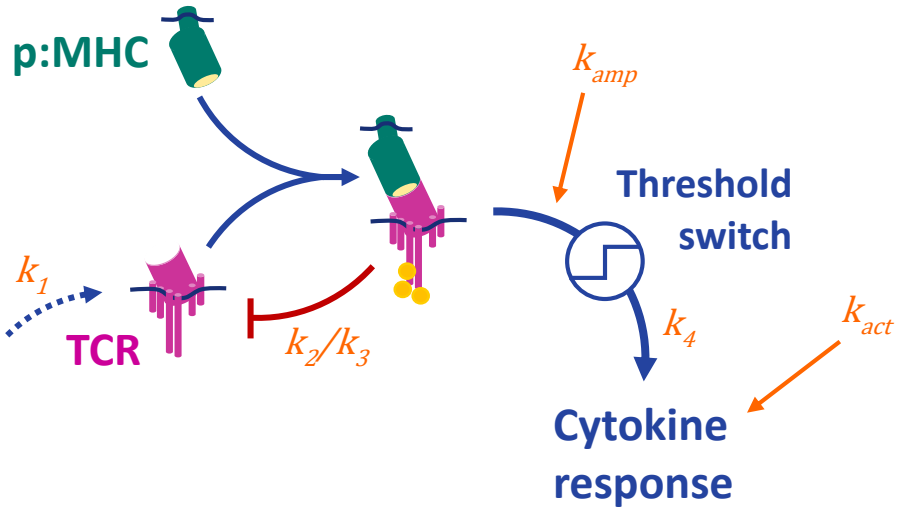

Affected parameter	CD27	4-1BB
k_1 ↑	×	×
k_2 ↓	(×)	×
k_3 ↓	(×)	×
k_{amp} ↑	✓	✓
k_4 ↑	✓	×
k_{act} ↑	×	✓

Table 3.7: Summary table of modelling results. ×: simulation inconsistent with experimental data from Chapter 2; ✓: simulation largely consistent with experimental data; k_1: rate of TCR (re)expression, k_2: rate of signalling-induced TCR downregulation, k_3: rate of ligand binding-induced TCR downregulation, k_4: rate of cytokine production, k_{amp}: rate of signalling amplification, k_{act}: rate of direct (TCR-independent) cytokine production.

3.2.3. Simulation of delayed co-stimulation allows for more conclusive distinction between models

When attempting to model CD27 and 4-1BB co-stimulation on their own, narrowing down their mechanism to a singular model proves to be difficult. While only the mechanism through k_{amp} is consistent with the experimental data for both TNFRSF members, this relies on the assumption that they share the same mechanism. An additional set of validation experiments could help provide more convincing support for this hypothesis.

Assuming that differences between 4-1BB and CD27 co-stimulation phenotypes are indeed only caused by their distinct expression patterns, CD27 would also be able to affect the T cell adaptation behaviour if it were expressed at the relevant time. This can happen when T cells are stimulated with pMHC in the absence of CD70 for a period of time sufficient to induce adaptation, before being co-stimulated through CD27. In this case, premature downregulation of CD27 would be prevented.

Figures 3.8 and 3.9 show simulations of the previous models under the conditions of such an experiment where cells were allowed to adapt to pMHC for 16 hours before CD70 is added. Confirming whether (and to what extent) the responsiveness of already adapted T cells could be rescued with the delayed CD27 co-stimulation might help us distinguish between these models.

Without co-stimulation, adapted T cells will not produce any further cytokines in the secondary stimulation phase. Here, co-stimulation through k_2 would not be

able to restore the cytokine response since this parameter governs the signalling-dependent TCR downregulation, which becomes irrelevant once TCR signalling shuts down due to adaptation (Fig. 3.8C). On the other hand, increasing k_1 and decreasing k_3 would lead to gradual recovery of TCR expression, preferentially rescuing the cytokine response at higher pMHC doses (Fig. 3.8B and D), effectively resulting in dose-response curves with higher EC_{50} compared to the first 16h stimulation phase (Fig. 3.8A). In contrast to this, co-stimulation through k_{amp} rescues the response by increasing the residual TCR signalling over the threshold, thereby slightly lowering the EC_{50} (Fig. 3.9B). The response is not restored by k_4 which offers no mechanism to revert adaptation, and k_{act} would once again induce a TCR-independent response (Fig. 3.9C and D).

Applying the same conditions to the 4-1BB co-stimulation models has very similar outcomes (Fig. 3.10 and 3.11), summarised in Table 3.12, with the exception of the k_{act} model (Fig. 3.11D) where the TCR-independent response still follows the pMHC dose due to 4-1BB expression being TCR signalling-dependent.

Figure 3.8: (next page) **Simulation of delayed CD27 co-stimulation modulating TCR expression and downregulation.** CD70 and CD27 were modelled as in Fig. 3.2. TCR expression and cytokine response were simulated for a 16-hour stimulation with pMHC only **(A)**, after which CD70 was either added (orange) or not (blue) for the remaining 8 hours. Simulations are shown for TCR expression and cytokine produced in this 8-hour time window for models in which the CD70-CD27 complex either increases k_1 **(B)** or decreases k_2 **(C)** or k_3 **(D).** k_1: rate of TCR (re)expression, k_2: rate of signalling-induced TCR downregulation, k_3: rate of ligand binding-induced TCR downregulation.

Figure 3.9: (page after next) **Simulation of delayed CD27 co-stimulation modulating downstream signalling.** CD70 and CD27 were modelled as in Fig. 3.2. The cytokine response was simulated for a 16-hour stimulation with pMHC only **(A)**, after which CD70 was either added (orange) or not (blue) for the remaining 8 hours. Simulations are shown for the cytokine produced in this 8-hour time window for models in which the CD70-CD27 complex increases k_{amp} **(B)**, k_4 **(C)** or k_{act} **(D)**. k_4: rate of cytokine production, k_{amp}: rate of signalling amplification, k_{act}: rate of direct (TCR-independent) cytokine production.

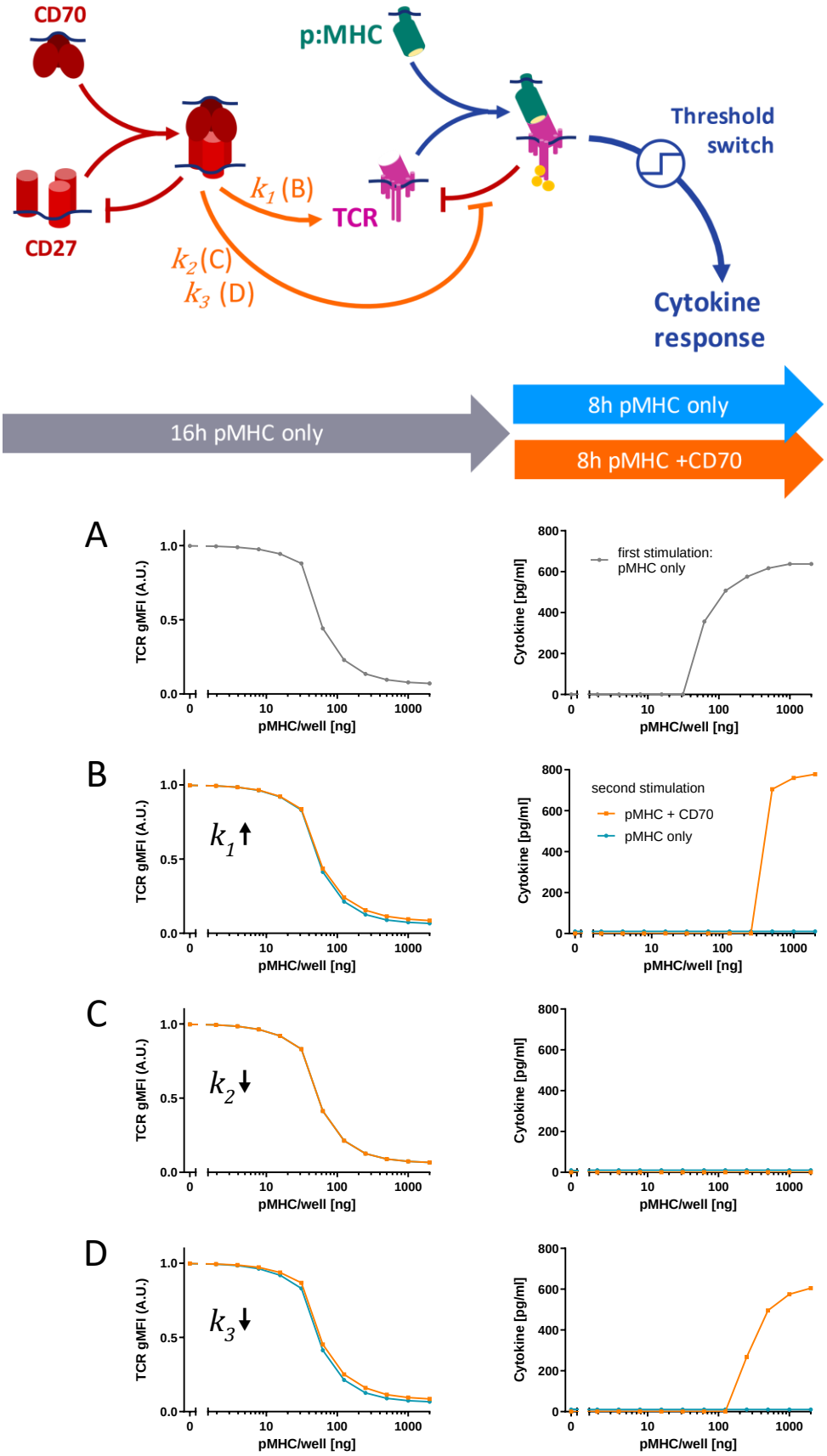

Figure 3.8: Simulation of delayed CD27 co-stimulation modulating TCR expression and downregulation. (Description on previous page.)

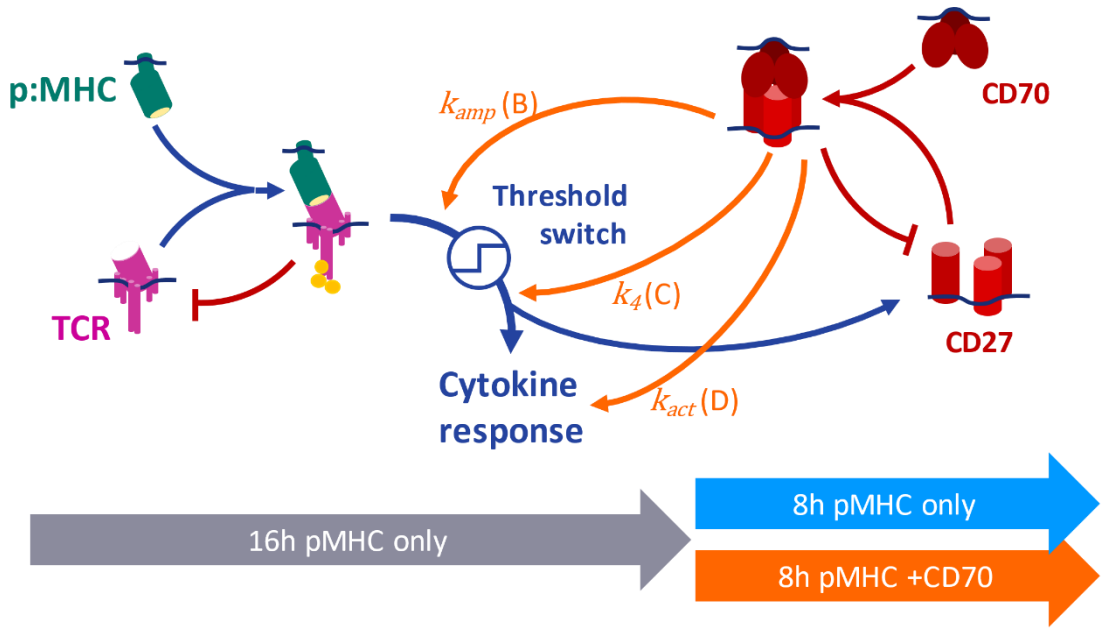

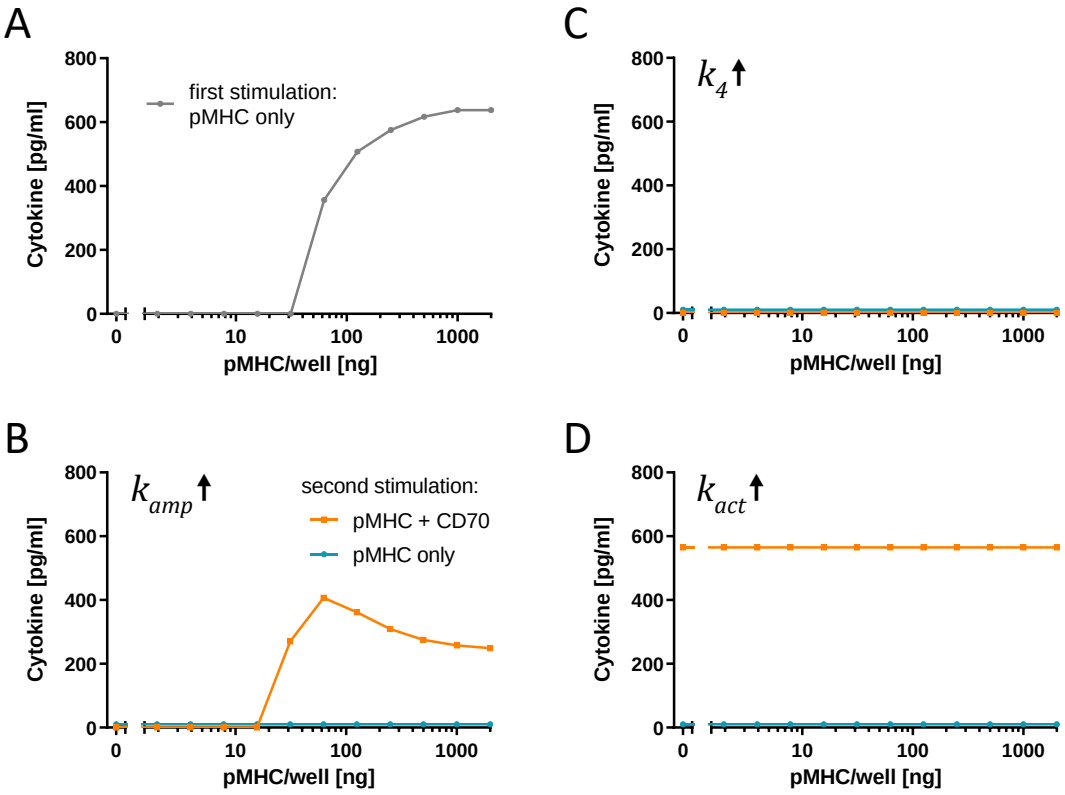

Figure 3.9: Simulation of delayed CD27 co-stimulation modulating downstream signalling. (Description on page before previous.)

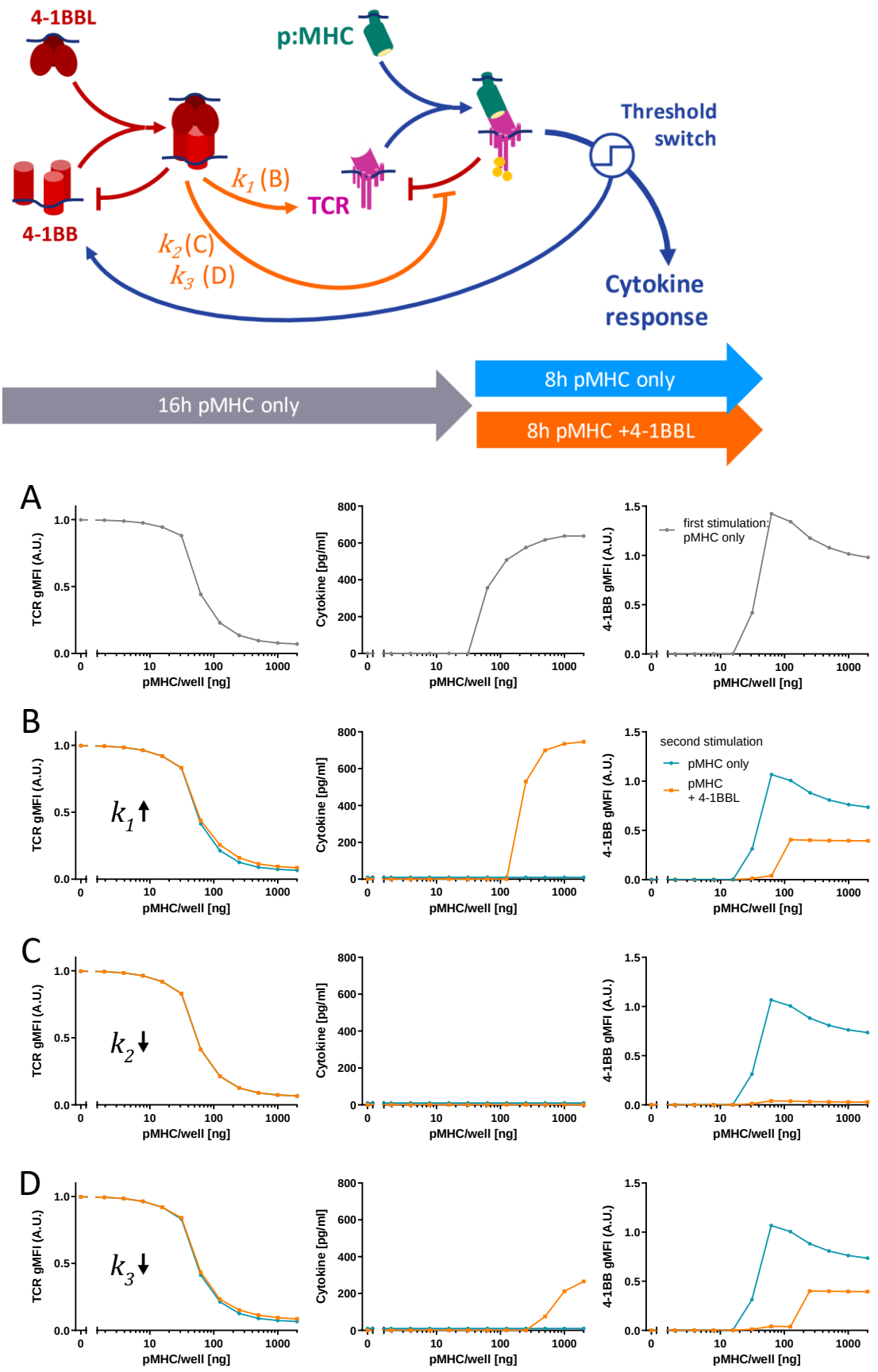

Figure 3.10: Simulation of delayed 4-1BB co-stimulation modulating TCR expression and downregulation. (Description on page after next)

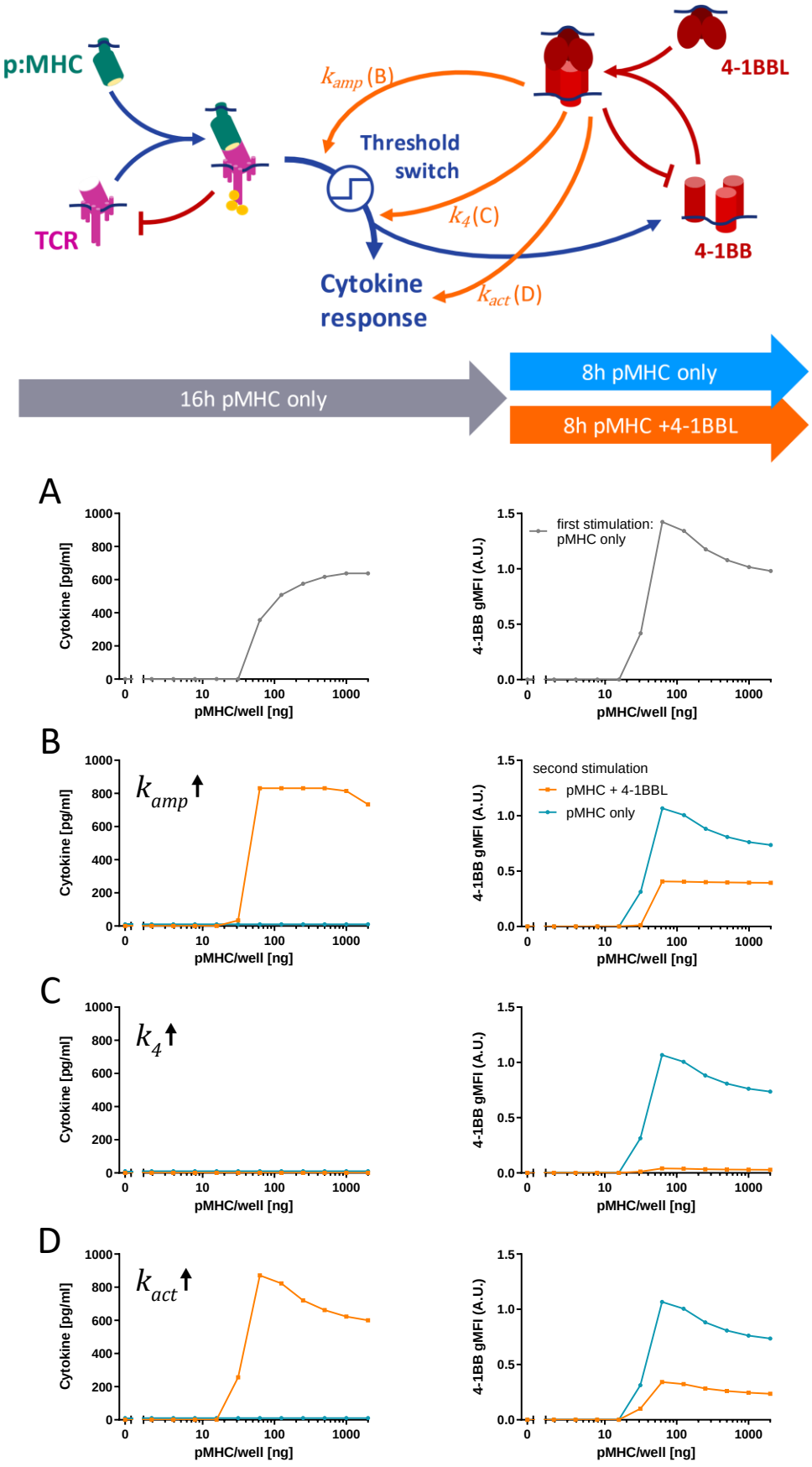

Figure 3.11: Simulation of delayed 4-1BB co-stimulation modulating downstream signalling. (Description on next page.)

Figure 3.10: (page before previous) **Simulation of delayed 4-1BB co-stimulation modulating TCR expression and downregulation.** 4-1BBL and 4-1BB were modelled as in Fig. 3.5. TCR expression, cytokine response and 4-1BB expression were simulated for a 16-hour stimulation with pMHC only **(A)**, after which 4-1BBL was either added (orange) or not (blue) for the remaining 8 hours. Simulations are shown for TCR and 4-1BB expression, as well as cytokine produced in this 8-hour time window, for models in which the 4-1BBL-4-1BB complex either increases k_1 **(B)** or decreases k_2 **(C)** or k_3 **(D)**. k_1: rate of TCR (re)expression, k_2: rate of signalling-induced TCR downregulation, k_3: rate of ligand binding-induced TCR downregulation.

Figure 3.11: (previous page) **Simulation of delayed 4-1BB co-stimulation modulating downstream signalling.** 4-1BBL and 4-1BB were modelled as in Fig. 3.5. Cytokine response and 4-1BB expression were simulated for a 16-hour stimulation with pMHC only **(A)**, after which 4-1BBL was either added (orange) or not (blue) for the remaining 8 hours. Simulations are shown for cytokine produced in this 8-hour time window and 4-1BB expression for models in which the 4-1BBL-4-1BB complex increases k_{amp} **(B)**, k_4 **(C)** or k_{act} **(D)**. k_4: rate of cytokine production, k_{amp}: rate of signalling amplification, k_{act}: rate of direct (TCR-independent) cytokine production.

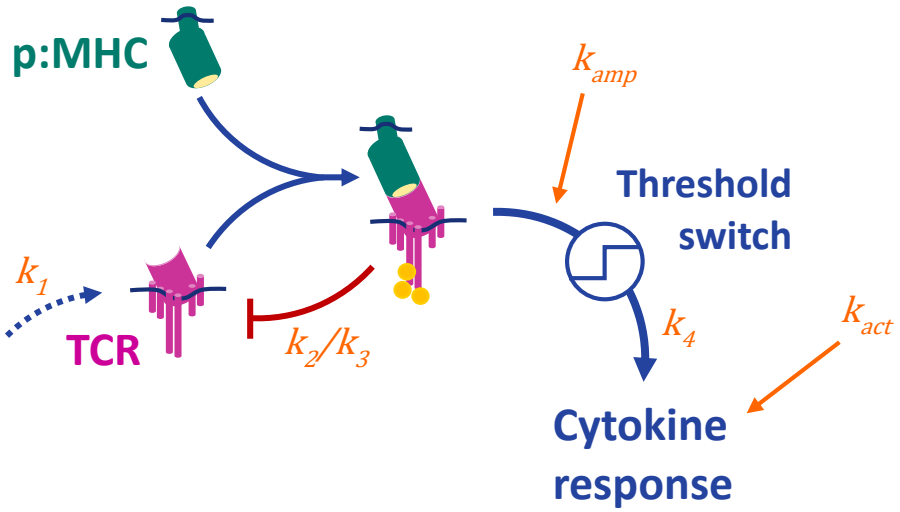

Affected parameter	Constitutive co-stimulation		Delayed co-stimulation	
	CD27	4-1BB	CD27	4-1BB
k_1 ↑	×	×	Response is rescued, and EC_{50} ↑	
k_2 ↓	(×)	×	Response cannot be rescued	
k_3 ↓	(×)	×	Response is rescued, and EC_{50} ↑	
k_{amp} ↑	✓	✓	Response is rescued, and EC_{50} ↓	
k_4 ↑	✓	×	Response cannot be rescued	
k_{act} ↑	×	✓	TCR-independent response is observed	

Table 3.12: Summary table of modelling results in Chapter 3. ×: simulation inconsistent with experimental data from Chapter 2; ✓: simulation largely consistent with experimental data; k_1: rate of TCR (re)expression, k_2: rate of signalling-induced TCR downregulation, k_3: rate of ligand binding-induced TCR downregulation, k_4: rate of cytokine production, k_{amp}: rate of signalling amplification, k_{act}: rate of direct (TCR-independent) cytokine production.

3.3. Discussion

3.3.1. Hypotheses to be tested in validation experiments

From the computational modelling results summarised in Table 3.12, a set of interesting open hypotheses can be derived which can be tested in follow-up experiments to determine the most appropriate models for TNFRSF co-stimulation, and to improve our conceptual understanding of these receptors:

1. 4-1BB is a bona-fide co-stimulatory receptor.

While CD27 signalling is apparently unable to induce a T cell cytokine response on its own, it is unclear from the data in Chapter 2 alone whether 4-1BB will behave the same, since its own expression is dependent on T cell activation through the TCR. There is controversy about TCR-independent T cell activation through TNFR family members, with So et al. reporting the antigen-independent assembly of an OX40L-OX40-induced signalosome containing components normally associated with TCR signalling (So et al., 2011b), suggesting that these receptors could activate T cell functions in the absence of antigen once their expression is induced. It is plausible that their survival-enhancing NFκB signalling can help maintain the pool of memory T cells after an immune response, once the antigen has been cleared (Pulle et al., 2006), but whether their signalling alone is sufficient to induce effector functions such as cytokine production in the absence of TCR stimuli remains questionable. Testing whether 4-1BB is a bona-fide co-stimulatory

receptor, i.e. requiring simultaneous TCR signalling to activate T cells, should be possible in our experimental system, where 4-1BB expression can be induced by presenting T cells with pMHC. 4-1BB-positve T cells can then be harvested and presented with 4-1BBL on its own or in combination with pMHC. This will either confirm or rule out the model of co-stimulation through the parameter k_{act}. Under the assumption that 4-1BB and CD27 share the same co-stimulatory mechanism due to similarities in their intracellular signalling, it is unlikely that cytokine production will be observed without the addition of pMHC.

2. 4-1BB signalling can revert unresponsiveness in adapted T cells.

Even though the data in Chapter 2 proved to be insufficient to convincingly narrow down the co-stimulatory mechanism of 4-1BB and CD27 to a single one of the models proposed in Chapter 3, simulations of delayed co-stimulation in 3.2.3. suggest that the phenotype observed on already adapted T cells may allow for a clearer distinction between possible models. Since the mechanisms through k_{amp} and k_{act} are currently the most plausible models for 4-1BB co-stimulation, this suggests that even delayed addition of 4-1BBL will be able to rescue the cytokine response in adapted T cells (Fig. 3.11). Past studies have shown that 4-1BB signalling can prevent and revert T cell anergy (Wilcox et al., 2004) and ameliorate the exhaustion phenotype caused by chimeric antigen receptor signalling (Long et al., 2015; Zhao et al., 2015), despite Watts and colleagues reporting desensitisation of 4-1BB in exhausted murine T cells due to TRAF1 loss (Wang et al., 2012). However, these forms of T cell unresponsiveness are likely distinct from the adaptation phenotype we observe in our experimental system.

3. Delayed CD27 signalling is capable of reverting unresponsiveness in adapted T cells.

If 4-1BB-mediated rescue of adapted T cells can be confirmed, the same hypothesis can be tested for CD27. This will allow us to more precisely test our proposed models of CD27 co-stimulation (Table 3.12) and thereby either support or disprove the assumption of a shared co-stimulatory mechanism between 4-1BB and CD27. Constitutive co-stimulation through CD27 was unable to prevent adaptation in the time course series of experiments in Chapter 2. If this is solely due to early ligand-induced downregulation of CD27, this can be prevented by delaying the addition of CD70 until the T cells have adapted in order to observe potential effects of CD27 signalling on this form of unresponsiveness.

3.3.2. Model limitations

As already indicated in Chapter 3.2.1., the deterministic models used in this chapter are scaled up from a single "cell" with fixed parameters, which means they only simulate the response of a theoretical population of identical cells. This causes several properties of the simulations which are irreconcilable with experimental data.

The threshold switch converts the T cell signalling into an all-or-nothing response, and the qualities and quantity of upstream stimuli only determine when cytokine production turns on or is shut off. Such a digital nature of the T cell response has been shown for the activation of signalling molecules, especially ERK (Altan-Bonnet and Germain, 2005; Das et al., 2009), as well as the synthesis of cytokines at mRNA and protein level (Bucy et al., 1994; Huang et al., 2013). Very sharp transitions in the response from 'on' to 'off', both in time and in the dose-response curves, are the consequence of this analogue-to-digital signal conversion in our simulations. However, population responses from real T cells do not produce such steep curves, owing to the heterogeneity in the cell population (Fig. 3.4).

Altan-Bonnet and Germain demonstrated the effects of this "biological variation" in their model of T cell antigen discrimination, where introduction of noise converts the digital response of the individual cell into a dose-response curve with a low Hill coefficient on the population level (Altan-Bonnet and Germain, 2005). Moreover, as discussed in Chapter 3.2.1., heterogeneity in the population would cause individual cells to start and stop cytokine production at variable times, smoothening out the response curves in time, as well.

Sources of biological variation in our experimental system can be T cell-intrinsic, e.g. expression of receptors and signalling proteins may slightly vary between cells, as well as the epigenetic and metabolic state of the cells. T cell-extrinsic sources of noise could be the time it takes for individual cells to make productive contact with the plate surface and micron-scale variation in ligand density. In the context of our model, there are no straightforward ways to determine the variation in each parameter, since many of them do not represent tangible biophysical quantities. While it is likely that there is some degree of heterogeneity in each parameter, they each contribute to noise to variable extents. Very small differences in the threshold, for example, produce large effects on the shape of the cytokine dose-response and time course, whereas even large variance in the parameter k_4 will hardly affect the population response, as differences in cytokine production rate between individual cells will be averaged out. Therefore, we decided against explicitly modelling this heterogeneity while keeping in mind the effects it will have on the T cell response.

Chapter 4: Validating a phenotypic model of CD8$^+$ T cell co-stimulation through TNFRSF members

In Chapter 2, we found that co-stimulation through two representative TNFRSF members produced quite different phenotypes, with 4-1BB co-stimulation being able to prevent the shutdown of cytokine production by T cell adaptation, whereas CD27 only enhanced the early cytokine response without affecting the adaptation behaviour. The similar signalling pathways downstream both receptors suggest that this discrepancy is likely due to the differential expression pattern of 4-1BB and CD27 rather than intrinsically different mechanisms.

In an attempt to confirm this using our phenotypic modelling approach, we systematically simulated potential mechanisms through which co-stimulation could potentially enhance the T cell response in our minimal model of T cell activation and adaptation in Chapter 3, and found one model to be applicable to both 4-1BB and CD27 co-stimulation. However, we were unable to conclusively reject two alternative models of signal integration based on the time course data from Chapter 2 alone. Instead, simulations of delayed co-stimulation generated another set of hypotheses (summarised in Section 3.3.1.) to test in order to narrow down the list of valid models. Most importantly, if 4-1BB and CD27 indeed share the same co-stimulation mechanism, delayed co-stimulation of already adapted T cells through either of these receptors should be able to rescue their ability to produce cytokine. This chapter focuses on testing these hypotheses, and on further validation experiments to support a confirmed model of TNFRSF co-stimulation.

4.1. Experimental design

In order to test the hypotheses derived from the computational modelling presented in Chapter 3, we sought to modify our plate-based experimental system to allow for introduction or removal of ligands mid-experiment. Simply adding the additional ligands to the cells at later time points would be sub-optimal, as we cannot guarantee timely immobilisation of these ligands, and a considerable fraction of binding sites on the plate-bound streptavidin is likely blocked by the biotin in the T cell culture medium. Removing receptor-ligand interactions with blocking antibodies also has the disadvantages of possible off- and on-target side-effects, and complete removal of binding might not be realistic at high ligand doses.

Therefore, we decided to prepare multiple plates with the desired conditions for each part of the experiment, and to change the doses and combinations of ligands mid-experiment by harvesting the T cells from the first stimulation plate and transferring them to another plate for secondary stimulation after a gentle wash at chosen time points. This also allowed us to easily separate the amounts of cytokine produced in the first and second stimulation phases as simulated in sub-chapter 3.2.3., since the supernatants of the primary stimulation are collected, and the cells receive fresh medium during the transfer. Several requirements had to be met by this method to ensure success:

1. The immobilisation of ligands has to be highly reproducible.

Technical variability was minimised by using streptavidin pre-coated plates from a manufacturer who guarantees a high standard and uniformity within the same batch, as well as using recombinant biotinylated ligands from the same production cycle.

2. Carry-over of ligands between stimulation plates has to be prevented.

Due to the extremely high affinity of the streptavidin-biotin interaction, it was relatively unlikely for ligands to be removed from the plates with the harvested cells. To demonstrate this, pMHC densities on the plates were quantified before addition of cells or after removal of cells from wells which were incubated with T cells (either with or without expression of the c58/c61 TCR; Fig. 4.1.). There was no detectable difference between the conditions for each pMHC, i.e. no sign of ligands being removed with the cells.

3. Viability of cells must not be impaired by the transfer process.

While additional harvesting and washing steps are likely to stress the cells, gentle handling of the cells minimises effects on their viability. To demonstrate this, cells that had undergone such a treatment were stained after the full experiment with 7-aminoactinomycin D (7-AAD), which allows for detection of dead cells with compromised membrane integrity (Fig. 4.2.). In this assay, cell viability remained around 90% at all conditions.

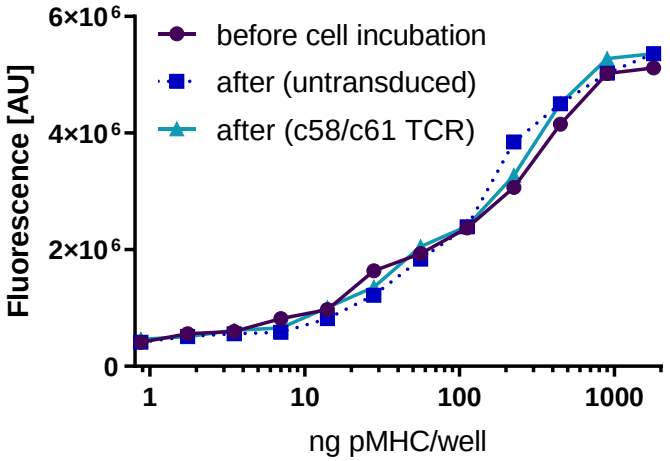

Figure 4.1: Harvesting cells from coated plates after stimulation does not dislodge detectable amounts of plate-bound pMHC. Densities of pMHC immobilised on streptavidin-coated plates were quantified using a conformation-sensitive anti-HLA-A/B/C antibody (clone w6/32) either before or after incubation with primary human $CD8^+$ T cells (either transduced with the c58/c61 TCR or untransduced) for 16h. Secondary antibody fluorescence was measured using a LICOR Odyssey® Sa Infrared Imaging System.

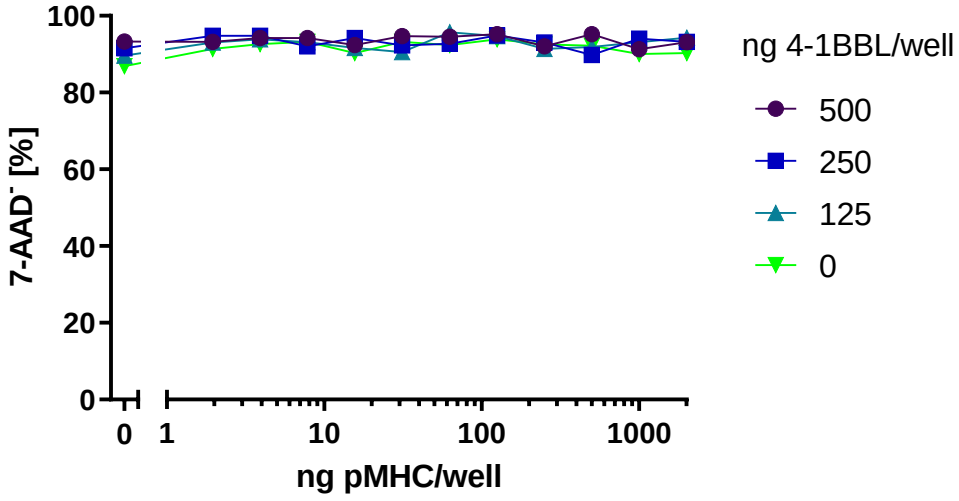

Figure 4.2: Transfer of cells between stimulation plates does not cause notable levels of cell death. Primary human CD8+ T cells transduced with the c58/c61 TCR were stimulated for 16h with pMHC and CD70 (each at 100 ng/well). Cells were harvested, washed, and stimulated for further 8h with pMHC and 4-1BBL at the indicated doses. Cell death after the experiment was quantified by 7-AAD staining and flow cytometry.

4.2. Results

4.2.1. 4-1BB is a bona-fide co-stimulatory receptor

Whether or not 4-1BB signalling can induce a T cell response on its own has been confounded by the requirement of TCR signalling for 4-1BB expression. To test this hypothesis, 4-1BB expression was induced by stimulating T cells with pMHC and CD70 at 100ng/well each for 16 hours. This combination of ligands was found in Chapter 2 to induce high 4-1BB expression without complete TCR downregulation (Fig. 4.3A) due to CD27 co-stimulation lowering the EC_{50} of 4-1BB expression without affecting the TCR levels.

These pre-stimulated cells were then harvested and transferred to a secondary plate containing a range of pMHC doses with or without 4-1BBL (Fig. 4.3B). Even in this secondary 8-hour stimulation, cytokine production was still strictly TCR signalling-dependent, as none was observed in absence or at low doses of pMHC. Therefore, this experiment shows that, like CD27, 4-1BB is unable to induce TCR-independent cytokine responses and can therefore be considered a bona-fide co-stimulatory receptor. This also means that the proposed model of 4-1BB co-stimulation through k_{act} can be rejected (see Table 3.12).

Interestingly, as the T cells were only adapted to 100ng/well of pMHC due to the primary round of stimulation, higher doses of pMHC were sufficient to induce IFN-γ and TNF responses in the secondary stimulation, which were boosted by the addition of 4-1BBL in a dose-dependent manner. IL-2 production was not observed, possibly due to IL-2 consumption (previously seen in the time course

experiments in Chapter 2) surpassing and thereby masking the IL-2 production rate. 4-1BB co-stimulation, however, rescued all cytokine responses, even at pMHC doses slightly below 100ng/well, providing a first indication that 4-1BB signalling can revert adaptation, which is tested in the subsequent set of experiments.

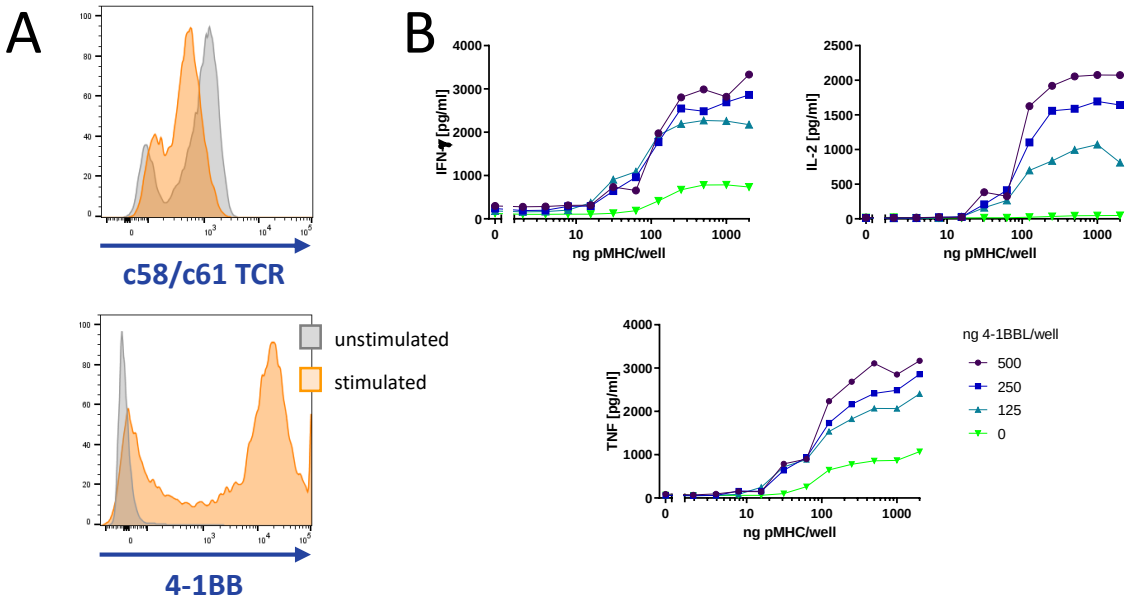

Figure 4.3: 4-1BB does not trigger TCR-independent cytokine responses. Primary human $CD8^+$ T cells transduced with the c58/c61 TCR were stimulated for 16h with pMHC and CD70 (each at 100 ng/well) in order to induce 4-1BB expression with minimal TCR downregulation. Cells were harvested, washed, and stimulated for a further 8h with pMHC and 4-1BBL at the indicated doses. **(A)** TCR and 4-1BB expression on cells before and after the 16h pre-stimulation from one representative experiment out of four. Surface c58/c61 TCR and 4-1BB were labelled with fluorescent high-affinity pMHC tetramers and anti-4-1BB antibodies, respectively, and quantified by flow cytometry. **(B)** T cell response during the secondary 8h stimulation from one representative experiment out of four. The production of the cytokines IFN-γ, IL-2 and TNF into the culture medium supernatant was quantified by ELISA.

4.2.2. 4-1BB co-stimulation rescues already adapted CD8$^+$ T cells from unresponsiveness

To formally test whether 4-1BB co-stimulation can revert (rather than prevent) this unresponsive phenotype, adaptation was induced by first stimulating T cells with a dose-range of pMHC for 16 hours (Fig. 4.4A). When transferred to the same doses of pMHC for another 8 hours, the cells hardly produced any further cytokine, which shows that they had become successfully adapted.

Addition of 4-1BBL to the secondary stimulation was indeed capable of rescuing the cytokine response of these adapted cells, with IFN-γ and TNF production even surpassing the levels of the primary 16-hour stimulation (Fig. 4.4B and C). In the case of IL-2, the rescue appeared to be weaker, but this might again be due to increased IL-2 consumption in the secondary stimulation, as activated T cells upregulate the expression of the IL-2 receptor alpha chain CD25 (Supplementary Figure S.9).

Extraction of EC_{50} values from the cytokine dose-response curves also shows a slight EC_{50} decrease with the delayed 4-1BB co-stimulation, in comparison to the primary stimulation or post-transfer to pMHC alone (Fig. 4.4D). Taken together, and with the k_{act} model rejected previously, this narrows down the likely mechanism of 4-1BB co-stimulation to k_{amp} in our model, according to the simulations in Chapter 3 summarised in Table 3.12.

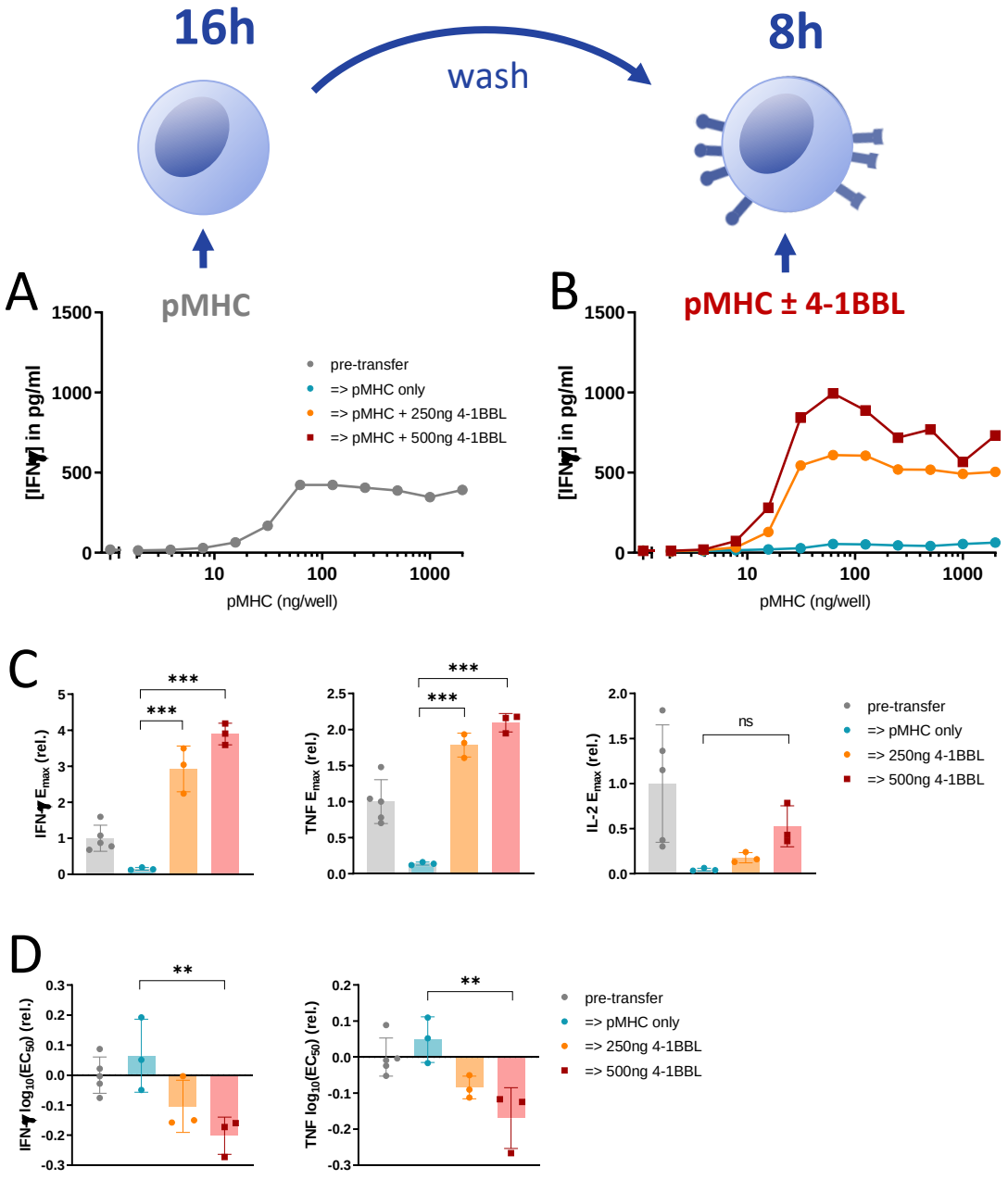

Figure 4.4: 4-1BB co-stimulation reverts T cell unresponsiveness to pMHC even after adaptation has set in. Primary human CD8$^+$ T cells transduced with the c58/c61 TCR were stimulated for 16h with pMHC doses varying from 0 to 2000 ng/well. Cells were harvested, washed and stimulated for further 8h with identical pMHC doses which they were adapted to, in absence or presence of 4-1BBL. The production of the cytokines IFN-γ, IL-2 and TNF into the culture medium supernatant was quantified by ELISA. **(A)** T cell response during the first 16h stimulation from one representative experiment. **(B)** T cell response during the secondary 8h stimulation from the same experiment. E_{max} **(C)** and EC_{50} **(D)** values from three separate experimental repeats were extracted from dose-response curve fits, normalised to the means of each individual experiment and plotted as fold change relative to the cytokine response during the 16h pre-stimulation. Post-transfer conditions were compared using one-way ANOVA with Šídák's correction for multiple comparisons. This statistical analysis was performed in GraphPad Prism 8. Abbreviations: ns = p-value > 0.05; * = p-value < 0.05; ** = p-value < 0.01; *** = p-value < 0.001

4.2.3. GITR co-stimulation can partially restore the cytokine response of adapted CD8⁺ T cells

By separating the cytokine measurements in the first 16 hours and a subsequent 8-hour stimulation phase, we are able to more reliably detect small changes in the later stages of the T cell response which might otherwise be masked by the large amounts of cytokine produced pre-adaptation. We suspected this might be the case for GITR co-stimulation which we found to be weak in the previous experiments in Chapter 2, due to measurements of cumulative cytokine produced in a time course.

If the relatively small effect of GITR co-stimulation (compared to 4-1BB) is merely due to its low expression on CD8⁺ T cells and if it otherwise shares the same co-stimulatory mechanism with 4-1BB, delayed GITR co-stimulation should also be able to rescue the cytokine response of adapted T cells to a certain extent. In order to test this hypothesis, an analogous experiment to the one presented in Section 4.2.2. was carried out, where CD8⁺ T cells were stimulated with a dose-range of pMHC for 16 hours to induce adaptation, and then transferred to the same dose-range of pMHC with or without the addition of GITRL (Fig. 4.5).

Once again, while pMHC on its own induced a greatly diminished cytokine response after adaptation, IFN-γ and TNF production were rescued by GITR co-stimulation (Fig. 4.5B and C), albeit to a lesser extent compared to 4-1BB, as expected: When comparing Figures 4.4C and 4.5C, on average 4-1BB co-stimulation led to 4-fold higher IFN-γ and 2-fold higher TNF production in the

secondary stimulation phase. However, no rescue of IL-2 production was observed. Whether this was due to the production rate remaining below the consumption rate, or whether GITR co-stimulation was simply unable to affect the expression of IL-2 could not be conclusively determined with the methods employed in this experiment.

The rescued IFN-γ and TNF responses also had a slightly lower EC_{50} compared to the cytokines measured during the primary stimulation or post-transfer to pMHC alone (Fig. 4.5D). This also confirms that the k_{amp} model is the most suitable for GITR amongst the ones proposed in Chapter 3, indicating that the co-stimulatory mechanism could indeed be shared between 4-1BB and GITR.

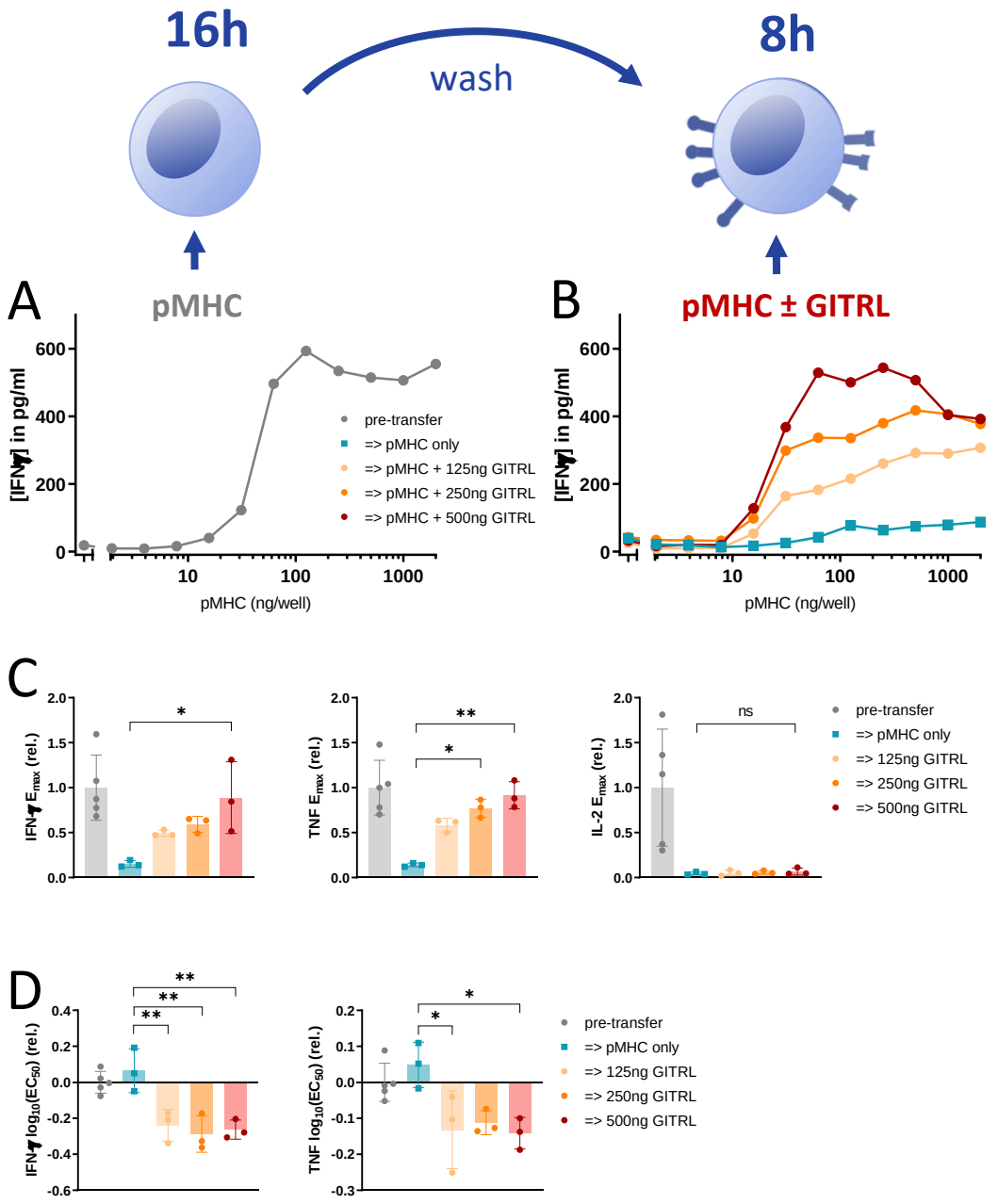

Figure 4.5: GITR co-stimulation reverts T cell unresponsiveness to pMHC after adaptation has set in. Primary human CD8⁺ T cells transduced with the c58/c61 TCR were stimulated for 16h with pMHC doses varying from 0 to 2000 ng/well. Cells were harvested, washed and stimulated for further 8h with identical pMHC doses which they were adapted to, in absence or presence of GITRL. The production of the cytokines IFN-γ, IL-2 and TNF into the culture medium supernatant was quantified by ELISA. **(A)** T cell response during the first 16h stimulation from one representative experiment. **(B)** T cell response during the secondary 8h stimulation from the same experiment. E_{max} **(C)** and EC_{50} **(D)** values from three separate experimental repeats were extracted from dose-response curve fits, normalised to the means of each individual experiment and plotted as fold change relative to the cytokine response during the 16h pre-stimulation. Post-transfer conditions were compared using one-way ANOVA with Šídák's correction for multiple comparisons. This statistical analysis was performed in GraphPad Prism 8. Abbreviations: ns (not significant) = p-value > 0.05; * = p-value < 0.05; ** = p-value < 0.01; *** = p-value < 0.001

4.2.4. Delayed, but not constitutive, CD27 co-stimulation rescues adapted CD8⁺ T cells from unresponsiveness

Another hypothesis to be tested was whether CD27 co-stimulation could also revert T cell adaptation, if CD27 is expressed during a relevant time frame. For this purpose, CD8⁺ T cells were stimulated with pMHC for 16 hours to induce adaptation, and were then transferred to another plate with the same pMHC dose-range, either with or without CD70, for a secondary stimulation of 8 hours (Fig. 4.6, blue curves, and Fig 4.7, blue bars). This experiment showed that CD27 co-stimulation was indeed able to rescue the cytokine response when added after adaptation had been induced. Moreover, the EC_{50} of the rescued responses was also slightly decreased compared to the cytokine dose-responses of pre- and post-transfer stimulation with pMHC only (Fig. 4.7C, blue bars), confirming that the k_{amp} model is indeed also most applicable to CD27 co-stimulation and therefore describes a shared co-stimulatory mechanism of the three TNFR family members tested (see Table 3.12).

Interestingly, despite the relatively high expression of CD27 on CD8⁺ T cells compared to GITR (Fig. 2.9), the secondary cytokine response rescued by CD27 co-stimulation (Fig. 4.7B, blue bars) is barely on par with the one achieved with GITR co-stimulation (Fig. 4.5C) and thus much weaker than the 4-1BB counterpart (Fig. 4.4C). This is likely a consequence of CD27 rapidly being downregulated in the presence of its ligand (Fig. 2.5), allowing only for a very transient rescue, whereas

the expression of activation-induced receptors is sustained as long as the T cells remain active. However, convincingly proving this would require another time course experiment.

The above transfer experiment was also performed with CD70 added also to the first stimulation phase (Fig. 4.6, orange curves, and Fig. 4.7, orange bars) to demonstrate that early and constant presentation of CD70 is unable to affect the adaptation phenotype (as seen in Chapter 2). As expected, CD27 co-stimulation becomes a lot less effective at rescuing the response in the second stimulation phase in this case (Fig. 4.6B and 4.7B).

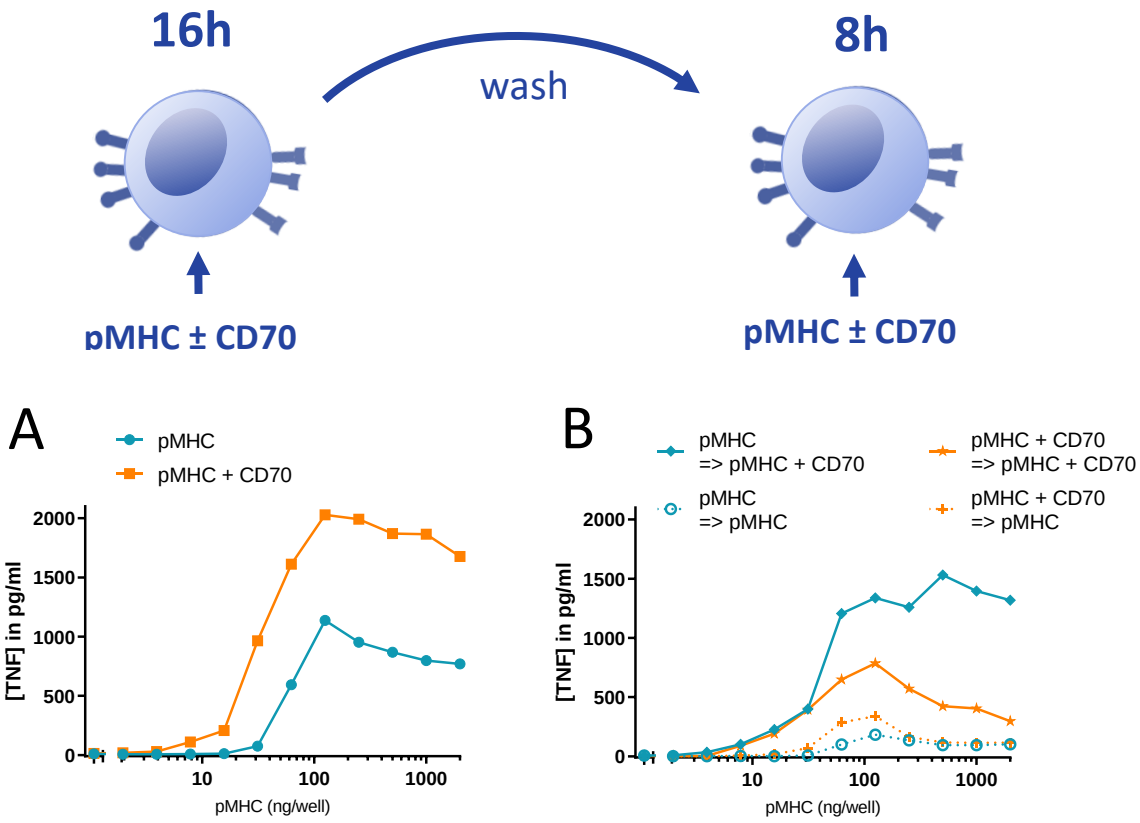

Figure 4.6: Delayed (but not constitutive) CD27 co-stimulation reverts T cell adaptation. Primary human $CD8^+$ T cells transduced with the c58/c61 TCR were stimulated for 16h with pMHC doses varying from 0 to 2000 ng/well in presence or absence of 200 ng/well CD70. Cells were harvested, washed and stimulated for further 8h with identical pMHC doses which they were adapted to, with or without addition of 200 ng/well CD70. The production of the cytokines IFN-γ, IL-2 and TNF into the culture medium supernatant was quantified by ELISA. **(A)** T cell response during the first 16h stimulation from one representative experiment. **(B)** T cell response during the secondary 8h stimulation from the same experiment.

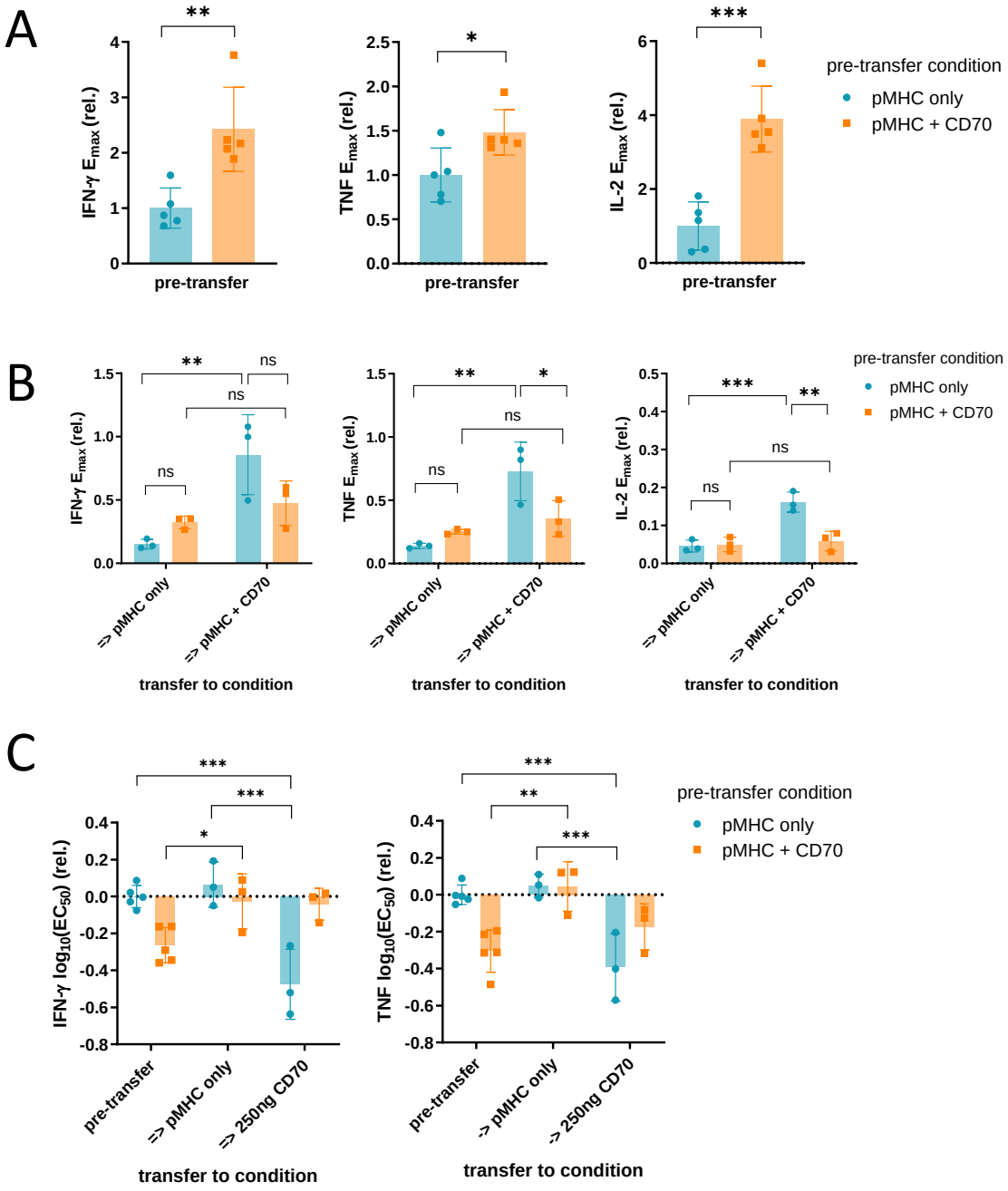

Figure 4.7: Delayed (but not constitutive) CD27 co-stimulation reverts T cell adaptation (statistical analysis). E_{max} **(A)(B)** and EC_{50} **(C)** values from three separate repeats of the experiment shown in Fig. 4.6 were extracted from dose-response curve fits, normalised to the means of each individual experiment and plotted as fold change relative to the cytokine response during the 16h pre-stimulation without co-stimulation. Pre-transfer conditions (pMHC with or without CD70) in (A) were compared with a two-tailed t-test. Conditions in (B) and (C) were compared using one-way ANOVA with Šídák's correction for multiple comparisons. This statistical analysis was performed in GraphPad Prism 8. Abbreviations: ns (not significant) = p-value > 0.05; * = p-value < 0.05; ** = p-value < 0.01; *** = p-value < 0.001

4.2.5. Phenotypic model simulations predict synergy between CD27 and inducible TNFRSF members

The results from the experiments in 4.2.1 through 4.2.4 are consistent with a model where 4-1BB, CD27 and GITR share the same co-stimulatory mechanism through the parameter k_{amp} which amplifies TCR signalling, allowing weaker stimuli (e.g. post-adaptation) to overcome the threshold to activate a T cell response. The divergent phenotypes observed with co-stimulation through each of these receptors are explained by differences in expression regulation and levels. Figure 4.8A visualises this model as a cartoon schematic. As 4-1BB and GITR are induced by T cell activation through the TCR, a positive feedback replenishes their expression, counteracting the ligand-induced downregulation to some extent. Therefore, co-stimulation through these receptors is less transient than CD27 co-stimulation, which has no such re-expression mechanism.

However, this circuit also suggests that CD27 co-stimulation, which can act during the early T cell activation phase (due to CD27 being expressed on resting T cells), will increase the expression of 4-1BB and GITR by enhancing the T cell response in general. The experimental data in sub-chapter 2.3.3. already hinted at this, with slightly higher 4-1BB expression on cells that received CD27 co-stimulation (Fig. 2.5C and D). It is plausible that this increased expression will later improve co-stimulation through these inducible TNFR family members.

To illustrate this, a simulation of this model was run, (similarly to the previous experiments) comprising a first 16-hour stimulation phase with pMHC with or

without CD70, and a subsequent transfer to pMHC with or without 4-1BBL for 8 hours (Fig. 4.8B). As shown before, the simulated T cell response in the first phase is improved by CD27 co-stimulation with increases in cytokine production and 4-1BB expression (Fig. 4.8C and E). A simulation of the secondary 8-hour stimulation shows that the 4-1BBL-mediated rescue of the cytokine response can indeed be enhanced by the elevated 4-1BB expression level (Fig. 4.8D).

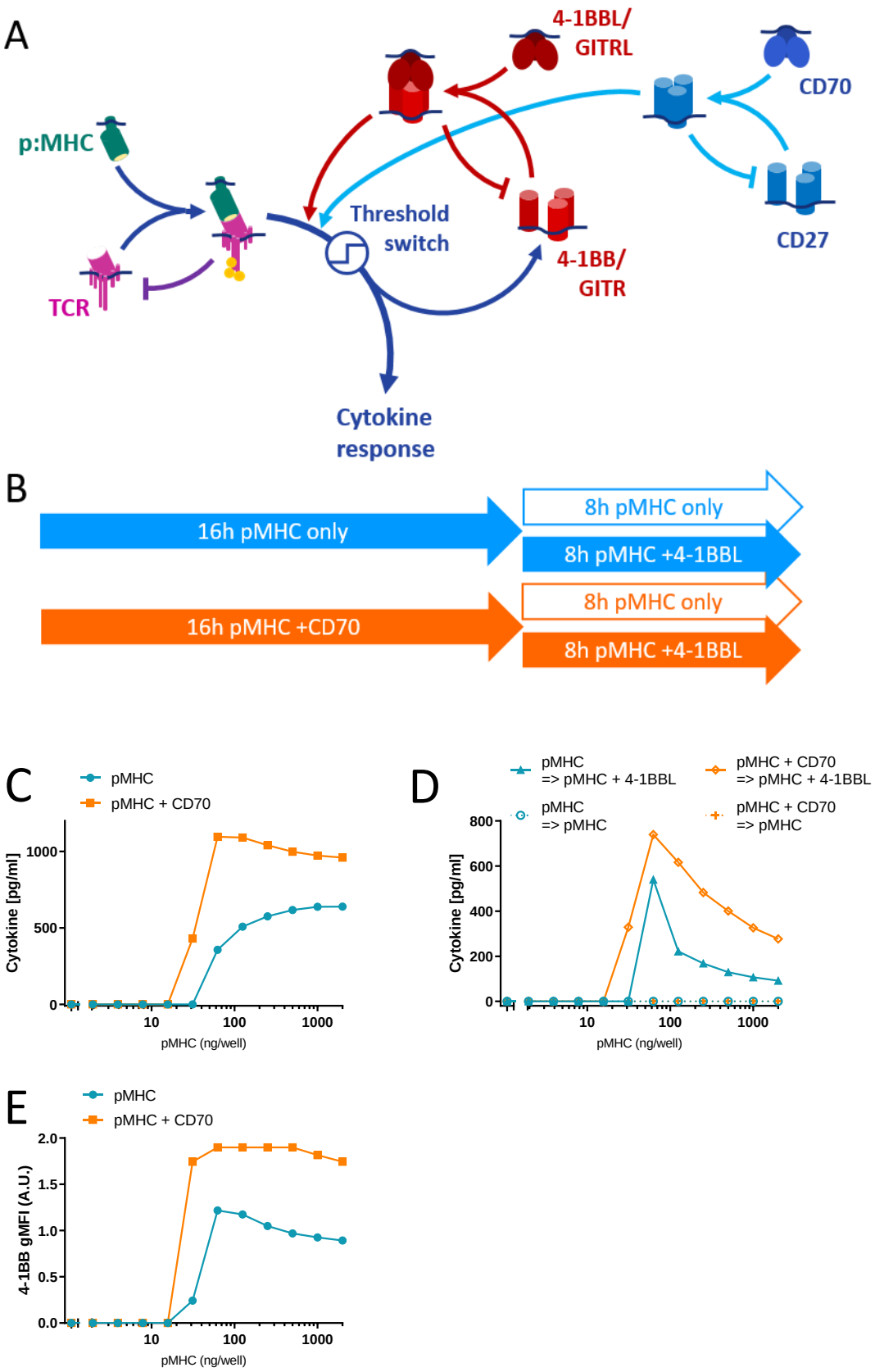

Figure 4.8: Simulation of both 4-1BB and CD27 co-stimulation modulating k_{amp} predicts synergy. (Description on next page.)

Figure 4.8: (previous page) **Simulation of both 4-1BB and CD27 co-stimulation modulating k_{amp} predicts synergy.** CD70 and CD27 were modelled as in Fig. 3.2 and 4-1BBL and 4-1BB were modelled as in Fig. 3.5, with co-stimulation through both receptors increasing k_{amp} **(A).** As indicated in **(B)**, cytokine response **(C)** and 4-1BB expression **(E)** were simulated for a 16-hour stimulation with pMHC only (blue) or presence of CD70 (orange). Afterwards, cells were transferred to identical pMHC doses for another 8 hours, with or without addition of 4-1BBL. Simulations are shown for the cytokine produced in this 8-hour time window **(D)**. k_{amp}: rate of signalling amplification, k_{act}: rate of direct (TCR-independent) cytokine production.

4.2.6. Co-stimulation through CD27 enhances 4-1BB expression and potency of co-stimulation with 4-1BBL

The experiment simulated in sub-chapter 4.2.5. was carried out by stimulating $CD8^+$ T cells with a dose-range of pMHC either with or without CD70 for 16 hours, before they were transferred to another plate with the same dose-range of pMHC, here with or without 4-1BBL.

As seen before, CD27 co-stimulation during the first stimulation phase resulted in increased cytokine production, but also enhanced the expression of 4-1BB (Fig. 4.9A and C). Figures 4.9B and 4.10A show that this high expression of 4-1BB had a functional effect in the second 8-hour stimulation, with significantly improved rescue of cytokine responses through 4-1BB co-stimulation, which is consistent with the simulated results. Most strikingly, cells that had received CD27 co-stimulation in the first stimulation produced high levels of IL-2 in the second stimulation in the presence of 4-1BBL, whereas 4-1BB co-stimulation was

relatively ineffective at rescuing the secondary IL-2 response from cells that had not been co-stimulated in the first 16 hours.

Interestingly, since CD27 co-stimulation also lowered the EC_{50} of 4-1BB expression, causing 4-1BB to be induced at lower pMHC doses (Fig. 4.9C, see also Fig. 2.8), this resulted in a further significant decrease in the EC_{50} of the cytokine response that was rescued by 4-1BBL in the second stimulation (Fig. 4.10B).

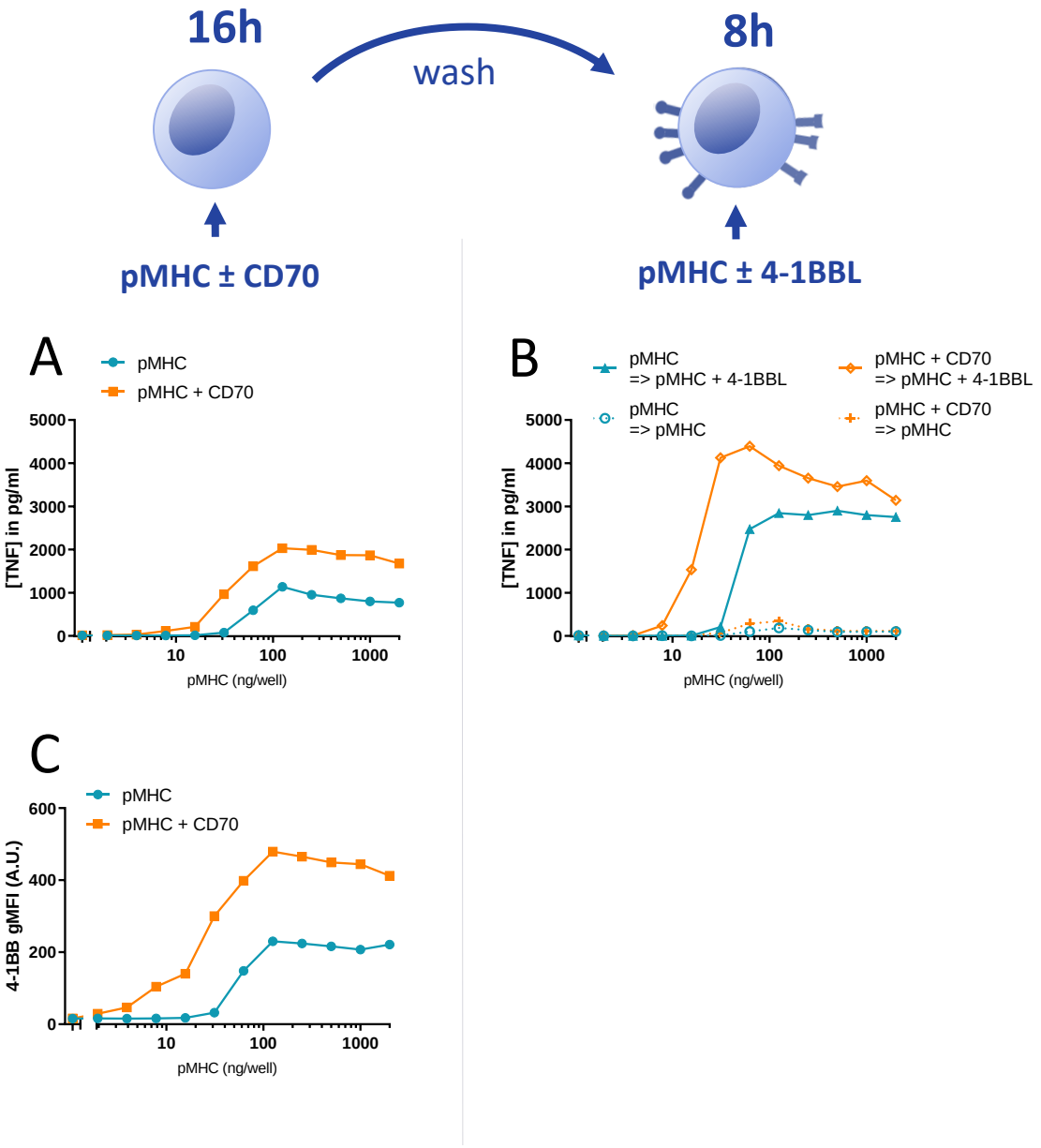

Figure 4.9: CD27 co-stimulation enhances 4-1BB expression and effectiveness. Primary human CD8+ T cells transduced with the c58/c61 TCR were stimulated for 16h with pMHC doses varying from 0 to 2000 ng/well in presence or absence of 200 ng/well CD70. Cells were harvested, washed and stimulated for further 8h with identical pMHC doses which they were adapted to, with or without addition of 500 ng/well 4-1BBL. The production of the cytokines IFN-γ, IL-2 and TNF into the culture medium supernatant was quantified by ELISA. **(A)** T cell response during the first 16h stimulation from one representative experiment. **(B)** T cell response during the secondary 8h stimulation from the same experiment. **(C)** Cells from designated duplicate samples in the same experiment were stained with fluorescent anti-4-1BB antibodies and analysed by flow cytometry.

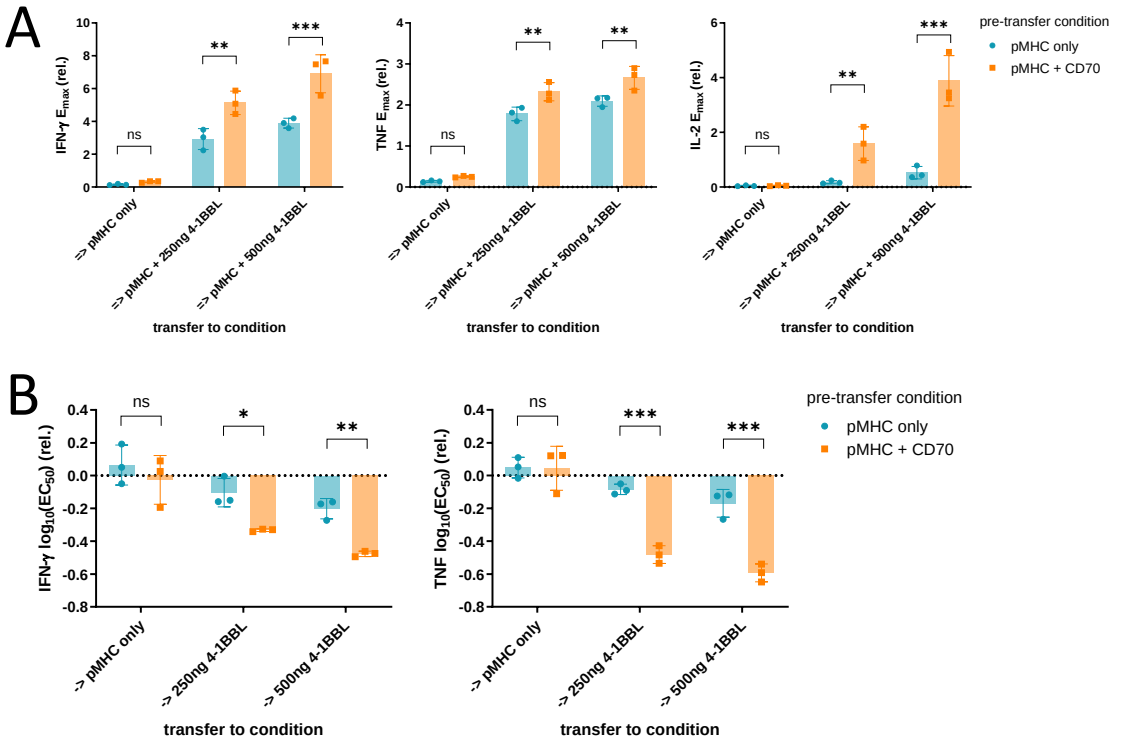

Figure 4.10: CD27 co-stimulation enhances 4-1BB expression and effectiveness (statistical analysis). E_{max} **(A)** and EC_{50} **(B)** values from three separate repeats of the experiment shown in Fig. 4.9 were extracted from dose-response curve fits, normalised to the means of each individual experiment and plotted as fold change relative to the cytokine response during the 16h pre-stimulation without co-stimulation. Post-transfer conditions in were compared using one-way ANOVA with Šídák's correction for multiple comparisons. This statistical analysis was performed in GraphPad Prism 8. Abbreviations: ns (not significant) = p-value > 0.05; * = p-value < 0.05; ** = p-value < 0.01; *** = p-value < 0.001

4.2.7. Co-stimulation through CD27 enhances GITR expression and potency of co-stimulation with GITRL

Like 4-1BB, GITR expression is T cell activation-induced, suggesting that it forms a very similar circuit that allows for synergy with CD27 co-stimulation (Fig. 4.8). Therefore, we carried out the same experiment as in 4.2.6., only replacing 4-1BBL with GITRL.

CD27 co-stimulation indeed enhanced GITR expression, especially at lower doses of pMHC (Fig. 4.11C). This resulted in improved rescue of the cytokine response by GITRL in the second stimulation (Fig. 4.11B and 4.12). While in terms of overall magnitude (E_{max}), this improvement was only statistically significant for IFN-γ when averaged across three independent repeats (Fig. 4.12A), a significant EC_{50} decrease was seen for TNF, and partially for IFN-γ (Fig. 4.12B).

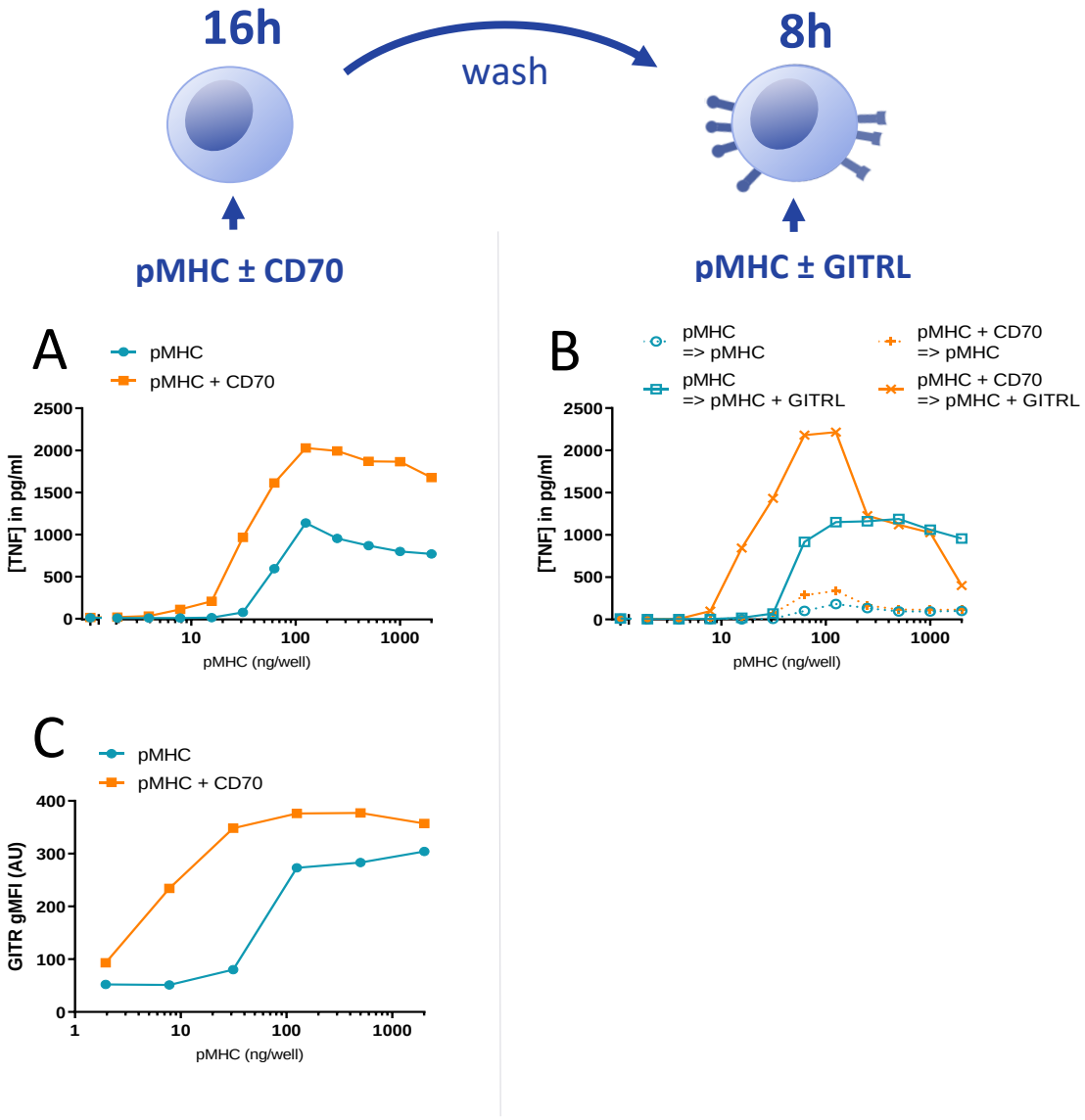

Figure 4.11: CD27 co-stimulation enhances GITR expression and effectiveness. Primary human CD8⁺ T cells transduced with the c58/c61 TCR were stimulated for 16h with pMHC doses varying from 0 to 2000 ng/well in presence or absence of 200 ng/well CD70. Cells were harvested, washed and stimulated for further 8h with identical pMHC doses which they were adapted to, with or without addition of 500 ng/well GITRL. The production of the cytokines IFN-γ, IL-2 and TNF into the culture medium supernatant was quantified by ELISA. **(A)** T cell response during the first 16h stimulation from one representative experiment. **(B)** T cell response during the secondary 8h stimulation from the same experiment. **(C)** Cells from designated duplicate samples in the same experiment were stained with fluorescent anti-GITR antibodies and analysed by flow cytometry.

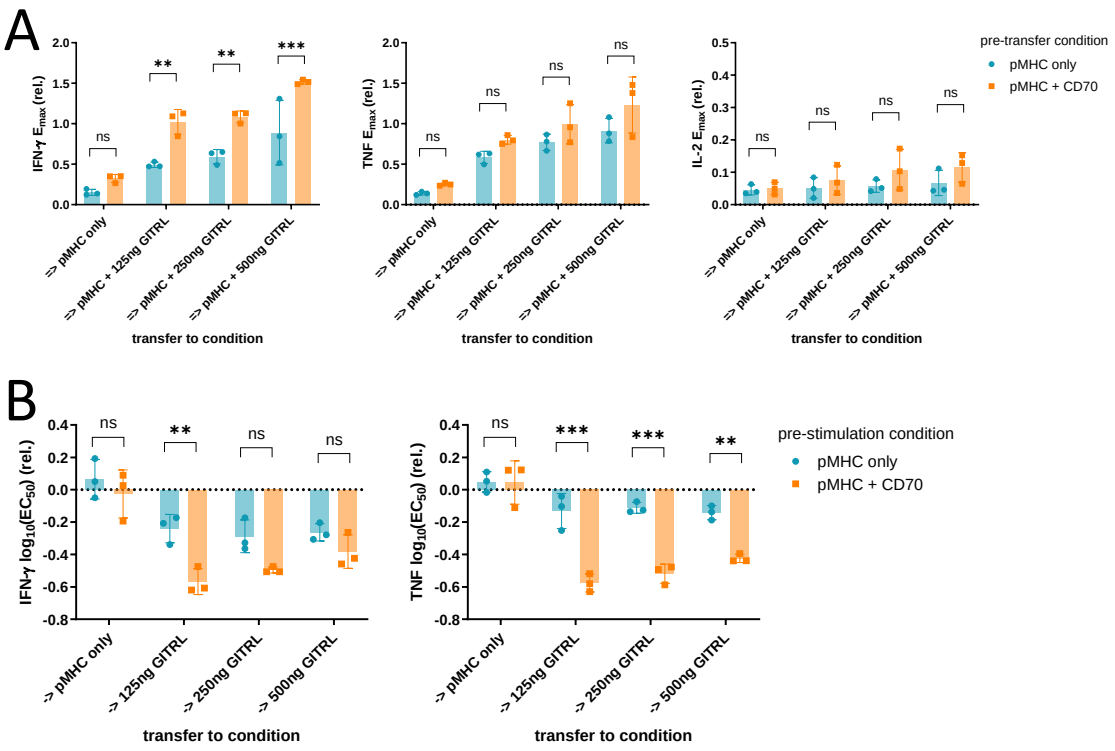

Figure 4.12: CD27 co-stimulation enhances GITR expression and effectiveness (statistical analysis). E_{max} **(A)** and EC_{50} **(B)** values from three separate experimental repeats were extracted from dose-response curve fits, normalised to the means of each individual experiment and plotted as fold change relative to the cytokine response during the 16h pre-stimulation without co-stimulation. Post-transfer conditions in were compared using one-way ANOVA with Šídák's correction for multiple comparisons. This statistical analysis was performed in GraphPad Prism 8. Abbreviations: ns (not significant) = p-value > 0.05; * = p-value < 0.05; ** = p-value < 0.01; *** = p-value < 0.001

4.3. Discussion

The set of experiments in this chapter allowed for the validation of a phenotypic model that captures the quantitative effects of co-stimulation through TNFRSF members on the T cell cytokine response. The results confirmed that TNFR family members share a common co-stimulatory mechanism, while variations in phenotype are primarily caused by differences in expression kinetics and levels.

A synergy between CD27 and the inducible TNFR family members 4-1BB and GITR based on receptor expression regulation was predicted by this model, which was later confirmed by a set of follow-up experiments in sub-chapters 4.2.6. and 4.2.7., where previous co-stimulation through CD27 enhanced both the expression of 4-1BB and GITR as well as the potency of reinvigoration of adapted T cells by 4-1BBL and GITRL.

Interestingly, not only were changes in the magnitude (E_{max}) observed, but early co-stimulation through CD27 also resulted in additional multiplicative decreases in EC_{50} during the later stimulation with 4-1BBL or GITRL, to a greater extent than predicted by the model. This is likely due to the limitation of our model when simulating responses of heterogeneous cell populations, as laid out in 3.3.2. (Model limitations). The simulated dose-responses are steeper than the experimental data, where small variability between cells will enable a proportion of them to respond and induce the expression of 4-1BB and GITR at lower doses, which allows them to benefit from stronger co-stimulation with further sensitivity-enhancing effects.

While these EC_{50} changes are still not comparable with those induced by additional adhesion molecules such as LFA-1 and CD2 (Bachmann et al., 1997, 1999), they arise through a different mechanism, which we identified for TNFRSF co-stimulation as the amplification of TCR signalling, lowering amount of signalling pMHC-TCR complexes required to overcome the intracellular machinery's threshold switch. This is comparable to previous studies of CD28 co-stimulation where threshold-lowering effects were observed (Iezzi et al., 1998; Viola and Lanzavecchia, 1996), even though CD28 is known to function as a signalling-enhancing receptor rather than mediating adhesion. This also suggests the possibility that on natural APCs where numerous co-stimulatory receptor-ligand pairs come into play, the multiplicative synergy of many minuscule effects on the EC_{50} could partially explain the reported extreme sensitivity of T cells to pMHC (Huang et al., 2013).

Chapter 5: Conclusions

5.1. Summary

A reductionist plate-based experimental system was used to stimulate primary human $CD8^+$ T cells with high throughput. Originally developed to characterise the T cell response to recombinant pMHCs with varying affinities (Lever et al., 2016), we observed a universal shutdown of pMHC-induced cytokine production within 4-8 hours, despite the continuous presence of ligand (Trendel et al., 2019). We interpreted this phenomenon as adaptation as seen for receptors in other cellular systems, a potentially TCR downregulation-dependent mechanism to limit the T cell response distinct from anergy and exhaustion. Extending this experimental platform to include additional recombinant ligands to other receptors on T cells allowed for the detailed study of co-stimulation, in this case with a focus on receptors of the TNFR superfamily, especially 4-1BB and CD27. The main advantage of such a minimal system here is that co-stimulation through a particular receptor can be examined in isolation, in contrast to experiments with natural APCs where numerous additional co-signalling ligands can have confounding effects.

In time course measurements of the T cell cytokine response to a dose-range of pMHC in absence or presence of co-stimulatory ligands, we confirmed differences in phenotypes for 4-1BB and CD27 co-stimulation despite the high degree of similarity between the signalling pathways downstream of these receptors. While 4-1BBL had little effect at the earliest time point (4 hours), it markedly increased the amount of cytokine produced by 16 and 24 hours. This was predominantly the result of adaptation apparently being prevented at sufficient doses of 4-1BBL.

CD70 (the ligand to CD27), on the other hand, boosted cytokine production at the early time points but did not prevent adaptation – thus, the response stopped at the same time scale of 4-8 hours. The enhancement of the cytokine response in both cases mainly manifested in the form of increases in magnitude (E_{max}), with only minor effects on EC_{50} and TCR downregulation.

Interestingly, the differences in phenotype between 4-1BB and CD27 co-stimulation coincided with the differential expression pattern of these receptors. 4-1BB is not expressed on resting T cells, a likely reason for the lack of effect at the earliest time point, and its surface expression is induced by T cell activation through the TCR, reaching its peak between 8 and 16 hours. In contrast, CD27 is highly expressed on resting T cells and rapidly (< 4 hours) downregulated in presence of its ligand CD70, while this ligand-induced downregulation in the case of 4-1BB is counter-acted to some extent by the activation-induced expression rate, possibly explaining why 4-1BB co-stimulation can act at later time points after adaptation whereas CD27 co-stimulation cannot.

Applying the same methods to examine GITR and OX40 co-stimulation, we observed weak effects reminiscent of low doses of 4-1BBL. Expression of GITR and OX40 is also activation-induced and relatively weak on the $CD8^+$ T cells in our experimental system, once again suggesting that the differences in phenotype are primarily determined by receptor expression levels and regulation.

To further analyse whether this is the case, we employed mathematical modelling to systematically simulate the various mechanisms through which co-stimulation could potentially enhance the T cell response in our minimal model of T cell

activation and adaptation. While the experimental data generated in Chapter 2 was insufficient to conclusively narrow down the likely co-stimulation mechanisms for the TNFR family, the simulations gave rise to a set of hypotheses that could be tested experimentally in order to either validate or reject the models of alternative co-stimulation mechanisms. Most importantly, simulation of whether and to what extent delayed co-stimulation through 4-1BB and CD27 is able to rescue adapted cells from unresponsiveness gave distinct predictions for the various models.

Testing these hypotheses in follow-up experiments, we were able to confirm that not only CD27, but also 4-1BB is a bona fide co-stimulatory receptor, i.e. to induce a cytokine response, additional TCR signalling is absolutely required. Moreover, 4-1BB, GITR and CD27 co-stimulation were able to rescue the T cell response in pre-stimulated (i.e. already adapted) T cells to varying degrees, depending on receptor expression dynamics, verifying a model in which TNFR superfamily members share the same mechanism of action. By amplifying TCR signalling upstream of a threshold switch, co-stimulation through these receptors allows for T cell responses at lower levels of TCR signalling, resulting in sustained responses as the TCR is downregulated. Simulations of this model predict that expression of activation induced TNFRSF members could be enhanced by co-stimulation, suggesting the possibility of synergy between these receptors, which we verified for CD27 with either 4-1BB or GITR.

5.2. Implications for the field of T cell signalling

Here, we built a minimal model which can reproduce the quantitative effects of co-stimulation through TNFRSF members on the cytokine response of $CD8^+$ T cells and offers a simple mechanistic explanation of their course of action in the amplification of TCR signalling and reversion of T cell adaptation.

This integration point of TNFRSF co-stimulation with TCR signalling in our model is consistent with the literature on the molecular pathways of these receptors that suggests a cooperation on the level of transcription factors. TNFRSF signalling primarily activates NFκB and MAPK pathways and is not known to interfere with TCR-proximal processes. On the other hand, TCR signalling results in the efficient and sustained nuclear trans-localisation of the transcription factor NFAT through the calcium pathway, whereas its ability to activate AP-1 and NFκB in the absence of co-stimulation is known to be relatively poor in comparison (Macián et al., 2002; Marangoni et al., 2013; Wells, 2009). As T cells adapt to the pMHC stimulus and downregulate TCR signalling, co-stimulation through TNFRSF members can mitigate the lack of active AP-1 and NFκB, thereby rescuing cytokine production post-adaptation. However, as bona-fide co-stimulatory receptors, TNFRSF members cannot trigger effector functions by themselves, since TCR signalling is still required for NFAT activation. Interestingly, this also suggests that TCR signalling in adapted T cells is still sufficient to activate NFAT through the calcium pathway.

While adaptation through downregulated or refractory receptors is common in many other cellular systems, unresponsive states in T cells are usually described

as anergy and exhaustion with distinct underlying mechanisms (Schwartz, 2003; Wherry, 2011). However, these also include reduction of TCR signalling, either through downregulation of signalling molecules or upregulation of co-inhibitory receptors. Furthermore, imbalanced and predominant NFAT activation is also considered to be a major factor in the induction and maintenance of T cell anergy and exhaustion (Macián et al., 2002; Martinez et al., 2015; Wells, 2009). By supplementing the other main transcription factors of T cell activation (AP-1 and NFκB), it is thus plausible for co-stimulation through TNFRSF members to at least partially counteract these mechanisms, which has been reported for both T cell anergy and exhaustion *in vivo* (Long et al., 2015; Wilcox et al., 2004; Zhao et al., 2015).

It is worth noting that a coarse-grained phenotypic model like ours lacks the ability to provide molecular details or information on further qualitative effects such as enhanced T cell survival and metabolism, which can to some extent be derived from molecular maps of signalling pathways based on reported biochemical data. However, the simplicity of the model allows for reliable simulations of more complex inputs, such as combinations of several co-stimulatory ligands, as long as models for their receptors are available. As an example, we have shown that a previous encounter of CD27 co-stimulation can synergise with later 4-1BBL- or GITRL-mediated rescue of adapted T cells.

5.3. Synergy between co-stimulatory receptors

The synergy between the co-stimulatory receptors predicted by the phenotypic model and validated in Chapter 4 has several interesting implications:

First, this synergy does not require simultaneous co-stimulation through both CD27 and one of the induced TNFRSF members; in fact, their temporally differential expression preclude this for the most part. This means that these co-stimulatory signals can be integrated from encounters on separate antigen-presenting cells or even different tissues, depending on the T cells' homing behaviour.

Furthermore, with the expression of these receptors staggered in time, T cells at different stages of the immune response and their differentiation will find themselves dependent on different sets of co-stimulatory signals. Receptors found on naïve and resting T cells, such as CD27 and CD28 can modulate the priming and early response, but become inhibited or downregulated and are even permanently removed from terminally differentiated effector T cells (Romero et al., 2007; Strioga et al., 2011). The baton is passed to transiently induced receptors such as 4-1BB, which modulate the response of already primed T cells but also seem to lose their effectiveness in the final stages of the immune response as antigen is either cleared, or T cells become severely exhausted, leading to downregulation of either the receptor or its signalling machinery (Wang et al., 2012). Receptors with slower expression kinetics such as GITR can then take over. This later group of induced receptors will likely be most dependent on synergistic effects and expressed at levels proportional to the magnitude of preceding stimulation and co-

stimulation, allowing for a mechanism to match the duration of the response to the severity of the threat. With a concomitant pattern of co-inhibitory receptors progressively accumulating on activated, differentiated and exhausted T cells, such a “tidal model” of the immune response was proposed by Chen and colleagues in a more generalised fashion in 2011 (Zhu et al., 2011).

Moreover, the synergy which we described between TNFRSF members here is based on the expression regulation of inducible co-stimulatory receptors rather than immediate integration of signalling pathways. It is thus highly likely that such relationships can span across receptor families. For example, as CD28 is a powerful early enhancer of T cell activation (Esensten et al., 2016), it is likely to improve 4-1BB and GITR upregulation, as well. Extending this study to include more T cell co-signalling receptors is therefore the logical next step in order to build a library of phenotypic models as a resource to simulate *in vitro* and *in vivo* scenarios of interest. Such a procedure will give rise to more precisely defined hypotheses to test experimentally, with the potential to accelerate progress in our understanding of T cell signalling.

5.4. Therapeutic implications

With co-signalling molecules being attractive targets for immunotherapy, quantitative modelling of these receptors can certainly also have a clinical impact. Despite impressive clinical results achieved with currently approved checkpoint inhibitors, a large proportion of patients does not respond to these therapies (Wolchok et al., 2017). In addition, immune-related adverse effects are a serious issue, and toxicity is a major obstacle in the development of co-stimulatory receptor agonists for clinical use (Sanmamed et al., 2019). There is hope for optimisation of efficacy and tolerability with synergistic combinations, and even targeted development of cocktails specifically for cohorts of patients identified with appropriate biomarkers (e.g. expression of co-signalling molecules on tumour-resident immune cells) (Khair et al., 2019; Nakamura, 2019). However, considering the range of drugs either already in use or in development, testing the vast number of possible combinations experimentally with sufficient coverage would be extremely costly and time-consuming. In this case, adequate models to simulate these options *in silico* would offer an efficient alternative to identify the most promising interactions for experimental follow-up.

Not only can the pre-existing immune response be invigorated with co-signalling-targeting interventions, synergies with adoptive cell therapies can also be expected (Redeker and Arens, 2016). In this context, second-generation chimeric antigen receptors (CARs) have been celebrated for their unprecedented effectiveness in B cell malignancies, but they fail to achieve the same results in solid tumours, largely owing to the immune-suppressive microenvironment

(Mardiana et al., 2019; Martinez and Moon, 2019). Third-generation CARs mark an attempt to improve the design of CARs by including additional co-stimulatory domains. However, our results illustrate that the timing of co-stimulatory signals, in part determined by the expression of the receptor, is crucial for their biological function. CARs are known to be downregulated by their ligands in a manner similar to the TCR (Eyquem et al., 2017), and as such, co-stimulatory domains of second- and third-generation CARs will be downregulated with them. As a consequence, it is likely that a co-stimulatory domain from 4-1BB will not be able to function to its fullest extent in a CAR, since its endogenous counterpart primarily acts after TCR downregulation. Targeting endogenous 4-1BB either with recombinant versions of 4-1BBL or agonistic antibodies might be more effective in this case. A direct *in vivo* comparison of second- and third-generation CARs with additional CD28 or 4-1BB co-stimulation carried out by Sadelain and colleagues confirms this hypothesis, with the combination of a second-generation CD28-CD3ζ CAR and exogenous expression of 4-1BBL on T cells showing superior performance (Zhao et al., 2015). Another approach is the engineering of "armored" CAR T cells with inducible expression of pro-inflammatory cytokines to modulate their immediate environment (Liu et al., 2019). Type-I interferons could be included here, as they have been shown to effectively induce TNFSF ligands on APCs, amongst other functions (Chang et al., 2017).

With that being said, even though ligand-induced downregulation is reported for CARs, depending on their promotors, their expression regulation might differ significantly from TCRs (Eyquem et al., 2017), which are rather known to be limited by CD3 expression (Ahmadi et al., 2011). It is thus presently unclear to

what extent CARs are affected in the long term by the phenomenon of adaptation and co-signalling through various endogenous receptors on T cells, and a quantitative study of these properties would be another interesting trajectory with the potential to improve the design of CAR-based immunotherapies.

5.5. Future directions

Apart from technical improvements to our plate-based stimulation platform (discussed in 2.4.2.) and extension of the study to other co-stimulatory and co-inhibitory receptors, including other T cell subpopulations would be another sensible next step. The conclusions from this thesis are inherently limited to primary human $CD8^+$ T cell blasts. Even though these cells were isolated and expanded *in vitro* according to a protocol similar to those used for adoptive cell therapy products, very different subsets of T cells will also become relevant when targeting co-stimulation and co-inhibition with systemic clinical interventions. Establishing an MHC class II-restricted TCR system and alternative methods of introducing the TCR into the cells in our lab, such as mRNA electroporation, will enable us to study the various $CD4^+$ T cell subpopulations, as well as unexpanded naïve and memory T cells. With regard to $CD8^+$ T cells, it would also be interesting to examine the effects of co-stimulation on other biologically relevant effector functions such as cytotoxic killing, which can be quantified indirectly in our *in vitro* system as Fas-ligand and CD107a surface expression (Ando et al., 1997; Betts and Koup, 2004).

Concerning our mathematical model, several refinement steps are planned. First, even though our current version is the simplest model which we found to reproduce our experimental findings, we have not formally tested all possible model architectures at this level of complexity. A systematic model search algorithm might be able to find alternative, equally simple models, in which case simulations and validation experiments are required to identify the most appropriate ones.

Furthermore, parameters for the simulations of the extended models in this thesis were manually estimated to recapitulate the experimental observations, while parameters of the base model of T cell activation and adaptation were based on best-fitting parameters for datasets in (Trendel et al., 2019), estimated by an ABC-SMC (Approximate Bayesian Computation / Sequential Monte Carlo) algorithm (Liepe et al., 2014). Application of such an algorithm on datasets collected as in Chapter 2 would produce unbiased parameter estimates, allowing for calibrated and possibly more specific model predictions. In addition, such estimates would offer a way to quantify and compare the relative strengths of co-stimulation through the individual TNFRSF members, providing useful information e.g. for the development of chimeric receptors.

Chapter 6: Materials and Methods

6.1. List of reagents

Reagent	Supplier
Agarose	Geneflow
Ampicillin	Sigma-Aldrich (now Merck)
ANTI-FLAG® M2 Affinity Gel	Sigma-Aldrich (now Merck)
BamHI, with NEB CutSmart® Buffer	New England Biolabs
BirA biotin-protein ligase bulk reaction kit	Avidity
dH_2O	made in-house with Purelab® flex 2 (Elga Labwater)
DNA Gel loading dye	Bioline Reagents
Ethanol	VWR Chemicals
Ethidium Bromide	Sigma-Aldrich (now Merck)
Glycine	Sigma-Aldrich (now Merck)
HiSpeed® Plasmid Maxi Kit	Qiagen
Hyperladder™ 1kb	Bioline Reagents
Isopropanol	Sigma-Aldrich (now Merck)
LB medium and agar plates	made in-house
Peptides for pMHC refolds	GenScript
PMSF	Sigma-Aldrich (now Merck)
Primers and other DNA oligos	Invitrogen, Thermo Fisher Scientific
QIAprep Spin® Miniprep Kit	Qiagen
QIAquick® Gel Extraction Kit	Qiagen
SOC medium	Takara Bio
Sulfuric acid	Sigma-Aldrich (now Merck)
T4 DNA ligase	Roche, Sigma-Aldrich (now Merck)
T4 polynucleotide kinase, with NEB T4 PNK Reaction Buffer	New England Biolabs

Table 6.1: List of reagents for general use.

Buffer	Supplier
Flow cytometry staining buffer	
PBS	
1% Bovine Serum Albumin (BSA)	Sigma-Aldrich (now Merck)
HBS-EP pH 7.4	
10 mM HEPES	Sigma-Aldrich (now Merck)
150 mM NaCl	Sigma-Aldrich (now Merck)
3 mM EDTA	Sigma-Aldrich (now Merck)
0.005% Tween® 20	Sigma-Aldrich (now Merck)
PBS pH 7.4	
from PBS tablets	Oxoid
OR sterile PBS	Sigma-Aldrich (now Merck)
PBS-Tween	
PBS from tablets	
0.05% Tween® 20	Sigma-Aldrich (now Merck)
pMHC refolding buffer	
100 mM Trizma® pH 8	Sigma-Aldrich (now Merck)
400 mM L-Arginine monohydrochloride	Sigma-Aldrich (now Merck)
2 mM EDTA	Sigma-Aldrich (now Merck)
5 mM reduced glutathione	Sigma-Aldrich (now Merck)
0.5 mM oxidised glutathione	Sigma-Aldrich (now Merck)
0.1 mM PMSF	Sigma-Aldrich (now Merck)
Storage buffer for M2 Affinity Gel	
PBS from tablets	
50% Glycerol	Sigma-Aldrich (now Merck)
0.02% sodium azide	Sigma-Aldrich (now Merck)
TAE buffer pH 8.0	
40 mM Trizma® base	Sigma-Aldrich (now Merck)
20 mM Acetic acid	Thermo Fisher Scientific
1 mM EDTA	Sigma-Aldrich (now Merck)

Table 6.2: List of buffers and their composition.

Antibodies				
Antibody target	**Species**	**Clone**	**Conjugate**	**Supplier**
human CD3ε	mouse	UCHT1	biotin	Biolegend
human CD25	mouse	BC96	Brilliant Violet® 421	Biolegend
human CD27	mouse	M-T271	PE or PerCp	Biolegend
human CD69	mouse	FN50	Alexa Fluor® 488	Biolegend
human GITR	mouse	DT5D3	PE	Miltenyi Biotec
human HLA-A/B/C	mouse	w6/32	-	Bio-Rad
human OX40	mouse	Ber-ACT35	Brilliant Violet® 421	Biolegend
human PD-1	mouse	EH12.2H7	Alexa Fluor® 488	Biolegend
human 4-1BB	mouse	4B4-1	Alexa Fluor® 647	Biolegend
mouse IgG Fc	goat	polyclonal	IRDye® 800CW	LI-COR
Streptavidin for flow cytometry				
Streptavidin			PE	Bio-Rad
Streptavidin			Alexa Fluor® 488	Invitrogen™, Thermo Fisher Scientific
ELISA kits				
human IFN-γ	Uncoated ELISA Kit			Invitrogen™, Thermo Fisher Scientific
human IL-2	Uncoated ELISA Kit			Invitrogen™, Thermo Fisher Scientific
human TNF-α	Uncoated ELISA Kit			Invitrogen™, Thermo Fisher Scientific

Table 6.3: List of flow cytometry reagents and ELISA kits.

Reagent	Supplier
DMSO, Hybri-Max™	Sigma-Aldrich (now Merck)
Dynabeads Human T-Activator CD3/CD28	Gibco™, Thermo Fisher Scientific
Fetal Bovine Serum (FBS)	Gibco™, Thermo Fisher Scientific
Ficoll-Paque PLUS density gradient medium	GE Healthcare
Recombinant human IL-2	Peprotech
Retronectin	Takara Bio
RosetteSep™ Human CD4+ T Cell Enrichment Cocktail	Stemcell Technologies
RosetteSep™ Human CD48+ T Cell Enrichment Cocktail	Stemcell Technologies
Solution 13	Chemometec
X-tremeGene™ 9	Roche, Sigma-Aldrich (now Merck)
HEK culture medium DMEM 10% FBS 100 U/ml Penicillin, 100 µg/ml Streptomycin	 Sigma-Aldrich (now Merck) Gibco™, Thermo Fisher Scientific Gibco™, Thermo Fisher Scientific
T cell culture medium RPMI 1640 10% FBS 100 U/ml Penicillin, 100 µg/ml Streptomycin	 Sigma-Aldrich (now Merck) Gibco™, Thermo Fisher Scientific Gibco™, Thermo Fisher Scientific

Table 6.4: List of cell culture reagents and media.

6.2. Molecular biology

6.2.1. Plasmid constructs

The c58/c61 TCR is an affinity-enhanced version of the 1G4 TCR (Chen et al., 2000; Li et al., 2005), and a pELNS (third-generation) lentiviral transfer vector encoding its alpha and beta chains under the control of the EF-1α promoter was kindly provided to us by Adaptimmune Ltd, together with the third-generation lentiviral packaging plasmids pRSV-Rev, pMDLg/pRRE and pMD2.G (Dull et al., 1998).

Expression vectors (pCR3 backbone with Ig signal peptide) for the FLAG-tagged tenascin-C-TNFSF-ligand fusion proteins for use as co-stimulatory ligands were a gift from Wajant and colleagues (Wyzgol et al., 2009). We used standard cloning techniques (see Sections 6.2.2.-6.2.5.) to insert an N-terminal AviTag for *in vitro* biotinylation. The FLAG-tag allows for purification of the fusion proteins from culture supernatant (see Section 6.3.3.), whereas the chicken tenascin C forms α-helical coiled coils to stabilise the trimers of 4-1BBL, CD70, GITRL and OX40L extracellular domains, respectively (Fig. 6.1).

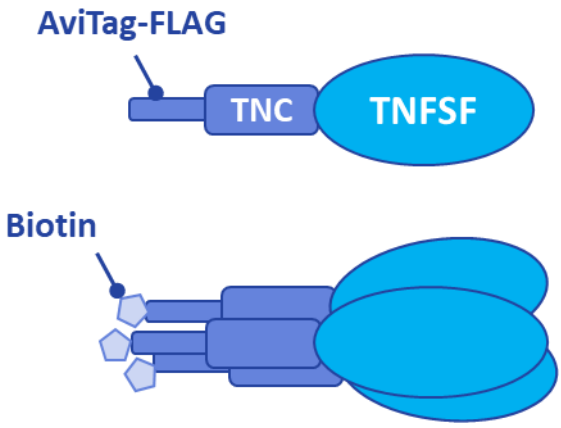

Figure 6.1: Schematic of tenascin C (TNC)-TNFSF ligand fusion proteins. The α-helical domain of chicken tenascin C (TNC) at the N-terminus stabilises trimers of the TNF superfamily ligand extracellular domains. FLAG-tag and AviTag allow for purification by affinity chromatography and *in vitro* biotinylation, respectively.

6.2.2. Transformation of *E. coli* DH5α

Rubidium chloride competent *E. coli* DH5α were prepared in-house by Marcus Bridge and stored at -80°C. 50 µl aliquots were thawed on ice and 100 ng of plasmid or 20 µl of a ligation reaction were added. After mixing and 30 min on ice, a 45 s heat shock at 42°C was applied. Tubes were placed back on ice for 2-3 min. Afterwards, 250 µl warm antibiotic-free SOC medium was added and the bacteria grown in a shaking incubator for 45-60 min. The bacteria were subsequently streaked onto 10 cm agar plates containing the appropriate antibiotic (100 µg/ml ampicillin). Plates were incubated overnight at 37°C.

For lentiviral transfer plasmids, commercially available NEB® Stable competent *E. coli* (New England Biolabs) were used instead of DH5α.

6.2.3. DNA extraction from bacterial cultures

Isolated single bacterial colonies were picked from the agar plates and used to inoculate 10 ml LB medium with the appropriate antibiotic (100 µg/ml ampicillin). The culture was placed in a shaking incubator at 37°C and 180 rpm, either overnight for sequencing only, or for 8 hours to be used for inoculation of a larger 500 ml overnight culture.

DNA from 10 ml or 500 ml overnight cultures was extracted using the QIAprep® Spin Miniprep Kit or HiSpeed® Plasmid Maxi Kit from Qiagen, respectively, according to the manufacturer's manual. DNA was eluted in TE buffer (1 mM EDTA in 10 mM Tris·Cl at pH 8.0) and stored at 4°C (short-term) or -20°C (long-term).

DNA concentrations were quantified using a Nanodrop 1000 (ThermoFisher Scientific) as absorbance at 260 nm. For sequencing, plasmids were sent to Source BioScience or Eurofins Genomics following their instructions.

6.2.4. Restriction enzyme digestion of DNA

To insert the AviTag into the FLAG-TNC-TNFSF expression vectors, each plasmid was cut with BamHI and dephosphorylated using CIP (calf intestinal phosphatase) to prevent re-ligation. 50 µl reactions were prepared with 1 µg of plasmid DNA and 1 µl each of BamHI (New England Biolabs, 20 units) and CIP (New England Biolabs, 10 units) in NEB CutSmart® Buffer.

After thorough mixing by pipetting, the reactions were incubated for 2 hours at 37°C and BamHI was subsequently inactivated at 65°C for 10 minutes. Cut and dephosphorylated plasmids were purified by agarose gel electrophoresis (1% Agarose in TAE buffer, 1 hour at 50V) and extracted from the gel using the QIAquick® Gel Extraction Kit (Qiagen).

6.2.5. Insertion of DNA oligomers into a prepared plasmid

```
5'-GATCCGGCCTGAACGATATTTTTGAAGCGCAGAAAATTGAATGGCATGAAA-3'
    3'-GCCGGACTTGCTATAAAAACTTCGCGTCTTTTAACTTACCGTACTTTCTAG-5'
        G  L  N  D  I  F  E  A  Q  K  I  E  W  H  E
```

Custom 51mer DNA oligonucleotides encoding the AviTag with BamHI-compatible overhangs, supplied by Invitrogen (ThermoFisher Scientific), were 5'-phosphorylated by T4 polynucleotide kinase (PNK, from New England Biolabs) and annealed. 100 µl reactions were prepared with final concentrations of 1 µM of each oligonucleotide, 3 µM ATP and 10 units of T4 PNK in NEB T4 PNK Reaction Buffer. The reaction was incubated for 1 hour at 37°C, heated up to 95°C for 5 minutes and slowly cooled down to 25°C over the course of 1 hour.

To insert the prepared phosphorylated DNA oligonucleotides into the BamHI-cut and dephosphorylated FLAG-TNC-TNFSF expression plasmids, 20 µl ligation reactions were prepared with 100 fmol plasmids, 1 pmol oligonucleotides and 1 unit of T4 DNA ligase in ligase buffer. The reaction was incubated at 16°C overnight and transformed into DH5α E. coli as described in 6.2.2.

6.3. Protein production and purification

6.3.1. pMHC refolding, biotinylation and purification

AviTag-tagged extracellular residues 1-287 of the HLA-A*02:01 α-chain and recombinant human β_2-microglobulin were produced in *E. coli*, purified from inclusion bodies by Marcus Bridge and Mikhail Kutuzov and stored in 8 M urea at -40°C. 1 mg peptide (Table 6.5), 26 mg β_2-microglobulin and 32 mg HLA-A2 α-chain were added dropwise to 100 ml cold Tris-arginine pMHC refolding buffer and stirred for 72 hours at 4°C. Aggregates were subsequently removed through 5 µm filtration and the filtrate concentrated in a Millipore Centricon® Plus-70 centrifugal filter (30 kDa NMWL) to a final volume of ~700 µl.

Peptide mutant of NY-ESO-$1_{157-165}$	**Amino acid sequence**	**K_D of peptide-HLA-A2 to c58/c61 TCR [M]**
C9V	SLLMWITQ**V**	7.07×10^{-11}
M4A-Q8K-C9V	SLL**A**WIT**KV**	7.23×10^{-6}

Table 6.5: List of peptides used for the generation of pMHCs. Peptides were ordered from Genscript and stored at 10 mg/ml in DMSO at -20°C. The affinity measurements were done by Marcus Bridge and Mikhail Kutuzov using surface plasmon resonance (SPR) and were reported in Trendel et al., 2019.

The refolded pMHC was biotinylated using the BirA biotin-protein ligase bulk reaction kit from Avidity following the manufacturer's manual. After overnight biotinylation at 4°C, the pMHC was purified by size-exclusion chromatography through a Superdex™ 200 column on an ÄKTA™ pure chromatography system (GE

Healthcare) with HBS-EP as the flow buffer. Eluted biotinylated pMHC was quantified using a Nanodrop 1000 (ThermoFisher Scientific) as absorbance at 280 nm and stored in aliquots at -80°C.

6.3.2. Production of recombinant TNFSF-TNC fusion proteins in HEK293T cells

HEK293T cells were seeded onto 150mm dishes with 9×10^6 cells in 30 ml HEK culture medium (DMEM / 10% FBS / 1× PenStrep). Seeded cells were cultured overnight (37°C, 10% CO_2) to reach ~50% confluency.

30 µg plasmid DNA (AviTag-FLAG-TNC-TNFSF in pCR3.1) were diluted in 1.5 ml serum-free DMEM per dish. 90 µl of X-tremeGENE™ 9 DNA transfection reagent (Roche) were added and, after thorough mixing, incubated for 15-20 min at room temperature. Culture medium of the HEK293T cells was reduced to 20 ml per dish and the prepared transfection mix added dropwise while gently swirling the dishes. The treated cells were cultured overnight (37°C, 10% CO_2).

The next day, the culture medium was replaced with 40 ml DMEM with 0.5% FBS per dish and the cells cultured for another 5 days. Culture supernatant was subsequently harvested, and cells removed by centrifugation (10 min at 520×g, 4°C) and filtration through a Millipore® Stericup (0.22 µm pore size). For short-term storage at 4°C, Tris·HCl (pH 8.0) and PMSF were added to final concentrations of 3 mM and 0.1 mM, respectively.

6.3.3. Purification and biotinylation of TNFSF-TNC fusion proteins

AviTag-FLAG-TNC-TNFSF fusion proteins were purified from culture supernatants through affinity chromatography using 2 ml ANTI-FLAG® M2 Affinity Gel (Sigma-Aldrich, now Merck), following the manufacturer's batch absorption protocol. Proteins were eluted in ten 1ml aliquots of 0.1 M glycine at pH 3.5, immediately neutralised with 20 µl of 1 M Tris·HCl at pH 8.0 per aliquot, and the pooled eluate concentrated in Millipore Amicon® Ultra-15 Centrifugal Filter Units (30 kDa NMWL) with buffer exchange into 10 mM Tris·HCl at pH 8.0 to a final volume of ~700 µl.

Purified AviTag-FLAG-TNC-TNFSF fusion proteins were biotinylated using the BirA biotin-protein ligase bulk reaction kit from Avidity following the manufacturer's manual. After overnight biotinylation at 4°C, excess biotin was removed using Millipore Amicon® Ultra-15 Centrifugal Filter Units (30 kDa NMWL) with buffer exchange into PBS. Biotinylated proteins were quantified using a Nanodrop 1000 (ThermoFisher Scientific) as absorbance at 280 nm and stored in aliquots at -80°C.

6.3.4. Preparation of fluorescent pMHC tetramers

15 µg PE-conjugated streptavidin (AbD Serotec, now Bio-Rad) were added to 100 µg biotinylated C9V (high-affinity) pMHC 10 times every 10 min while shaking the mix at room temperature. The resulting pMHC tetramers were stored at 4°C under protection from light. Working dilutions (1:200 to 1:1000) were titrated for each batch on cells expressing the c58/c61 TCR.

6.4. Cell culture

6.4.1. Cell lines and maintenance

HEK293T cells (ATCC® CRL-3216™) were cultured in HEK culture medium (DMEM / 10% FBS / 1×PenStrep) at 37°C and 10% CO_2 and passaged every 2-3 days. For passaging, the cells were gently flushed off the flask bottom with fresh pre-warmed medium and re-seeded at 1-2×10^6 cells in 20 ml culture medium per 75 cm^2 flask.

6.4.2. Cryopreservation

1.5×10^7 cells which had been passaged the day before were harvested, carefully resuspended in 1 ml cold FBS with 10% DMSO, and transferred into a cryogenic vial. These were placed inside a Nalgene® Mr. Frosty freezing container and frozen at -80°C. For long-term storage in liquid nitrogen, frozen vials were transferred to the institute's cell bank.

To thaw frozen cells, vials were briefly placed inside a 37°C water bath until almost completely thawed and wiped with 70% ethanol. The contents were carefully resuspended and slowly transferred into a 75 cm^2 flask with 30 ml pre-warmed culture medium while swirling. The flask was placed into a 37°C / 10% CO_2 incubator. Culture medium was replaced the next day and the cells were cultured as in 6.4.1.

6.4.3. Cell Counting

Automated cell counted was carried out using the Chemometec Nucleocounter® NC-3000™ Image Cytometer with NC-Slide A8™ and the acridine orange / DAPI-based Nucleocounter® Solution 13 following the manufacturer's instructions.

6.4.4. Production of lentiviral particles for T cell transduction

For the transduction of 1×10^6 T cells, 6×10^5 HEK293T were seeded in 3 ml HEK culture medium (DMEM / 10% FBS / 1×PenStrep) in one well of a 6-well plate on the day prior to T cell isolation and HEK293T transfection. The plate was returned to the incubator (37°C / 10% CO_2). The next day, lentiviral packaging plasmids (0.95 µg pRSV-Rev, 0.37µg pMD2.g, 0.95 µg pMDLg/pRRE) and 0.8 µg lentiviral transfer plasmid for the c58/c61 TCR were diluted in plain DMEM to a final volume of 191 µl and mixed by pipetting. 9 µl of X-tremeGENE™ 9 transfection reagent (Roche) was added to the DNA-DMEM solution and mixed thoroughly by pipetting. After 20 min of incubation at room temperature, the culture medium of the prepared HEK293T cells was reduced to 2 ml and the transfection mix was added dropwise and dispersed by swirling the plate. The plate was returned to the incubator (37°C / 10% CO_2).

Culture supernatant with lentiviral particles was harvested 24 hours post-transfection, filtered through a 0.45 µm Minisart® cellulose acetate syringe end

filter (Sartorius) and used fresh after supplementing with 50 U/ml recombinant human IL-2 (PeproTech)(see 6.4.6).

6.4.5. Isolation of primary T cells

Leukocyte cones were purchased from National Health Services Blood and Transplant and tested by Enas Abu-Shah for HLA-A2 expression via flow cytometry. $CD4^+$ and $CD8^+$ T cells were isolated from HLA-A2-negative leukocyte cones using the RosetteSep™ Human $CD4^+$ T Cell Enrichment Cocktail (Stemcell Technologies) or its $CD8^+$ T cell variant, respectively, following the manufacturer's protocol under sterile conditions. Briefly, 300 µl antibody cocktail were added to 2 ml leucocyte cone, mixed and incubated for 20 minutes. This mix was subsequently diluted with room temperature PBS to a final volume of 6.25 ml and carefully layered over 5 ml Ficoll-Paque PLUS density gradient medium (GE Healthcare) in a 15 ml centrifuge tube. Density gradient centrifugation was performed at 1200×g and room temperature for 20 min with the brake disabled. The layer of enriched $CD4^+$ or $CD8^+$ T cells on the Ficoll phase was carefully harvested using a pipette, washed with room temperature PBS (300×g for 10 min, low brake) and resuspended in 15 ml pre-warmed T cell culture medium (RPMI / 10% FBS / 1×PenStrep) for counting and pelleted again (300×g for 10 min, low brake). T cells were then resuspended in pre-warmed T cell culture medium at 1×10^6 cells/ml. Dynabeads® Human T-Activator CD3/CD28 (ThermoFisher Scientific) were added at a 1:1 bead:cell ratio and recombinant human IL-2

(PeproTech) to a final concentration of 50 U/ml. T cells were cultured at 37°C / 5% CO_2.

6.4.6. Transduction and culture of primary $CD8^+$ T cells

On the day of T cell isolation and HEK293T transfection, non-tissue culture-treated 24-well plates were coated with 10 µg RetroNectin (Takara Clontech) in 500 µl PBS per well and left overnight. Plates were subsequently blocked with sterile 2% BSA in PBS for 30 min and washed with PBS before use.

The day after isolation, T cells and beads were distributed over the RetroNectin-coated 24-well plate (1 ml per well). Freshly prepared culture supernatant with lentiviral particles and recombinant human IL-2 (see 6.4.4.) was added to the T cells (2 ml per well) and mixed. One untransduced control well received filtered culture supernatant from untransfected HEK293T instead, supplemented with IL-2. T cells were returned to the incubator (37°C / 5% CO_2).

On day 3 post-transduction, 2.5 ml medium per well was carefully aspirated and replaced with fresh T cell culture medium (RPMI / 10% FBS / 1×PenStrep) with 50 U/ml IL-2. On day 5 post-transduction, cells and beads were resuspended and beads removed using a Dynal MPC-1 magnet (ThermoFisher Scientific). Cells were counted and resuspended in fresh T cell culture medium with 50 U/ml IL-2 at 1×10^6 cells/ml.

From this point onwards, T cells were passaged every other day to a density of 1×10^6 cells/ml in T cell culture medium with 50 U/ml IL-2. The size of the culture vessel was chosen to keep the between 1×10^5 and 5×10^5 cells/cm^2.

6.4.7. Quality control

To confirm transduction efficiency, expression of the c58/c61 TCR on transduced cells was quantified by cytometry after day 7 post-transduction and compared against untransduced control cells. 1×10^5 cells were pelleted in FACS tubes. Fluorescent pMHC tetramers were diluted in 1% BSA in PBS to a previously determined working concentration (see 6.3.4.) and the cell pellets resuspended in this staining solution (200 µl/tube). After staining for 20 min at 4°C, cells were washed twice with PBS (4 ml/tube, 5 min at 520×g) and resuspended in 200 µl PBS for analysis on a custom Cytek® flow cytometer.

Cells used for the experiments in this thesis were generally 50-80% c58/c61 TCR-positive.

6.5. T cell stimulation assays

6.5.1. Ligand immobilisation

Ligands for T cell stimulation were produced in-house (see 6.3.). Pierce™ Streptavidin Coated High Capacity 96-well Plates (ThermoFisher Scientific) were rinsed with 200 µl/well sterile PBS. Serial dilutions of pMHC were made with sterile PBS and transferred onto the streptavidin pre-coated plates (50 µl per well). After a minimum of 90 min at 4°C, wells were aspirated and washed once with 200 µl/well sterile PBS. Co-stimulatory ligands were also diluted in sterile PBS and added to the washed plates in the same manner. After a minimum of 90 min at 4°C, wells were aspirated and washed twice with 200 µl/well sterile PBS.

Fig. 6.2 shows an example of the layout of such a 96-well plate. After the last PBS wash, plates were immediately used for T cell stimulation experiments.

Optionally, to confirm adequate levels of pMHC immobilisation, duplicate plates were produced as described above and set aside for a fluorescence-based immobilisation assay. After the last PBS wash, 50 µl/well of a conformation-sensitive anti-HLA-A/B/C antibody (clone w6/32) diluted 1:500 in PBS with 1% BSA were added and incubated for 30 min at 4°C. Wells were aspirated and washed twice with 0.05% Tween in PBS. 50 µl/well of an IRDye® 800CW-conjugated anti-mouse secondary antibody (LI-COR) diluted 1:5000 in PBS with 1% BSA were added and incubated for 30 min at 4°C. Wells were aspirated and washed twice with 0.05% Tween in PBS, after which fluorescence was quantified using a LICOR Odyssey® Sa Infrared Imaging System.

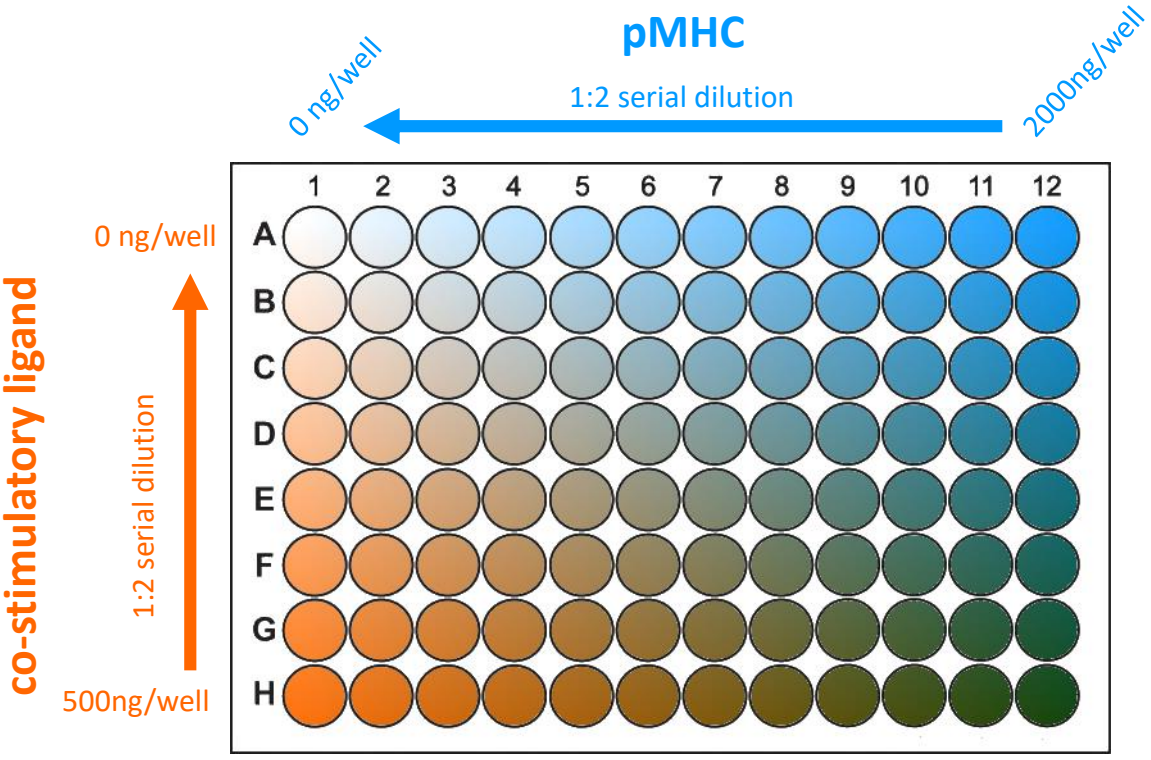

Figure 6.2: Example plate layout for one time point and one co-stimulatory ligand of the data sets collected for Chapter 2. Serial dilutions were prepared on separate plates and transferred onto streptavidin pre-coated plates for ligand capture. pMHC and co-stimulatory ligand were immobilised sequentially.

6.5.2. T cell stimulation

Expanded and c58/c61 TCR-transduced CD8⁺ T cells were used for experiments on days 10-14 post-transduction. Cells were counted, pelleted (5 min at 520×g) and resuspended in pre-warmed T cell culture medium (RPMI / 10% FBS / 1×PenStrep, without addition of IL-2) to 3.75×10^5 cells/ml. This cell suspension was added to the prepared stimulation plates (200 µl/well) to a final number of 7.5×10^4 cells/well. To settle down the cells, plates were briefly spun for 1 min at

100×g with slow acceleration and deceleration and returned to the incubator (37°C / 5% CO_2) for the specified times.

6.5.3. Cell transfer experiments

To stimulate T cells in two phases with different conditions, stimulation plates were prepared for each phase as in 6.5.1., and cells treated as in 6.5.2. for the first phase, after which the cells were harvested by pipetting and transferred to V-bottom 96-well plates. The harvested cells were pelleted (5 min at 520×g) and the supernatants collected for later ELISAs. Pellets were resuspended in fresh pre-warmed T cell culture medium (200 µl/well) and transferred to prepared stimulation plates for the second phase. To settle down the cells again, plates were briefly spun for 1 min at 100×g with slow acceleration and deceleration and returned to the incubator (37°C / 5% CO_2) for the specified times.

6.5.4. Flow cytometry

After the specified timepoints of the stimulation experiments, cells were harvested by pipetting and transferred to V-bottom 96-well plates. The harvested cells were pelleted (5 min at 520×g) and the supernatants collected for ELISAs. Pellets were resuspended in 50 µl/well of a staining solution containing 1% BSA in PBS with fluorescently labelled pMHC tetramers and/or fluorophore-conjugated antibodies at previously titrated working concentrations (usually 1:200 for commercially

available antibodies from BioLegend). After 20 min at 4°C, cells were washed twice with 1% BSA in PBS (200 µl/well, 5 min at 520×g) and resuspended in 80 µl/well PBS for flow cytometry.

Samples were analysed on a BD FACSCalibur™ or BD LSRFortessa™ X-20 with a BD High Throughput Sampler for automated acquisition. Flow cytometry data was analysed in FlowJo V10.

6.5.5. ELISA

After harvesting the cells from the stimulation experiments, the supernatants were separated from the cell pellets, collected in round-bottom 96-well plates and kept at 4°C for short-term storage (< 12 hours). To quantify the cytokines IFN-γ, IL-2 and TNF, ELISAs were performed using Nunc MaxiSorp™ flat-bottom 96-well plates and the respective Invitrogen™ Uncoated ELISA Kits (ThermoFisher Scientific) according to the manufacturer's protocol. A BioTek ELx405 plate washer was used for washing steps, and absorbance at 450 nm and 570 nm was measured using a SpectraMax M5 plate reader (Molecular Devices). Standards in duplicates were included for each plate to generate calibration curves for the calculation of cytokine concentrations.

6.6. Data analysis

6.6.1. Curve fitting

Dose-response curves were fit in order to extract E_{max} and/or EC_{50} values. For this purpose, TCR downregulation curves were fit in GraphPad Prism 8 with the non-linear regression function "*inhibitor dose response curve with variable slope*" which fits the data with a monotonically decreasing sigmoid function and calculates an "IC_{50}" that is interpreted as EC_{50} in the context of our experiments.

For the often bell-shaped cytokine response and 4-1BB expression curves, GraphPad Prism did not offer any appropriate functions. Therefore, a script was written with the assistance of Omer Dushek which uses the Matlab *lsqcurvefit* solver to fit the dose-response data with a composite of two Hill equations:

$$y = E_{min} + \frac{a + \frac{b - a}{1 + (\frac{c_1}{x})^{n_1}} - E_{min}}{1 + (\frac{c_2}{x})^{n_2}}$$

With these fits, E_{max} and EC_{50} values could be determined numerically in Matlab as highest y-value and x-value at $y = \frac{E_{max}}{2}$, respectively (Fig. 6.3). However, in certain cases, the cytokine response was so weak that the technical noise in the ELISA made it unfeasible to accurately estimate the EC_{50}. Therefore, EC_{50} values were excluded for dose-responses where the fit E_{max} was below 50 pg/ml, which was often the case for IL-2 at late time points.

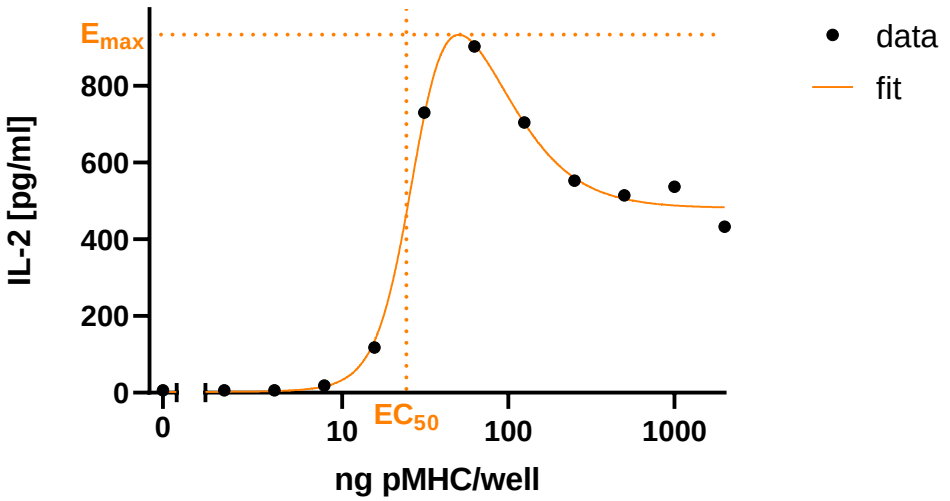

Figure 6.3: Dose-response curve fit and extraction of metrics. As an example, an IL-2 dose-response data set was fit with a bell-shaped function using the Matlab *lsqcurvefit* solver. Graphically shown as dotted lines are the E_{max} and EC_{50} which were numerically determined in Matlab.

6.6.2. Normalisation

To further minimise the contribution of technical variability between experiments, originating, for instance, from differences in quality of stimulatory ligands, transduction efficiency of the cells and donor variability, the extracted absolute E_{max} and EC_{50} values were normalised to the mean E_{max} and EC_{50} values of each readout in each experiment. Therefore, pooled and averaged E_{max} and EC_{50} values were not plotted as absolute values but as relative fold-change compared to one standard condition (e.g. pMHC without co-stimulation), as indicated for each figure.

6.6.3. Statistical analysis

Statistical tests with appropriate corrections for multiple testing were performed as indicated for each figure in GraphPad Prism 8.

6.7. Mathematical modelling

6.7.1. Base model of T cell activation

The mathematical model used as foundation for all subsequent models in this thesis has been developed iteratively by testing various model architectures against T cell stimulation data generated by multiple members of the lab. Most importantly, it can reproduce the cytokine dose-responses as well as the kinetics observed in time course experiments, including the T cell adaptation phenotype, as discussed in detail in (Trendel et al., 2019). It is described by the following set of ordinary differential equations (ODEs):

(1) $$\frac{dTCR}{dt} = k_1 \cdot (1 - TCR) - k_2 \cdot H(C - K_2) \cdot TCR - k_3 \cdot C$$

(2) $$\frac{dOut}{dt} = k_4 \cdot H(C - K_4) \cdot H(t - t_{delay})$$

with $C = \frac{pMHC^n}{(\frac{1}{K_A})^n + pMHC^n} \cdot TCR$ (amount of pMHC-TCR complexes)

and $H(x)$ being Heaviside step functions (threshold switches in the model).

Parameters are annotated in Table 6.6. Parameter values were based on the best fitting values for the data sets in (Trendel et al., 2019), estimated by an ABC-SMC algorithm written and run by Nicola Trendel and Omer Dushek.

The Matlab *ode23* solver was used to numerically integrate the ODE system of the models for simulations.

Parameter / Species	Description	Value / Initial condition
$pMHC$	pMHC dose [ng/well]	Variable
TCR	T cell receptor expression level [dimensionless between 0 and 1]	1
Out	Cytokine response [pg/ml]	0
K_A	pMHC-TCR association constant [(ng/well)$^{-1}$]	$10^{2.5}$
n	pMHC-TCR binding cooperativity	1.35
k_1	TCR expression rate [s^{-1}]	$10^{-5.7}$
k_2	Activation-induced TCR downregulation rate [s^{-1}]	10^{-4}
K_2	Activation-induced TCR downregulation threshold	$10^{-1.1}$
k_3	Ligand binding-induced TCR downregulation rate [s^{-1}]	$10^{-4.5}$
k_4	Cytokine production rate [pg·ml^{-1}·s^{-1}]	$10^{-1.5}$
K_4	Cytokine production activation threshold	$10^{-1.11}$
t_{delay}	Delay between start of stimulation and earliest possible cytokine response [s]	$10^{3.4}$

Table 6.6: Annotated species and parameters for the basic model.

6.7.2. Models of CD27 and 4-1BB expression and downregulation

ODEs were added to model the expression of CD27 and 4-1BB:

(3) $$\frac{dCD27}{dt} = k_5 \cdot (1 - CD27) - k_6 \cdot C_{CD27}$$

(4) $$\frac{dBB}{dt} = k_7 \cdot H(C - K_7) \cdot H\left(t - t_{BBdelay}\right) - k_8 \cdot C_{BB} - k_9 \cdot BB$$

with $$C_{CD27} = \frac{CD70}{KD_{CD70} + CD70} \cdot CD27$$ (amount of CD70-CD27 complexes)

and $$C_{BB} = \frac{BBL}{KD_{BBL} + BBL} \cdot BB$$ (amount of 4-1BBL-4-1BB complexes).

Parameter / Species	Description	Value / Initial condition
$CD27$	CD27 expression level [dimensionless between 0 and 1]	1
k_5	CD27 expression rate [s^{-1}]	$10^{-4.5}$
k_6	Ligand binding-induced CD27 downregulation rate [s^{-1}]	$10^{-3.7}$
$CD70$	CD70 dose [ng/well]	Variable
KD_{CD70}	CD70-CD27 dissociation constant [ng/well]	$10^{1.5}$
BB	4-1BB expression level	0
k_7	4-1BB expression rate [s^{-1}]	$10^{-4.3}$
K_7	4-1BB expression activation threshold	$10^{-1.15}$
$t_{BBdelay}$	Delay between start of stimulation and earliest possible 4-1BB expression [s]	10^{4}
k_8	Ligand binding-induced 4-1BB downregulation rate [s^{-1}]	$10^{-3.8}$
k_9	Basal 4-1BB downregulation rate [s^{-1}]	10^{-5}
BBL	4-1BBL dose [ng/well]	Variable
KD_{BBL}	4-1BBL-4-1BB dissociation constant [ng/well]	$10^{2.3}$

Table 6.7: Annotated species and parameters for the models of CD27 and 4-1BB expression.

6.7.3. Co-stimulation models

For co-stimulation to increase k_1, equation (1) was modified as follows:

(5) $$\frac{dTCR}{dt} = k_1 \cdot (1 + k_{10} \cdot C_{costim}) \cdot (1 - TCR) - k_2 \cdot H(C - K_2) \cdot TCR - k_3 \cdot C$$

For co-stimulation to decrease k_2, equation (1) was modified as follows:

(6) $$\frac{dTCR}{dt} = k_1 \cdot (1 - TCR) - \frac{k_2}{(1+k_{10} \cdot C_{costim})} \cdot H(C - K_2) \cdot TCR - k_3 \cdot C$$

For co-stimulation to decrease k_3, equation (1) was modified as follows:

(7) $$\frac{dTCR}{dt} = k_1 \cdot (1 - TCR) - k_2 \cdot H(C - K_2) \cdot TCR - \frac{k_3}{(1+k_{10} \cdot C_{costim})} \cdot C$$

For co-stimulation to increase k_{amp}, equations (2) and (4) were modified as follows:

(8) $$\frac{dOut}{dt} = k_4 \cdot H(C \cdot (1 + k_{10} \cdot C_{costim}) - K_4) \cdot H(t - t_{delay})$$

(9) $$\frac{dBB}{dt} = k_7 \cdot H(C \cdot (1 + k_{11} \cdot C_{costim}) - K_7) \cdot H\left(t - t_{BBdelay}\right) - k_8 \cdot C_{BB} - k_9 \cdot BB$$

For co-stimulation to increase k_4, equations (2) and (4) were modified as follows:

(10) $$\frac{dOut}{dt} = k_4 \cdot (1 + k_{10} \cdot C_{costim}) \cdot H(C - K_4) \cdot H(t - t_{delay})$$

(11) $$\frac{dBB}{dt} = k_7 \cdot (1 + k_{11} \cdot C_{costim}) \cdot H(C - K_7) \cdot H\left(t - t_{BBdelay}\right) - k_8 \cdot C_{BB} - k_9 \cdot BB$$

For co-stimulation to increase k_{act}, equations (2) and (4) were modified as follows:

(10) $$\frac{dOut}{dt} = k_4 \cdot \left(k_{10} \cdot C_{costim} + H(C - K_4)\right) \cdot H(t - t_{delay})$$

(11) $$\frac{dBB}{dt} = k_7 \cdot \left(k_{11} \cdot C_{costim} + H(C - K_7)\right) \cdot H\left(t - t_{BBdelay}\right) - k_8 \cdot C_{BB} - k_9 \cdot BB$$

with C_{costim} being either C_{CD27} or C_{BB} (see 6.7.2.) for CD27 and 4-1BB co-stimulation, respectively.

Figure	Parameter modulated	Value for k_{10}	Value for k_{11}	Value for $CD70$ [ng/well]	Value for BBL [ng/well]
3.2 B	k_1	$10^{0.4}$	-	200	-
3.2 C	k_2	$10^{0.5}$	-	200	-
3.2 D	k_3	$10^{0.3}$	-	200	-
3.3 B	k_{amp}	$10^{-0.3}$	-	200	-
3.3 C	k_4	$10^{0.8}$	-	200	-
3.3 D	k_{act}	1	-	200	-
3.5 A	k_1	$10^{0.1}$	-	-	500
3.5 B	k_2	10^{2}	-	-	500
3.5 C	k_3	$10^{0.1}$	-	-	500
3.6 A	k_{amp}	$10^{-0.2}$	$10^{-0.3}$	-	500
3.6 B	k_4	10	$10^{0.5}$	-	500
3.6 C	k_{act}	$10^{0.4}$	$10^{0.4}$	-	500
3.8 B	k_1	$10^{0.5}$	-	200	-
3.8 C	k_2	10^{2}	-	200	-
3.8 D	k_3	10	-	200	-
3.9 B	k_{amp}	1	-	200	-
3.9 C	k_4	$10^{0.8}$	-	200	-
3.9 D	k_{act}	$10^{0.5}$	-	200	-
3.10 B	k_1	$10^{0.5}$	-	-	500
3.10 C	k_2	10^{2}	-	-	500
3.10 D	k_3	$10^{0.5}$	-	-	500
3.11 B	k_{amp}	1	$10^{-0.3}$	-	500
3.11 C	k_4	10^{2}	$10^{0.5}$	-	500
3.11 D	k_{act}	$10^{0.4}$	$10^{0.4}$	-	500

Table 6.8: List of parameter values used for the simulations in Chapter 3.

For the confirmed model in Chapter 4, equations (2) and (4) were modified as follows:

(12) $$\frac{dOut}{dt} = k_4 \cdot H(C \cdot (1 + k_{10} \cdot C_{CD27} + k_{11} \cdot C_{BB}) - K_4) \cdot H(t - t_{delay})$$

(13) $$\frac{dBB}{dt} = k_7 \cdot H(C \cdot (1 + k_{12} \cdot C_{CD27} + k_{13} \cdot C_{BB}) - K_7) \cdot H(t - t_{BBdelay}) - k_8 \cdot C_{BB} - k_9 \cdot BB$$

Species / Parameter	Description	Value
CD70	CD70 dose [ng/well]	200 -> 0
BBL	4-1BBL dose [ng/well]	0 -> 500
k_{10}	Cytokine modulation by CD27 co-stim.	$10^{-0.3}$
k_{11}	Cytokine modulation by 4-1BB co-stim.	$10^{-0.2}$
k_{12}	4-1BB modulation by CD27 co-stim.	$10^{-0.2}$
k_{13}	4-1BB modulation by 4-1BB co-stim.	$10^{-0.03}$

Table 6.9: Annotated species and additional parameters for the model simulation in Chapter 4, Fig. 4.8.

Appendix

Supplementary figures

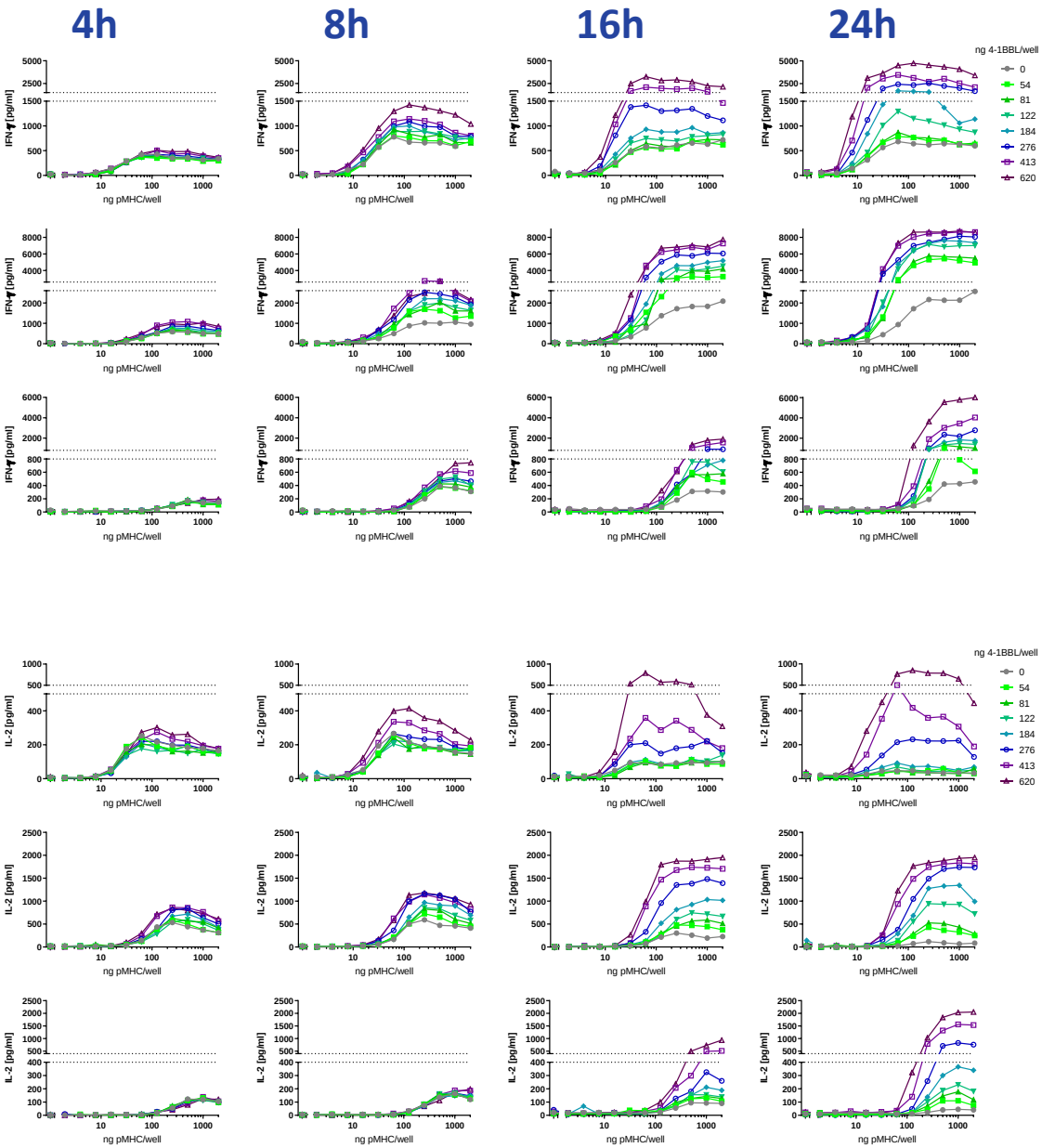

Supplementary Figure S.1: Co-stimulation through 4-1BB increases T cell cytokine production especially after 8 hours. Primary human CD8⁺ T cells transduced with the c58/c61 TCR were stimulated for 4, 8, 16 and 24 hours with pMHC, with or without 4-1BBL, at the indicated doses. The production of the cytokines IFN-γ, IL-2 into the culture medium supernatant was quantified by ELISA. Shown here are the raw dose-response curves for the 4 time points of each of the 3 experimental repeats.

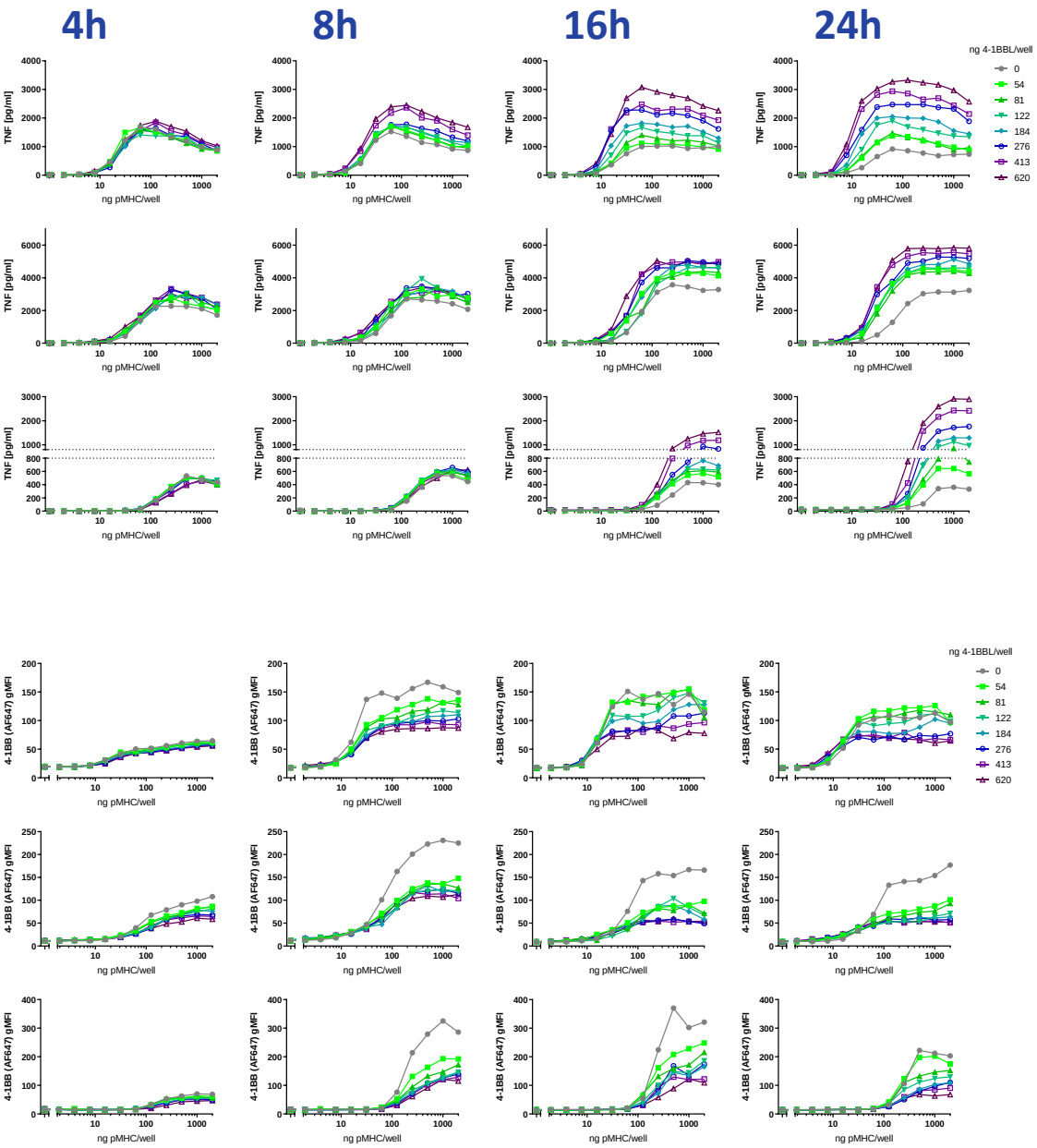

Supplementary Figure S.2: Addition of 4-1BBL increases T cell cytokine production especially after 8 hours and leads to ligand-induced 4-1BB downregulation. Primary human CD8$^+$ T cells transduced with the c58/c61 TCR were stimulated for 4, 8, 16 and 24 hours with pMHC, with or without 4-1BBL, at the indicated doses. The production of the cytokine TNF into the culture medium supernatant was quantified by ELISA. Surface 4-1BB was labelled with a fluorescent anti-4-1BB antibody and quantified by flow cytometry. Shown here are the raw dose-response curves for the 4 time points of each of the 3 experimental repeats.

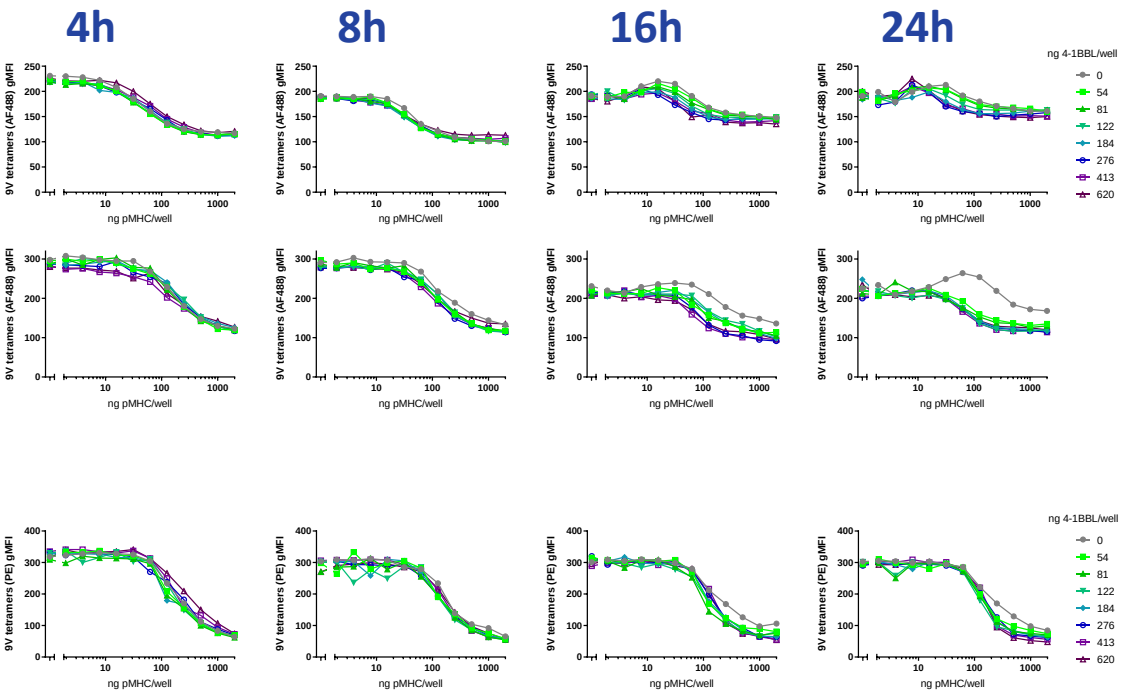

Supplementary Figure S.3: 4-1BB co-stimulation does not significantly affect TCR downregulation. Primary human CD8$^+$ T cells transduced with the c58/c61 TCR were stimulated for 4, 8, 16 and 24 hours with pMHC, with or without 4-1BBL, at the indicated doses. Surface TCR was labelled with fluorescent pMHC tetramers and quantified by flow cytometry. Shown here are the raw dose-response curves for the 4 time points of each of the 3 experimental repeats. We decided to exclude the first two data sets from further analysis due to the use of an unsuitable staining panel with a weak fluorophore for the pMHC tetramers. The signal-to-noise ratio was compromised and changes in cell size and morphology appeared to markedly affect the fluorescence readout.

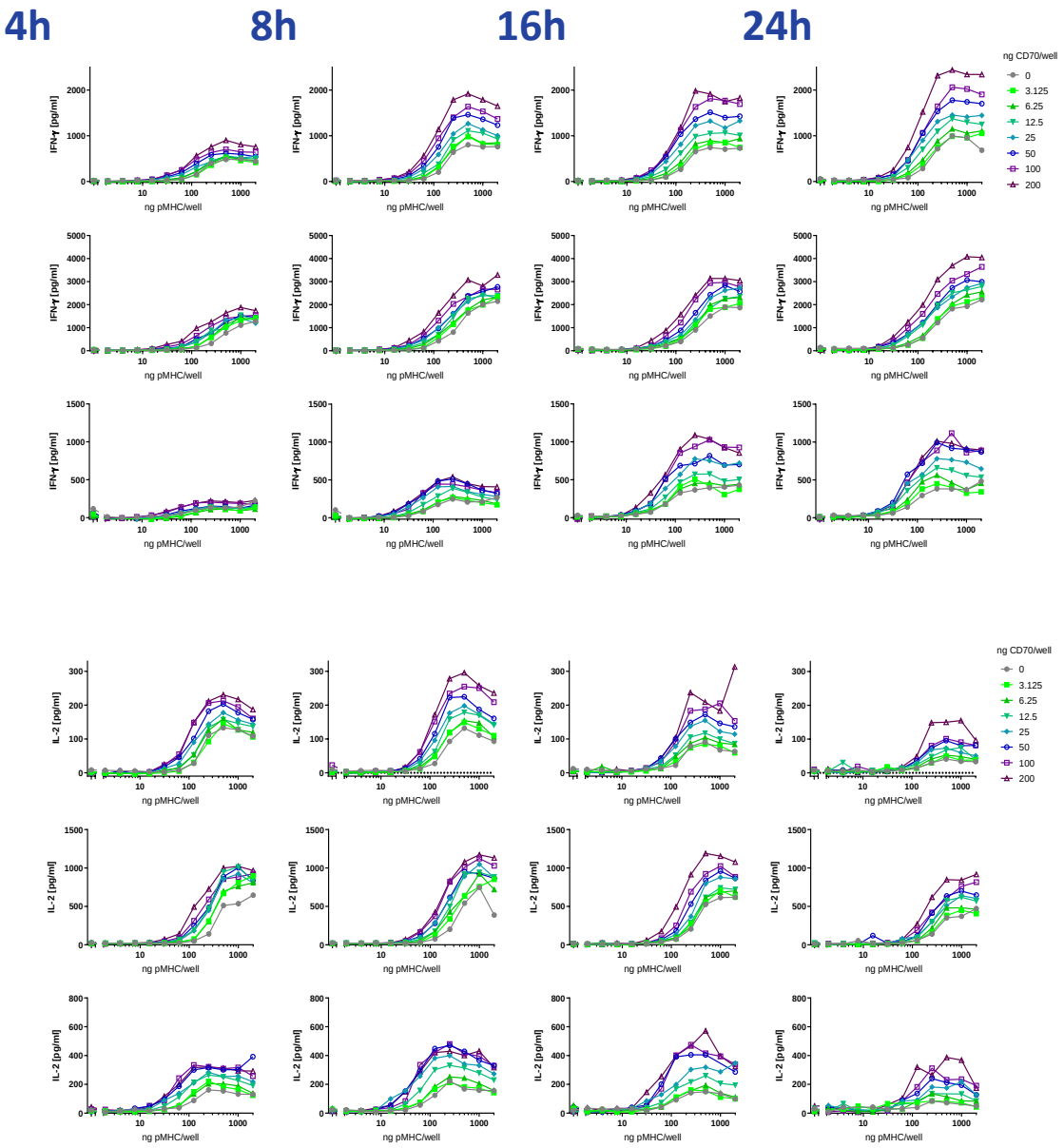

Supplementary Figure S.4: Co-stimulation through CD27 increases T cell cytokine production. Primary human $CD8^+$ T cells transduced with the c58/c61 TCR were stimulated for 4, 8, 16 and 24 hours with pMHC, with or without CD70, at the indicated doses. The production of the cytokines IFN-γ, IL-2 into the culture medium supernatant was quantified by ELISA. Shown here are the raw dose-response curves for the 4 time points of each of the 3 experimental repeats.

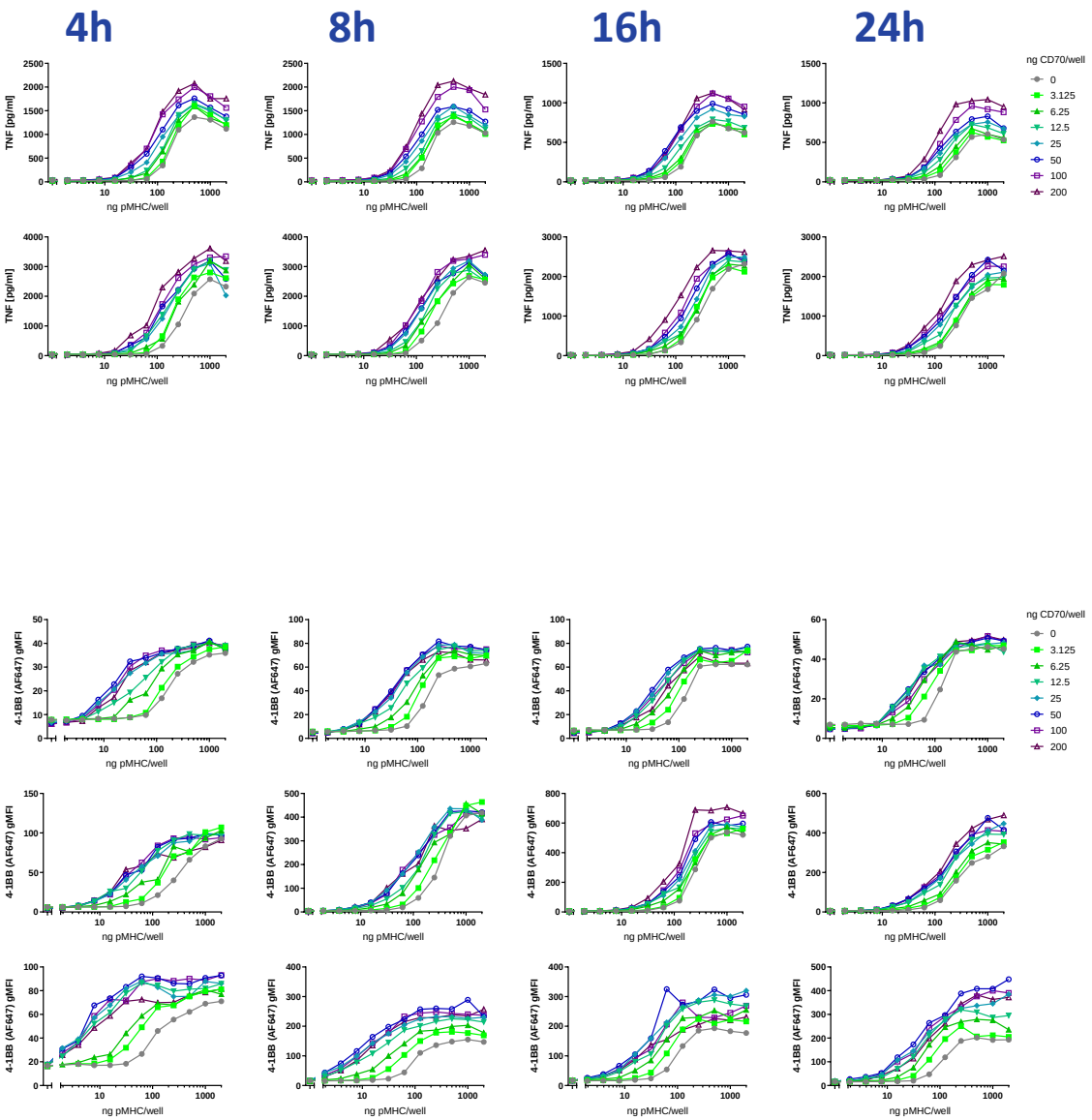

Supplementary Figure S.5: Co-stimulation through CD27 increases T cell cytokine production and 4-1BB expression. Primary human $CD8^+$ T cells transduced with the c58/c61 TCR were stimulated for 4, 8, 16 and 24 hours with pMHC, with or without CD70, at the indicated doses. The production of the cytokines IFN-γ, IL-2 into the culture medium supernatant was quantified by ELISA. Surface 4-1BB was labelled with a fluorescent anti-4-1BB antibody and quantified by flow cytometry. Shown here are the raw dose-response curves for the 4 time points of each of the 3 experimental repeats.

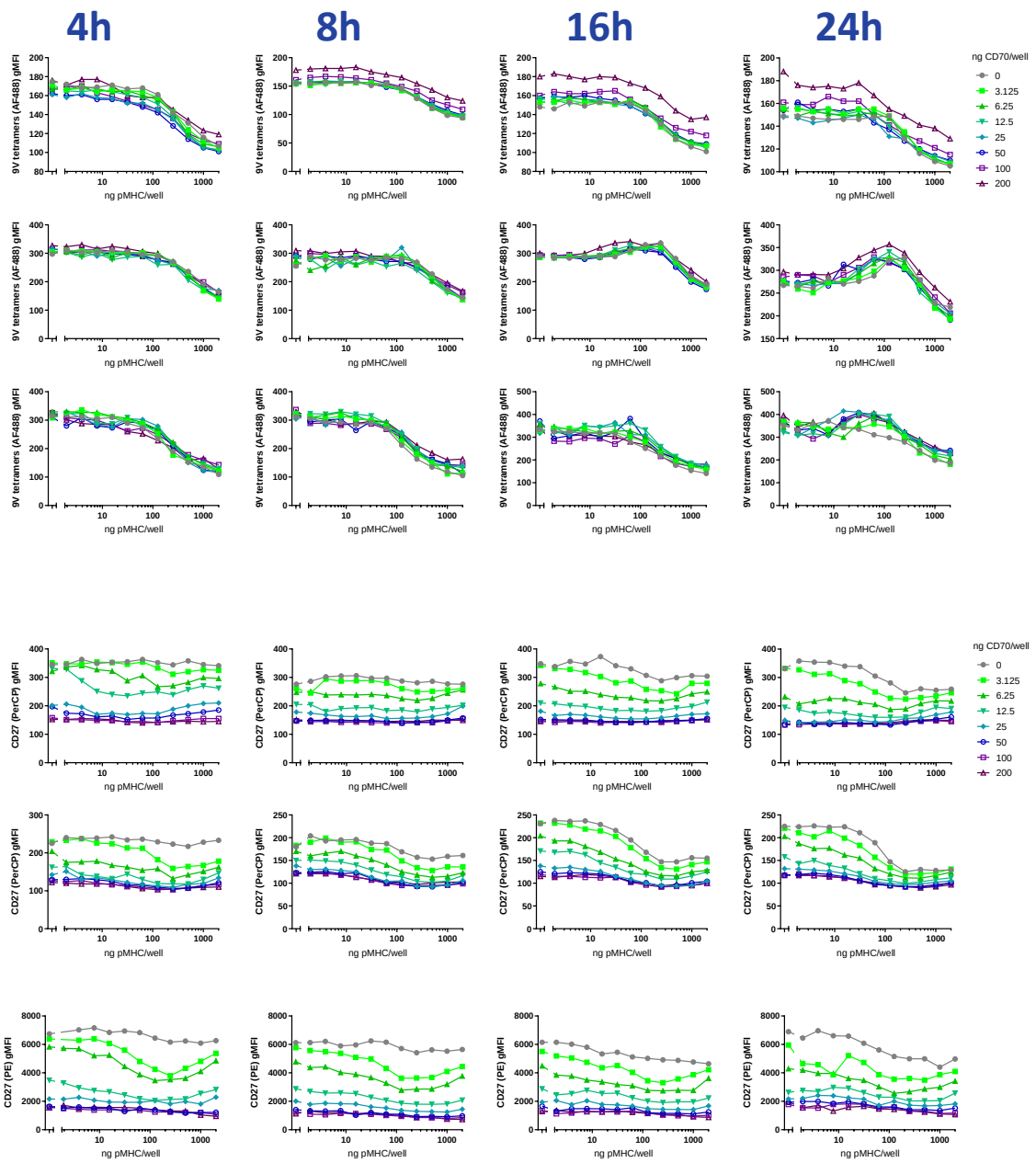

Supplementary Figure S.6: Addition of CD70 leads to a reduction in CD27 surface expression but does not significantly affect TCR downregulation. Primary human CD8$^+$ T cells transduced with the c58/c61 TCR were stimulated for 4, 8, 16 and 24 hours with pMHC, with or without CD70, at the indicated doses. Surface TCR and CD27 were labelled with fluorescent pMHC tetramers a fluorescent anti-CD27 antibody, respectively, and quantified by flow cytometry. Shown here are the raw dose-response curves for the 4 time points of each of the 3 experimental repeats. We decided to exclude the TCR data sets and the first two CD27 data sets from further analysis due to the use of an unsuitable staining panel with a weak fluorophore for the pMHC tetramers / anti-CD27 antibody. The signal-to-noise ratio was compromised and changes in cell size and morphology appeared to markedly affect the fluorescence readout.

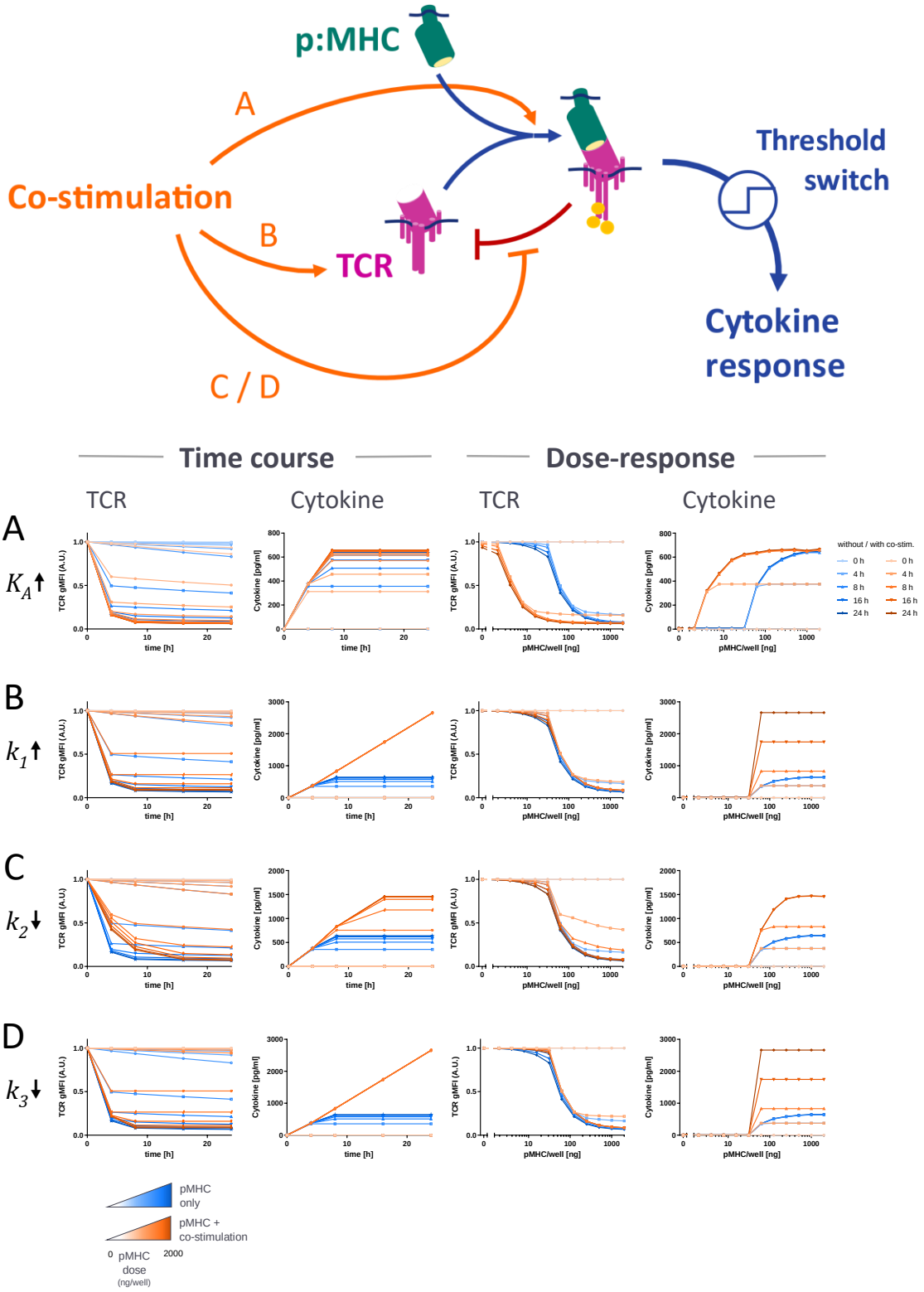

Supplementary Figure S.7: Simulation of constant co-stimulation modulating TCR expression and downregulation. TCR expression and cytokine response were simulated over time and across pMHC doses for models in which constant co-stimulation either increases **(A)** K_A, k_1 **(B)** or decreases k_2 **(C)** or k_3 **(D)** in the base model. K_A: pMHC-TCR association constant, k_1: rate of TCR (re)expression, k_2: rate of signalling-induced TCR downregulation, k_3: rate of ligand binding-induced TCR downregulation.

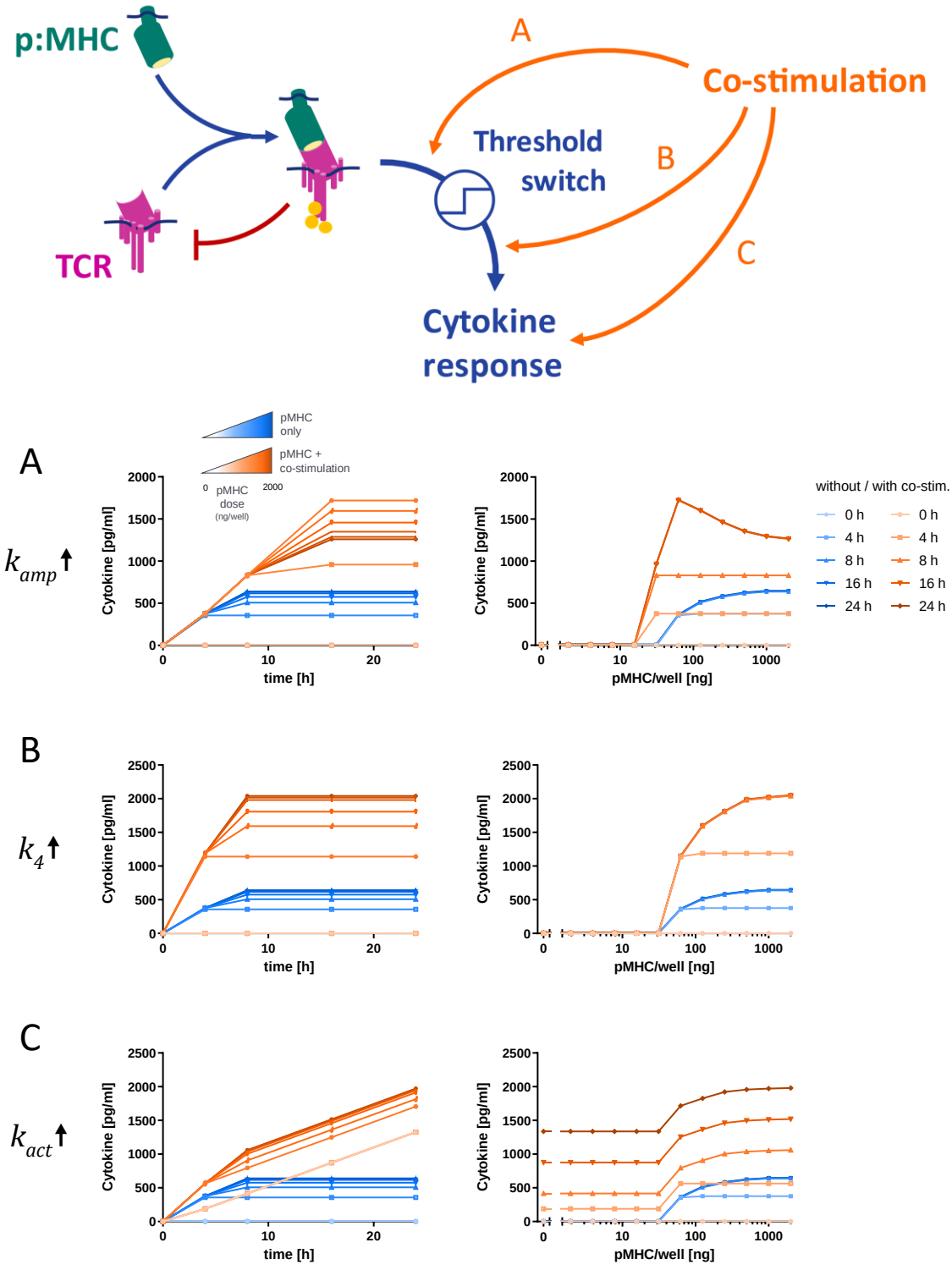

Supplementary Figure S.8: Simulation of constant co-stimulation modulating downstream signalling. The cytokine response was simulated over time and across pMHC doses for models in which the constant co-stimulation increases k_{amp} **(A),** k_4 **(B)** or k_{act} **(C)**. k_4: rate of cytokine production, k_{amp}: rate of signalling amplification, k_{act}: rate of direct (TCR-independent) cytokine production.

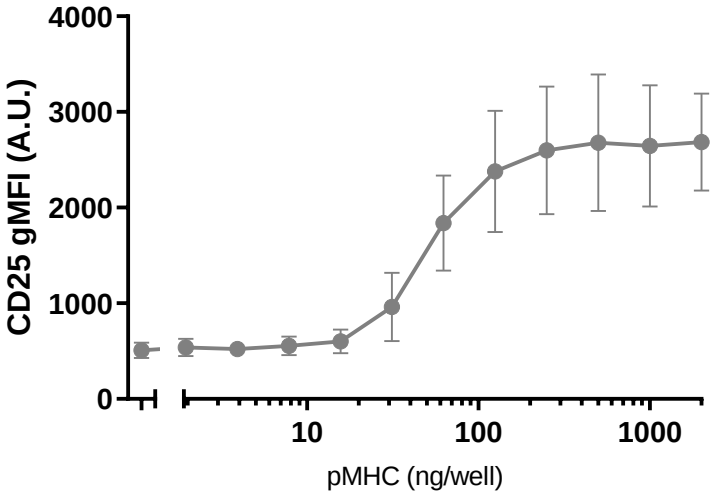

Supplementary Figure S.9: T cell activation induces the expression of CD25, the IL-2 receptor α chain. Primary human $CD8^+$ T cells transduced with the c58/c61 TCR were stimulated for 16 hours with pMHC at the indicated doses. Surface CD25 was labelled with a fluorescent anti-CD25 antibody and quantified by flow cytometry. Shown here is the averaged dose-response curve for 3 experimental repeats.

List of abbreviations

7-AAD	7-aminoactinomycin D
A.U.	arbitrary units
ABC-SMC	Approximate Bayesian Computation - Sequential Monte Carlo
ANOVA	Analysis of variance
AP-1	Activator protein 1
APC	Antigen-presenting cell
Bcl	B cell lymphoma
CAR	Chimeric Antigen Receptor
Cbl-b	Casitas B-lineage Lymphoma Proto-Oncogene B
CD	Cluster of differentiation
cDC	Conventional dendritic cell
CDR	Complementarity determining region
CRD	Cysterine-rich domain
cSMAC	Central supramolecular activation cluster
CTL	Cytotoxic T lymphocyte
CTLA-4	Cytotoxic T lymphocyte-associated protein 4
DAG	Diacylglycerol
DC	Dendritic cell
DMEM	Dulbecco's modified Eagle medium
DMSO	Dimethyl Sulfoxide
DNA	Desoxyribonucleic acid
e.g.	exempli gratia (for example)
EBV	Epstein-Barr virus
EC_{50}	Half-maximal effective concentration

EDTA	Ethylenediaminetetraacetic acid
EF-1α	Eukaryotic translation elongation factor 1 alpha
ELISA	Enzyme-linked immunosorbent assay
E_{max}	Maximum effect
ERK	Extracellular-signal regulated kinase
Fas	First apoptosis signal
FBS	Fetal bovine serum
FoxP3	Forkhead box P3
GITR	Glucocorticoid-induced TNFR-related protein
gMFI	Geometric mean fluorescence intensity
GRAIL	Gene related to anergy in lymphocytes
HBS	HEPES-buffered saline
HBV	Hepatitis B virus
HCV	Hepatitis C virus
HEK293T	Human embryonic kidney 293 cells expressing the simian virus 40 large T antigen
HEPES	4-(2-hydroxyethyl)-1-piperazineethanesulfonic acid
HIV	Human immunodeficiency virus
HLA	Human leukocyte antigen
i.e.	id est (in other words)
ICAM-1	Intercellular adhesion molecule 1
ICOS	Inducible T cell costimulator
IFN	Interferon
IgSF	Immunoglobulin superfamily
IL	Interleukin
IP_3	Inositol 1,4,5-trisphosphate

ITAM	Immunoreceptor tyrosine-based activation motif
Itch	E3 ubiquitin-protein ligase Itchy homolog
JNK	c-jun N-terminal kinase
K_D	Dissociation constant
LAT	Linker for activation of T cells
Lck	Lymphocyte-specific protein tyrosine kinase
LFA-1	Lymphocyte function-associated antigen
MAPK	Mitogen-activated protein kinase
moDC	Monocyte-derived dendritic cell
mRNA	Messenger ribonucleic acid
NEB	New England Biolabs
NFAT	Nuclear factor of activated T cells
NFκB	Nuclear factor kappa-light-chain enhancer of activated B cells
NK cell	Natural killer cell
NY-ESO-1	New York esophageal squamous cell carcinoma 1
PAMP	Pathogen-associated Molecular Pattern
PBS	Phosphate-buffered saline
PD-1	Programmed cell death protein 1
PE	Phycoerythrin
PerCP	Peridinin-chlorophyll-protein
PI3K	Phosphoinositide 3-kinase
PKC	Protein kinase C
PLC	Phospholipase C
pMHC	Peptide major histocompatibility complex
PMSF	Phenylmethanesulfonyl fluoride
PRR	Pattern Recognition Receptor

pSMAC	Peripheral supramolecular activation cluster
rel.	relative
RPMI	Roswell Park Memorial Institute
scFv	Single-chain variable fragment of an antibody
SLP-76	SH2 domain-containing leukocyte protein of 76 KDa
SOC medium	Super optimal broth with catabolite repression
TAE	Tris, Acetic acid, EDTA
TBS	Tris-buffered saline
TCR	T cell receptor
TGF-β	Transforming growth factor beta
T_H	T helper cell
TNF	Tumour necrosis factor
TNFR	Tumour necrosis factor receptor
TNFRSF	Tumour necrosis factor receptor superfamily
TNFSF	Tumour necrosis factor superfamily
TRAF	TNF receptor-associated factor
T_{reg}	Regulatory T cell
Tris	Tris(hydroxymethyl)aminomethane
Vav	Proto-oncogene vav
WASp	Wiskott-Aldrich Syndrome protein
ZAP-70	Zeta chain-associated protein of 70 kDa

List of figures

List of tables

List of references

Ahmadi, M., King, J.W., Xue, S.A., Voisine, C., Holler, A., Wright, G.P., Waxman, J., Morris, E., and Stauss, H.J. (2011). CD3 limits the efficacy of TCR gene therapy in vivo. Blood.

Akiba, H., Nakano, H., Nishinaka, S., Shindo, M., Kobata, T., Atsuta, M., Morimoto, C., Ware, C.F., Malinin, N.L., Wallach, D., et al. (1998). CD27, a member of the tumor necrosis factor receptor superfamily, activates NF-κB and stress-activated protein kinase/c-Jun N-terminal kinase via TRAF2, TRAF5, and NF-κB-inducing kinase. J. Biol. Chem.

Alcover, A., Alarcón, B., and Di Bartolo, V. (2018). Cell Biology of T Cell Receptor Expression and Regulation. Annu. Rev. Immunol.

Alderson, M.R., Smith, C.A., Tough, T.W., Davis-Smith, T., Armitage, R.J., Falk, B., Roux, E., Baker, E., Sutherland, G.R., Din, W.S., et al. (1994). Moslecular and biological characterization of human 4-1BB and its ligands. Eur. J. Immunol.

Allie, N., Grivennikov, S.I., Keeton, R., Hsu, N.J., Bourigault, M.L., Court, N., Fremond, C., Yeremeev, V., Shebzukhov, Y., Ryffel, B., et al. (2013). Prominent role for T cell-derived Tumour Necrosis Factor for sustained control of Mycobacterium tuberculosis infection. Sci. Rep.

Altan-Bonnet, G., and Germain, R.N. (2005). Modeling T cell antigen discrimination based on feedback control of digital ERK responses. PLoS Biol.

Ando, K., Hiroishi, K., Kaneko, T., Moriyama, T., Imawari, M., Muto, Y., Kayagaki, N., Yagita, H., and Okumura, K. (1997). Perforin, Fas/Fas ligand, and TNF-α pathways as specific and bystander killing mechanisms of hepatitis C virus-specific human CTL. J. Immunol.

Apetoh, L., Smyth, M.J., Drake, C.G., Abastado, J.P., Apte, R.N., Ayyoub, M., Blay, J.Y., Bonneville, M., Butterfield, L.H., Caignard, A., et al. (2015). Consensus nomenclature for CD8+ T cell phenotypes in cancer. Oncoimmunology.

Apostolou, I., and Von Boehmer, H. (2004). In vivo instruction of suppressor commitment in naive T cells. J. Exp. Med.

Arch, R.H., and Thompson, C.B. (1998). 4-1BB and Ox40 Are Members of a Tumor Necrosis Factor (TNF)-Nerve Growth Factor Receptor Subfamily That Bind TNF Receptor-Associated Factors and Activate Nuclear Factor κB. Mol. Cell. Biol.

Bachmann, M.F., McKall-Faienza, K., Schmits, R., Bouchard, D., Beach, J., Speiser, D.E., Mak, T.W., and Ohashi, P.S. (1997). Distinct roles for LFA-1 and CD28 during activation of naive T cells: Adhesion versus costimulation. Immunity.

Bachmann, M.F., Barner, M., and Kopf, M. (1999). CD2 sets quantitative thresholds in T cell activation. J. Exp. Med.

Baine, I., Abe, B.T., and Macian, F. (2009). Regulation of T-cell tolerance by calcium/NFAT signaling. Immunol. Rev.

Balagopalan, L., Coussens, N.P., Sherman, E., Samelson, L.E., and Sommers, C.L. (2010). The LAT story: a tale of cooperativity, coordination, and choreography. Cold Spring Harb. Perspect. Biol.

Bansal-Pakala, P., Gebre-Hiwot Jember, A., and Croft, M. (2001). Signaling through OX40 (CD134) breaks peripheral T-cell tolerance. Nat. Med.

Beatty, G.L., O'Hara, M.H., Lacey, S.F., Torigian, D.A., Nazimuddin, F., Chen, F., Kulikovskaya, I.M., Soulen, M.C., McGarvey, M., Nelson, A.M., et al. (2018). Activity of Mesothelin-Specific Chimeric Antigen Receptor T Cells Against Pancreatic Carcinoma Metastases in a Phase 1 Trial. Gastroenterology.

Berman, D., Korman, A., Peck, R., Feltquate, D., Lonberg, N., and Canetta, R. (2015). The development of immunomodulatory monoclonal antibodies as a new therapeutic modality for cancer: The Bristol-Myers Squibb experience. Pharmacol. Ther.

Betts, M.R., and Koup, R.A. (2004). Detection of T-Cell Degranulation: CD107a and b. Methods Cell Biol.

Boussiotis, V.A., Freeman, G.J., Griffin, J.D., Gray, G.S., Gribben, J.G., and Nadler, L.M. (1994). CD2 Is Involved in Maintenance and Reversal of Human Alloantigen-specific Clonal Anergy. J. Exp. Med.

Bromley, S.K., Iaboni, A., Davis, S.J., Whitty, A., Green, J.M., Shaw, A.S., Weiss, A., and Dustin, M.L. (2001). The immunological synapse and CD28-CD80 interactions. Nat. Immunol.

Buchan, S.L., Dou, L., Remer, M., Booth, S.G., Dunn, S.N., Lai, C., Semmrich, M., Teige, I., Mårtensson, L., Penfold, C.A., et al. (2018). Antibodies to Costimulatory Receptor 4-1BB Enhance Anti-tumor Immunity via T Regulatory Cell Depletion and Promotion of CD8 T Cell Effector Function. Immunity *49*, 958-970.e7.

Bucy, R.P., Panoskaltsis-Mortari, A., Huang, G.Q., Li, J., Karr, L., Ross, M., Russell, J.H., Murphy, K.M., and Weaver, C.T. (1994). Heterogeneity of single cell cytokine gene expression in clonal T cell populations. J. Exp. Med.

Bulliard, Y., Jolicoeur, R., Zhang, J., Dranoff, G., Wilson, N.S., and Brogdon, J.L. (2014). OX40 engagement depletes intratumoral Tregs via activating FcγRs, leading to antitumor efficacy. Immunol. Cell Biol.

Butz, E.A., and Bevan, M.J. (1998). Massive expansion of antigen-specific CD8+ T

cells during an acute virus infection. Immunity.

Call, M.E., Pyrdol, J., and Wucherpfennig, K.W. (2004). Stoichiometry of the T-cell receptor-CD3 complex and key intermediates assembled in the endoplasmic reticulum. EMBO J.

Carpenito, C., Milone, M.C., Hassan, R., Simonet, J.C., Lakhal, M., Suhoski, M.M., Varela-Rohena, A., Haines, K.M., Heitjan, D.F., Albelda, S.M., et al. (2009). Control of large, established tumor xenografts with genetically retargeted human T cells containing CD28 and CD137 domains. Proc. Natl. Acad. Sci. U. S. A.

Chan, A.C., Iwashima, M., Turck, C.W., and Weiss, A. (1992). ZAP-70: A 70 kd protein-tyrosine kinase that associates with the TCR ζ chain. Cell.

Chang, Y.H., Wang, K.C., Chu, K.L., Clouthier, D.L., Tran, A.T., Torres Perez, M.S., Zhou, A.C., Abdul-Sater, A.A., and Watts, T.H. (2017). Dichotomous Expression of TNF Superfamily Ligands on Antigen-Presenting Cells Controls Post-priming Anti-viral CD4+ T Cell Immunity. Immunity.

Chen, L., and Flies, D.B. (2013). Molecular mechanisms of T cell co-stimulation and co-inhibition. Nat. Rev. Immunol.

Chen, J.-L., Dunbar, P.R., Gileadi, U., Jäger, E., Gnjatic, S., Nagata, Y., Stockert, E., Panicali, D.L., Chen, Y.-T., Knuth, A., et al. (2000). Identification of NY-ESO-1 Peptide Analogues Capable of Improved Stimulation of Tumor-Reactive CTL. J. Immunol.

Chiodetti, L., Choi, S., Barber, D.L., and Schwartz, R.H. (2006). Adaptive Tolerance and Clonal Anergy Are Distinct Biochemical States. J. Immunol.

Clouthier, D.L., Zhou, A.C., Wortzman, M.E., Luft, O., Levy, G.A., and Watts, T.H. (2015). GITR Intrinsically Sustains Early Type 1 and Late Follicular Helper CD4 T Cell Accumulation to Control a Chronic Viral Infection. PLoS Pathog.

Courtney, A.H., Lo, W.L., and Weiss, A. (2018). TCR Signaling: Mechanisms of Initiation and Propagation. Trends Biochem. Sci.

Croft, M. (2003). Co-stimulatory members of the TNFR family: Keys to effective T-cell immunity? Nat. Rev. Immunol.

Das, J., Ho, M., Zikherman, J., Govern, C., Yang, M., Weiss, A., Chakraborty, A.K., and Roose, J.P. (2009). Digital Signaling and Hysteresis Characterize Ras Activation in Lymphoid Cells. Cell.

Davey, G.M., Kurts, C., Miller, J.F.A.P., Bouillet, P., Strasser, A., Brooks, A.G., Carbone, F.R., and Heath, W.R. (2002). Peripheral deletion of autoreactive CD8 T cells by cross presentation of self-antigen occurs by a Bcl-2-inhibitable pathway mediated by Bim. J. Exp. Med.

Davila, M.L., Riviere, I., Wang, X., Bartido, S., Park, J., Curran, K., Chung, S.S., Stefanski, J., Borquez-Ojeda, O., Olszewska, M., et al. (2014). Efficacy and toxicity management of 19-28z CAR T cell therapy in B cell acute lymphoblastic leukemia. Sci. Transl. Med.

Davis, M.M., and Bjorkman, P.J. (1988). T-cell antigen receptor genes and T-cell recognition. Nature.

Davis, S.J., and van der Merwe, P.A. (2006). The kinetic-segregation model: TCR triggering and beyond. Nat. Immunol.

Derbinski, J., Gäbler, J., Brors, B., Tierling, S., Jonnakuty, S., Hergenhahn, M., Peltonen, L., Walter, J., and Kyewski, B. (2005). Promiscuous gene expression in thymic epithelial cells is regulated at multiple levels. J. Exp. Med.

Dotti, G., Gottschalk, S., Savoldo, B., and Brenner, M.K. (2014). Design and development of therapies using chimeric antigen receptor-expressing T cells. Immunol. Rev.

Dull, T., Zufferey, R., Kelly, M., Mandel, R.J., Nguyen, M., Trono, D., and Naldini, L. (1998). A third-generation lentivirus vector with a conditional packaging system. J. Virol.

Dushek, O., and Dustin, M.L. (2018). CD8 helps TCR catch slippery self pMHC. Nat. Immunol.

Dustin, M.L. (2008). T-cell activation through immunological synapses and kinapses. Immunol. Rev.

Dustin, M.L. (2014). The immunological synapse. Cancer Immunol. Res.

Dustin, M.L., Golan, D.E., Zhu, D.M., Miller, J.M., Meier, W., Davies, E.A., and Van Der Merwe, P.A. (1997). Low affinity interaction of human or rat T cell adhesion molecule CD2 with its ligand aligns adhering membranes to achieve high physiological affinity. J. Biol. Chem.

Esensten, J.H., Helou, Y.A., Chopra, G., Weiss, A., and Bluestone, J.A. (2016). CD28 Costimulation: From Mechanism to Therapy. Immunity.

von Essen, M., Menné, C., Nielsen, B.L., Lauritsen, J.P.H., Dietrich, J., Andersen, P.S., Karjalainen, K., Ødum, N., and Geisler, C. (2002). The CD3γ Leucine-Based Receptor-Sorting Motif Is Required for Efficient Ligand-Mediated TCR Down-Regulation. J. Immunol.

Eyquem, J., Mansilla-Soto, J., Giavridis, T., Van Der Stegen, S.J.C., Hamieh, M., Cunanan, K.M., Odak, A., Gönen, M., and Sadelain, M. (2017). Targeting a CAR to the TRAC locus with CRISPR/Cas9 enhances tumour rejection. Nature.

Fritz, J.H., Le Bourhis, L., Magalhaes, J.G., and Philpott, D.J. (2008). Innate immune recognition at the epithelial barrier drives adaptive immunity: APCs take the back seat. Trends Immunol.

Giardino Torchia, M.L., Munitic, I., Castro, E., Herz, J., Mcgavern, D.B., and Ashwell, J.D. (2015). c-IAP ubiquitin protein ligase activity is required for 4-1BB signaling and CD8+ memory T-cell survival. Eur. J. Immunol.

van Gisbergen, K.P.J.M., van Olffen, R.W., van Beek, J., van der Sluijs, K.F., Arens, R., Nolte, M.A., and van Lier, R.A. (2009). Protective CD8 T Cell Memory Is Impaired during Chronic CD70-Driven Costimulation. J. Immunol.

van Gisbergen, K.P.J.M., Klarenbeek, P.L., Kragten, N.A.M., Unger, P.P.A., Nieuwenhuis, M.B.B., Wensveen, F.M., ten Brinke, A., Tak, P.P., Eldering, E., Nolte, M.A., et al. (2011). The costimulatory molecule CD27 maintains clonally diverse CD8+ T cell responses of low antigen affinity to protect against viral variants. Immunity.

Gotter, J., Brors, B., Hergenhahn, M., and Kyewski, B. (2004). Medullary Epithelial Cells of the Human Thymus Express a Highly Diverse Selection of Tissue-specific Genes Colocalized in Chromosomal Clusters. J. Exp. Med.

Gottschalk, R.A., Hathorn, M.M., Beuneu, H., Corse, E., Dustin, M.L., Altan-Bonnet, G., and Allison, J.P. (2012). Distinct influences of peptide-MHC quality and quantity on in vivo T-cell responses. Proc. Natl. Acad. Sci. U. S. A.

Hausmann, J., Pagenstecher, A., Baur, K., Richter, K., Rziha, H.-J., and Staeheli, P. (2005). CD8 T Cells Require Gamma Interferon To Clear Borna Disease Virus from the Brain and Prevent Immune System-Mediated Neuronal Damage. J. Virol.

Heczey, A., Louis, C.U., Savoldo, B., Dakhova, O., Durett, A., Grilley, B., Liu, H., Wu, M.F., Mei, Z., Gee, A., et al. (2017). CAR T Cells Administered in Combination with Lymphodepletion and PD-1 Inhibition to Patients with Neuroblastoma. Mol. Ther.

Hendriks, J., Xiao, Y., and Borst, J. (2003). CD27 Promotes Survival of Activated T Cells and Complements CD28 in Generation and Establishment of the Effector T Cell Pool. J. Exp. Med.

Hendriks, J., Xiao, Y., Rossen, J.W.A., van der Sluijs, K.F., Sugamura, K., Ishii, N., and Borst, J. (2005). During Viral Infection of the Respiratory Tract, CD27, 4-1BB, and OX40 Collectively Determine Formation of CD8+ Memory T Cells and Their Capacity for Secondary Expansion. J. Immunol. *175*, 1665–1676.

Hewitt, E.W. (2003). The MHC class I antigen presentation pathway: Strategies for viral immune evasion. Immunology.

Hong, J., Ge, C., Jothikumar, P., Yuan, Z., Liu, B., Bai, K., Li, K., Rittase, W., Shinzawa,

M., Zhang, Y., et al. (2018). A TCR mechanotransduction signaling loop induces negative selection in the thymus. Nat. Immunol.

Huang, C.Y.F., and Ferrell, J.E. (1996). Ultrasensitivity in the mitogen-activated protein kinase cascade. Proc. Natl. Acad. Sci. U. S. A.

Huang, J., Brameshuber, M., Zeng, X., Xie, J., Li, Q. jing, Chien, Y. hsiu, Valitutti, S., and Davis, M.M. (2013). A Single peptide-major histocompatibility complex ligand triggers digital cytokine secretion in CD4+ T Cells. Immunity.

Hünig, T. (2016). The rise and fall of the CD28 superagonist TGN1412 and its return as TAB08: a personal account. FEBS J. *283*, 3325–3334.

Iezzi, G., Karjalainen, K., and Lanzavecchia, A. (1998). The duration of antigenic stimulation determines the fate of naive and effector T cells. Immunity.

Itoh, M., Takahashi, T., Sakaguchi, N., Kuniyasu, Y., Shimizu, J., Otsuka, F., and Sakaguchi, S. (1999). Thymus and autoimmunity: production of CD25+CD4+ naturally anergic and suppressive T cells as a key function of the thymus in maintaining immunologic self-tolerance. J. Immunol.

Iwasaki, A., and Medzhitov, R. (2015). Control of adaptive immunity by the innate immune system. Nat. Immunol.

Izawa, K., Martin, E., Soudais, C., Bruneau, J., Boutboul, D., Rodriguez, R., Lenoir, C., Hislop, A.D., Besson, C., Touzot, F., et al. (2017). Inherited CD70 deficiency in humans reveals a critical role for the CD70-CD27 pathway in immunity to Epstein-Barr virus infection. J. Exp. Med.

Janeway Jr., C.A., and Medzhitov, R. (2002). Innate immune recognition. Annu Rev Immunol.

Jordan, M.S., Boesteanu, A., Reed, A.J., Petrone, A.L., Holenbeck, A.E., Lerman, M.A., Naji, A., and Caton, A.J. (2001). Thymic selection of CD4+CD25+ regulatory T cells induced by an agonist self-peptide. Nat. Immunol.

June, C.H., Ledbetter, J.A., Gillespie, M.M., Lindsten, T., and Thompson, C.B. (1987). T-cell proliferation involving the CD28 pathway is associated with cyclosporine-resistant interleukin 2 gene expression. Mol. Cell. Biol.

Kalekar, L.A., Schmiel, S.E., Nandiwada, S.L., Lam, W.Y., Barsness, L.O., Zhang, N., Stritesky, G.L., Malhotra, D., Pauken, K.E., Linehan, J.L., et al. (2016). CD4+ T cell anergy prevents autoimmunity and generates regulatory T cell precursors. Nat. Immunol.

Kamphorst, A.O., Wieland, A., Nasti, T., Yang, S., Zhang, R., Barber, D.L., Konieczny, B.T., Daugherty, C.Z., Koenig, L., Yu, K., et al. (2017). Rescue of exhausted CD8 T cells by PD-1-targeted therapies is CD28-dependent. Science (80-.).

Kashii, Y., Giorda, R., Herberman, R.B., Whiteside, T.L., and Vujanovic, N.L. (1999). Constitutive expression and role of the TNF family ligands in apoptotic killing of tumor cells by human NK cells. J. Immunol.

Kawahata, K., Misaki, Y., Yamauchi, M., Tsunekawa, S., Setoguchi, K., Miyazaki, J., and Yamamoto, K. (2002). Generation of CD4 + CD25 + Regulatory T Cells from Autoreactive T Cells Simultaneously with Their Negative Selection in the Thymus and from Nonautoreactive T Cells by Endogenous TCR Expression . J. Immunol.

Kawamata, S., Hori, T., Imura, A., Takaori-Kondo, A., and Uchiyama, T. (1998). Activation of OX40 signal transduction pathways leads to tumor necrosis factor receptor-associated factor (TRAF) 2- and TRAF5-mediated NF-≃B activation. J. Biol. Chem.

Keller, A.M., Groothuis, T.A., Veraar, E.A.M., Marsman, M., Wenniger, L.M.D.B., Janssen, H., Neefjes, J., and Borst, J. (2007). Costimulatory ligand CD70 is delivered to the immunological synapse by shared intracellular trafficking with MHC class II molecules. Proc. Natl. Acad. Sci. U. S. A.

Kershaw, M.H., Westwood, J.A., Parker, L.L., Wang, G., Eshhar, Z., Mavroukakis, S.A., White, D.E., Wunderlich, J.R., Canevari, S., Rogers-Freezer, L., et al. (2006). A phase I study on adoptive immunotherapy using gene-modified T cells for ovarian cancer. Clin. Cancer Res.

Khair, D.O., Bax, H.J., Mele, S., Crescioli, S., Pellizzari, G., Khiabany, A., Nakamura, M., Harris, R.J., French, E., Hoffmann, R.M., et al. (2019). Combining immune checkpoint inhibitors: Established and emerging targets and strategies to improve outcomes in melanoma. Front. Immunol.

Khoshnan, A., Tindell, C., Laux, I., Bae, D., Bennett, B., and Nel, A.E. (2000). The NF-κB Cascade Is Important in Bcl-x L Expression and for the Anti-Apoptotic Effects of the CD28 Receptor in Primary Human CD4 + Lymphocytes . J. Immunol.

Klein, L., Kyewski, B., Allen, P.M., and Hogquist, K.A. (2014). Positive and negative selection of the T cell repertoire: What thymocytes see (and don't see). Nat. Rev. Immunol.

Konstorum, A., Vella, A.T., Adler, A.J., and Laubenbacher, R.C. (2019). A mathematical model of combined CD8 T cell costimulation by 4-1BB (CD137) and OX40 (CD134) receptors. Sci. Rep.

Koyasu, S., Lawton, T., Novick, D., Recny, M.A., Siliciano, R.F., Wallner, B.P., and Reinherz, E.L. (1990). Role of interaction of CD2 molecules with lymphocyte function-associated antigen 3 in T-cell recognition of nominal antigen. Proc. Natl. Acad. Sci. U. S. A.

Krause, P., Bruckner, M., Uermösi, C., Singer, E., Groettrup, M., and Legler, D.F.

(2009). Prostaglandin e2 enhances T-cell proliferation by inducing the costimulatory molecules OX40L, CD70, and 4-1BBL on dendritic cells. Blood.

Kristensen, N.N., Madsen, A.N., Thomsen, A.R., and Christensen, J.P. (2004). Cytokine production by virus-specific CD8+ T cells varies with activation state and localization, but not with TCR avidity. J. Gen. Virol.

Kurts, C., Kosaka, H., Carbone, F.R., Miller, J.F.A.P., and Heath, W.R. (1997). Class I-restricted cross-presentation of exogenous self-antigens leads to deletion of autoreactive CD8+ T cells. J. Exp. Med.

Lamers, C.H.J., Sleijfer, S., Van Steenbergen, S., Van Elzakker, P., Van Krimpen, B., Groot, C., Vulto, A., Den Bakker, M., Oosterwijk, E., Debets, R., et al. (2013). Treatment of metastatic renal cell carcinoma with CAIX CAR-engineered T cells: Clinical evaluation and management of on-target toxicity. Mol. Ther.

Lavoie, J.N., L'Allemain, G., Brunei, A., Müller, R., and Pouysségur, J. (1996). Cyclin D1 expression is regulated positively by the p42/p44(MAPK) and negatively by the p38/HOG(MAPK) pathway. J. Biol. Chem.

Lee, H.-W., Park, S.-J., Choi, B.K., Kim, H.H., Nam, K.-O., and Kwon, B.S. (2002). 4-1BB Promotes the Survival of CD8 + T Lymphocytes by Increasing Expression of Bcl-x L and Bfl-1 . J. Immunol.

Lee, K.H., Dinner, A.R., Tu, C., Campi, G., Raychaudhuri, S., Varma, R., Sims, T.N., Burack, W.R., Wu, H., Wang, J., et al. (2003). The Immunological Synapse Balances T Cell Receptor Signaling and Degradation. Science (80-.).

Lever, M., Maini, P.K., Van Der Merwe, P.A., and Dushek, O. (2014). Phenotypic models of T cell activation. Nat. Rev. Immunol.

Lever, M., Lim, H.S., Kruger, P., Nguyen, J., Trendel, N., Abu-Shah, E., Maini, P.K., Van Der Merwe, P.A., and Dushek, O. (2016). Architecture of a minimal signaling pathway explains the T-cell response to a 1 million-fold variation in antigen affinity and dose. Proc. Natl. Acad. Sci. U. S. A.

Li, Y., Moysey, R., Molloy, P.E., Vuidepot, A.L., Mahon, T., Baston, E., Dunn, S., Liddy, N., Jacob, J., Jakobsen, B.K., et al. (2005). Directed evolution of human T-cell receptors with picomolar affinities by phage display. Nat. Biotechnol.

Liepe, J., Kirk, P., Filippi, S., Toni, T., Barnes, C.P., and Stumpf, M.P.H. (2014). A framework for parameter estimation and model selection from experimental data in systems biology using approximate Bayesian computation. Nat. Protoc.

van Lier, R.A., Borst, J., Vroom, T.M., Klein, H., Van Mourik, P., Zeijlemaker, W.P., and Melief, C.J. (1987). Tissue distribution and biochemical and functional properties of Tp55 (CD27), a novel T cell differentiation antigen. J. Immunol.

Lin, G.H.Y., Snell, L.M., Wortzman, M.E., Clouthier, D.L., and Watts, T.H. (2013). GITR-Dependent Regulation of 4-1BB Expression: Implications for T Cell Memory and Anti–4-1BB–Induced Pathology. J. Immunol.

Liu, Y., Di, S., Shi, B., Zhang, H., Wang, Y., Wu, X., Luo, H., Wang, H., Li, Z., and Jiang, H. (2019). Armored Inducible Expression of IL-12 Enhances Antitumor Activity of Glypican-3–Targeted Chimeric Antigen Receptor–Engineered T Cells in Hepatocellular Carcinoma. J. Immunol.

Long, A.H., Haso, W.M., Shern, J.F., Wanhainen, K.M., Murgai, M., Ingaramo, M., Smith, J.P., Walker, A.J., Kohler, M.E., Venkateshwara, V.R., et al. (2015). 4-1BB costimulation ameliorates T cell exhaustion induced by tonic signaling of chimeric antigen receptors. Nat. Med.

Ma, Z., Discher, D.E., and Finkel, T.H. (2012). Mechanical force in T cell receptor signal initiation. Front. Immunol.

Macian, F. (2005). NFAT proteins: Key regulators of T-cell development and function. Nat. Rev. Immunol.

Macián, F., García-Cózar, F., Im, S.H., Horton, H.F., Byrne, M.C., and Rao, A. (2002). Transcriptional mechanisms underlying lymphocyte tolerance. Cell.

Malek, T.R., and Castro, I. (2010). Interleukin-2 Receptor Signaling: At the Interface between Tolerance and Immunity. Immunity.

Marangoni, F., Murooka, T.T., Manzo, T., Kim, E.Y., Carrizosa, E., Elpek, N.M., and Mempel, T.R. (2013). The Transcription Factor NFAT Exhibits Signal Memory during Serial T Cell Interactions with Antigen-Presenting Cells. Immunity.

Mardiana, S., Solomon, B.J., Darcy, P.K., and Beavis, P.A. (2019). Supercharging adoptive T cell therapy to overcome solid tumor-induced immunosuppression. Sci. Transl. Med.

Martinez, M., and Moon, E.K. (2019). CAR T cells for solid tumors: New strategies for finding, infiltrating, and surviving in the tumor microenvironment. Front. Immunol.

Martinez, G.J., Pereira, R.M., Äijö, T., Kim, E.Y., Marangoni, F., Pipkin, M.E., Togher, S., Heissmeyer, V., Zhang, Y.C., Crotty, S., et al. (2015). The Transcription Factor NFAT Promotes Exhaustion of Activated CD8+ T Cells. Immunity.

Maude, S.L., Laetsch, T.W., Buechner, J., Rives, S., Boyer, M., Bittencourt, H., Bader, P., Verneris, M.R., Stefanski, H.E., Myers, G.D., et al. (2018). Tisagenlecleucel in children and young adults with B-cell lymphoblastic leukemia. N. Engl. J. Med.

Mempel, T.R., Henrickson, S.E., and Von Andrian, U.H. (2004). T-cell priming by dendritic cells in lymph nodes occurs in three distinct phases. Nature.

Van Der Merwe, P.A., and Dushek, O. (2011). Mechanisms for T cell receptor triggering. Nat. Rev. Immunol.

Mescher, M.F., Curtsinger, J.M., Agarwal, P., Casey, K.A., Gerner, M., Hammerbeck, C.D., Popescu, F., and Xiao, Z. (2006). Signals required for programming effector and memory development by CD8+ T cells. Immunol. Rev.

Michalek, R.D., and Rathmell, J.C. (2010). The metabolic life and times of a T-cell. Immunol. Rev.

Minguet, S., Swamy, M., Alarcón, B., Luescher, I.F., and Schamel, W.W.A. (2007). Full Activation of the T Cell Receptor Requires Both Clustering and Conformational Changes at CD3. Immunity.

Monjas, A., Alcover, A., and Alarcón, B. (2004). Engaged and bystander T cell receptors are down-modulated by different endocytotic pathways. J. Biol. Chem.

Monks, C.R.F., Freiberg, B.A., Kupfer, H., Sciaky, N., and Kupfer, A. (1998). Three-dimensional segregation of supramolecular activation clusters in T cells. Nature.

Morales, M.S., and Mueller, D. (2018). Anergy into T regulatory cells: An integration of metabolic cues and epigenetic changes at the Foxp3 conserved non-coding sequence 2 [version 1; referees: 2 approved]. F1000Research.

Mueller, D.L., Jenkins, M.K., and Schwartz, R.H. (1989). An accessory cell-derived costimulatory signal acts independently of protein kinase C activation to allow T cell proliferation and prevent the induction of unresponsiveness. J. Immunol.

Muise-Helmericks, R.C., Grimes, H.L., Bellacosa, A., Malstrom, S.E., Tsichlis, P.N., and Rosen, N. (1998). Cyclin D expression is controlled post-transcriptionally via a phosphatidylinositol 3-kinase/Akt-dependent pathway. J. Biol. Chem.

Nakamura, Y. (2019). Biomarkers for Immune Checkpoint Inhibitor-Mediated Tumor Response and Adverse Events. Front. Med.

Nakanishi, Y., Lu, B., Gerard, C., and Iwasaki, A. (2009). CD8 + T lymphocyte mobilization to virus-infected tissue requires CD4 + T-cell help. Nature.

Pollok, K.E., Kim, Y.J., Zhou, Z., Hurtado, J., Kim, K.K., Pickard, R.T., and Kwon, B.S. (1993). Inducible T cell antigen 4-1BB. Analysis of expression and function. J. Immunol.

Pollok, K.E., Kim, Y. -J, Hurtado, J., Zhou, Z., Kim, K.K., and Kwon, B.S. (1994). 4-1BB T-cell antigen binds to mature B cells and macrophages, and costimulates anti-μ-primed splenic B cells. Eur. J. Immunol.

Prévost-Blondel, A., Roth, E., Rosenthal, F.M., and Pircher, H. (2000). Crucial Role of TNF-α in CD8 T Cell-Mediated Elimination of 3LL-A9 Lewis Lung Carcinoma Cells

In Vivo. J. Immunol.

Proulx-Giraldeau, F., Rademaker, T.J., and François, P. (2017). Untangling the Hairball: Fitness-Based Asymptotic Reduction of Biological Networks. Biophys. J.

Pulle, G., Vidric, M., and Watts, T.H. (2006). IL-15-Dependent Induction of 4-1BB Promotes Antigen-Independent CD8 Memory T Cell Survival. J. Immunol.

Redeker, A., and Arens, R. (2016). Improving adoptive T cell therapy: The particular role of T cell costimulation, cytokines, and post-transfer vaccination. Front. Immunol.

Reis E Sousa, C. (2006). Dendritic cells in a mature age. Nat. Rev. Immunol.

Reth, M. (1989). Antigen receptor tail clue [5]. Nature.

Riedhammer, C., and Weissert, R. (2015). Antigen presentation, autoantigens, and immune regulation in multiple sclerosis and other autoimmune diseases. Front. Immunol.

Rock, K.L., Reits, E., and Neefjes, J. (2016). Present Yourself! By MHC Class I and MHC Class II Molecules. Trends Immunol.

Romero, P., Zippelius, A., Kurth, I., Pittet, M.J., Touvrey, C., Iancu, E.M., Corthesy, P., Devevre, E., Speiser, D.E., and Rufer, N. (2007). Four Functionally Distinct Populations of Human Effector-Memory CD8 + T Lymphocytes . J. Immunol.

Saeidi, A., Zandi, K., Cheok, Y.Y., Saeidi, H., Wong, W.F., Lee, C.Y.Q., Cheong, H.C., Yong, Y.K., Larsson, M., and Shankar, E.M. (2018). T-cell exhaustion in chronic infections: Reversing the state of exhaustion and reinvigorating optimal protective immune responses. Front. Immunol.

San José, E., Borroto, A., Niedergang, F., Alcover, A., and Alarcón, B. (2000). Triggering the TCR complex causes the downregulation of nonengaged receptors by a signal transduction-dependent mechanism. Immunity.

Sanmamed, M.F., Pastor, F., Rodriguez, A., Perez-Gracia, J.L., Rodriguez-Ruiz, M.E., Jure-Kunkel, M., and Melero, I. (2015). Agonists of Co-stimulation in Cancer Immunorapy Directed Against CD137, OX40, GITR, CD27, CD28, and ICOS. Semin. Oncol.

Sanmamed, M.F., Etxeberría, I., Otano, I., and Melero, I. (2019). Twists and turns to translating 4-1BB cancer immunotherapy. Sci. Transl. Med.

Saoulli, K., Lee, S.Y., Cannons, J.L., Yeh, W.C., Santana, A., Goldstein, M.D., Bangia, N., DeBenedette, M.A., Mak, T.W., Choi, Y., et al. (1998). CD28-independent, TRAF2-dependent costimulation of resting T cells by 4- 1BB ligand. J. Exp. Med.

Savoldo, B., Ramos, C.A., Liu, E., Mims, M.P., Keating, M.J., Carrum, G., Kamble, R.T.,

Bollard, C.M., Gee, A.P., Mei, Z., et al. (2011). CD28 costimulation improves expansion and persistence of chimeric antigen receptor-modified T cells in lymphoma patients. J. Clin. Invest.

Schmidt, A., Oberle, N., and Krammer, P.H. (2012). Molecular mechanisms of Treg-mediated T cell suppression. Front. Immunol.

Schwartz, R.H. (2003). T CELL ANERGY. Annu. Rev. Immunol.

Seko, Y., Ishiyama, S., Nishikawa, T., Kasajima, T., Hiroe, M., Suzuki, S., Ishiwata, S., Kawai, S., Tanaka, Y., Azuma, M., et al. (2002). Expression of tumor necrosis factor ligand superfamily costimulatory molecules CD27L, CD30L, OX40L and 4-1BBL in the heart of patients with acute myocarditis and dilated cardiomyopathy. Cardiovasc. Pathol.

Serghides, L., Bukczynski, J., Wen, T., Wang, C., Routy, J.-P., Boulassel, M.-R., Sekaly, R.-P., Ostrowski, M., Bernard, N.F., and Watts, T.H. (2005). Evaluation of OX40 Ligand as a Costimulator of Human Antiviral Memory CD8 T Cell Responses: Comparison with B7.1 and 4-1BBL. J. Immunol.

Shuford, W.W., Klussman, K., Tritchler, D.D., Loo, D.T., Chalupny, J., Siadak, A.W., Brown, T.J., Emswiler, J., Raecho, H., Larsen, C.P., et al. (1997). 4-1BB costimulatory signals preferentially induce CD8+ T cell proliferation and lead to the amplification in vivo of cytotoxic T cell responses. J. Exp. Med.

Slifka, M.K., and Whitton, J.L. (2000). Activated and Memory CD8 + T Cells Can Be Distinguished by Their Cytokine Profiles and Phenotypic Markers . J. Immunol.

Snell, L.M., McPherson, A.J., Lin, G.H.Y., Sakaguchi, S., Pandolfi, P.P., Riccardi, C., and Watts, T.H. (2010). CD8 T Cell-Intrinsic GITR Is Required for T Cell Clonal Expansion and Mouse Survival following Severe Influenza Infection. J. Immunol.

Snell, L.M., Lin, G.H.Y., and Watts, T.H. (2012). IL-15–Dependent Upregulation of GITR on CD8 Memory Phenotype T Cells in the Bone Marrow Relative to Spleen and Lymph Node Suggests the Bone Marrow as a Site of Superior Bioavailability of IL-15. J. Immunol.

So, T., Choi, H., and Croft, M. (2011a). OX40 Complexes with Phosphoinositide 3-Kinase and Protein Kinase B (PKB) To Augment TCR-Dependent PKB Signaling. J. Immunol.

So, T., Soroosh, P., Eun, S.Y., Altman, A., and Croft, M. (2011b). Antigen-independent signalosome of CARMA1, PKCθ, and TNF receptor-associated factor 2 (TRAF2) determines NF-κB signaling in T cells. Proc. Natl. Acad. Sci. U. S. A.

Steinman, R.M. (1998). Dendritic cells and the control of immunity. Exp. Hematol.

Strioga, M., Pasukoniene, V., and Characiejus, D. (2011). CD8+CD28- and

CD8+CD57+ T cells and their role in health and disease. Immunology.

Sznol, M., Hodi, F.S., Margolin, K., McDermott, D.F., Ernstoff, M.S., Kirkwood, J.M., Wojtaszek, C., Feltquate, D., and Logan, T. (2008). Phase I study of BMS-663513, a fully human anti-CD137 agonist monoclonal antibody, in patients (pts) with advanced cancer (CA). J. Clin. Oncol.

Takahashi, C., Vella, A.T., and Mittler, R.S. (1999). Cutting edge: 4-1BB is a bona fide CD8 T cell survival signal. J. Immunol.

Takeuchi, O., and Akira, S. (2010). Pattern Recognition Receptors and Inflammation. Cell.

Tham, E.L., Shrikant, P., and Mescher, M.F. (2002). Activation-Induced Nonresponsiveness: A Th-Dependent Regulatory Checkpoint in the CTL Response. J. Immunol.

Thompson, C.B. (1995). New insights into V(D)J recombination and its role in the evolution of the immune system. Immunity.

Trendel, N., Kruger, P., Nguyen, J., Gaglione, S., and Dushek, O. (2019). Perfect adaptation of CD8 + T cell responses to constant antigen input over a wide range of affinity is overcome by costimulation. Biorxiv.

Varga, S.M., and Welsh, R.M. (2000). High Frequency of Virus-Specific Interleukin-2-Producing CD4+ T Cells and Th1 Dominance during Lymphocytic Choriomeningitis Virus Infection. J. Virol.

Varma, R., Campi, G., Yokosuka, T., Saito, T., and Dustin, M.L. (2006). T Cell Receptor-Proximal Signals Are Sustained in Peripheral Microclusters and Terminated in the Central Supramolecular Activation Cluster. Immunity.

Vera, J., Savoldo, B., Vigouroux, S., Biagi, E., Pule, M., Rossig, C., Wu, J., Heslop, H.E., Rooney, C.M., Brenner, M.K., et al. (2006). T lymphocytes redirected against the κ light chain of human immunoglobulin efficiently kill mature B lymphocyte-derived malignant cells. Blood.

Vignali, D.A.A., Collison, L.W., and Workman, C.J. (2008). How regulatory T cells work. Nat. Rev. Immunol.

Vinay, D.S., and Kwon, B.S. (2012). Immunotherapy of cancer with 4-1BB. Mol. Cancer Ther.

Viola, A., and Lanzavecchia, A. (1996). T cell activation determined by T cell receptor number and tunable thresholds. Science (80-.).

Van Der Vliet, H.J.J., and Nieuwenhuis, E.E. (2007). IPEX as a result of mutations in FOXP3. Clin. Dev. Immunol.

Volterra, V. (1928). Variations and Fluctuations of the Number of Individuals in Animal Species living together. ICES J. Mar. Sci.

Voskoboinik, I., Whisstock, J.C., and Trapani, J.A. (2015). Perforin and granzymes: Function, dysfunction and human pathology. Nat. Rev. Immunol.

Wang, C., McPherson, A.J., Jones, R.B., Kawamura, K.S., Lin, G.H.Y., Lang, P.A., Ambagala, T., Pellegrini, M., Calzascia, T., Aidarus, N., et al. (2012). Loss of the signaling adaptor TRAF1 causes CD8+ T cell dysregulation during human and murine chronic infection. J. Exp. Med.

Wang, Y., Chung, Y.R., Eitzinger, S., Palacio, N., Gregory, S., Bhattacharyya, M., and Penaloza-MacMaster, P. (2019). TLR4 signaling improves PD-1 blockade therapy during chronic viral infection. PLoS Pathog.

Wells, A.D. (2009). New Insights into the Molecular Basis of T Cell Anergy: Anergy Factors, Avoidance Sensors, and Epigenetic Imprinting. J. Immunol.

Wherry, E.J. (2011). T cell exhaustion. Nat. Immunol.

Wilcox, R.A., Tamada, K., Flies, D.B., Zhu, G., Chapoval, A.I., Blazar, B.R., Kast, W.M., and Chen, L. (2004). Ligation of CD137 receptor prevents and reverses established anergy of CD8+ cytolytic T lymphocytes in vivo. Blood.

Wolchok, J.D., Chiarion-Sileni, V., Gonzalez, R., Rutkowski, P., Grob, J.J., Cowey, C.L., Lao, C.D., Wagstaff, J., Schadendorf, D., Ferrucci, P.F., et al. (2017). Overall Survival with Combined Nivolumab and Ipilimumab in Advanced Melanoma. N. Engl. J. Med.

Wyzgol, A., Müller, N., Fick, A., Munkel, S., Grigoleit, G.U., Pfizenmaier, K., and Wajant, H. (2009). Trimer Stabilization, Oligomerization, and Antibody-Mediated Cell Surface Immobilization Improve the Activity of Soluble Trimers of CD27L, CD40L, 41BBL, and Glucocorticoid-Induced TNF Receptor Ligand. J. Immunol.

Yu, Q., Yue, F.Y., Gu, X.X., Schwartz, H., Kovacs, C.M., and Ostrowski, M.A. (2006). OX40 Ligation of CD4 + T Cells Enhances Virus-Specific CD8 + T Cell Memory Responses Independently of IL-2 and CD4 + T Regulatory Cell Inhibition . J. Immunol.

Zapata, J.M., Perez-Chacon, G., Carr-Baena, P., Martinez-Forero, I., Azpilikueta, A., Otano, I., and Melero, I. (2018). CD137 (4-1BB) signalosome: Complexity is a matter of TRAFs. Front. Immunol.

Zhao, Z., Condomines, M., van der Stegen, S.J.C., Perna, F., Kloss, C.C., Gunset, G., Plotkin, J., and Sadelain, M. (2015). Structural Design of Engineered Costimulation Determines Tumor Rejection Kinetics and Persistence of CAR T Cells. Cancer Cell.

Zheng, C., Kabaleeswaran, V., Wang, Y., Cheng, G., and Wu, H. (2010). Crystal

Structures of the TRAF2: cIAP2 and the TRAF1: TRAF2: cIAP2 Complexes: Affinity, Specificity, and Regulation. Mol. Cell.

Zhu, J., Yamane, H., and Paul, W.E. (2010). Differentiation of Effector CD4 T Cell Populations. Annu. Rev. Immunol.

Zhu, Y., Yao, S., and Chen, L. (2011). Cell Surface Signaling Molecules in the Control of Immune Responses: A Tide Model. Immunity.

Zinkernagel, R.M., and Doherty, P.C. (1974). Restriction of in vitro T cell-mediated cytotoxicity in lymphocytic choriomeningitis within a syngeneic or semiallogeneic system. Nature.